

NASA CR-145

327

Study of the Effect of Scattering from Turbid Water on the Polarization of a Laser Beam

(NASA-CR-145327) STUDY OF THE EFFECT OF
SCATTERING FROM TURBID WATER ON THE
POLARIZATION OF A LASER BEAM (Mitre Corp.)
138 p HC A07/MF A01

N78-26426

CSCL 20E

Unclassified

G3/36 23347

Robert G. Henderson

Ali H. Ghovanlou

METREK Division of The MITRE Corporation

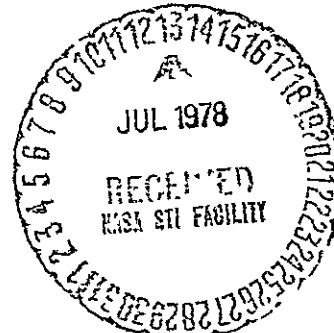
Contract No. F19628-77-C-0001

March 1978



National Aeronautics and
Space Administration

Langley Research Center
Hampton, Virginia 23665



NASA CR-145 327

Study of the Effect of Scattering from Turbid Water on the Polarization of a Laser Beam

**Robert G. Henderson
Ali H. Ghovanlou**

**METREK Division of The MITRE Corporation
1820 Dolley Madison Blvd.
McLean, Virginia 22101**

**Contract No. F19628-77-C-0001
March 1978**



National Aeronautics and
Space Administration

Langley Research Center
Hampton, Virginia 23665

Department Approval: Tracy Wright

MITRE Project Approval Ali Ghoussous

ABSTRACT

This report documents a study which was carried out using a Monte Carlo Simulation method to determine the effect of scattering from turbid water on the polarization of a backscattered beam of laser light. The relationship between the polarization and the type and amount of suspended particulates in the water was investigated.

TABLE OF CONTENTS

| | <u>Page</u> |
|---|-------------|
| LIST OF ILLUSTRATIONS | vii |
| LIST OF TABLES | ix |
| 1.0 INTRODUCTION | 1 |
| 2.0 SUMMARY AND CONCLUSIONS | 5 |
| 3.0 METREK'S MONTE CARLO RADIATIVE TRANSFER MODEL | 9 |
| 3.1 Monte Carlo Simulation for Narrow Beam Transmission | 10 |
| 4.0 CALCULATION OF SCATTERING FUNCTIONS | 15 |
| 4.1 Mie Theory for Single Particle Scattering | 15 |
| 4.2 Mie Theory for Scattering from Polydispersions | 18 |
| 4.3 Computational Methods | 20 |
| 4.4 Properties of Clay samples | 22 |
| 4.4.1 Physical Characteristics of Clay Samples | 22 |
| 4.4.2 Particle Size Distributions | 25 |
| 4.5 Results of Computations | 37 |
| 4.5.1 Volume Scattering Phase Functions | 37 |
| 4.5.2 Volume Scattering Distribution Functions | 44 |
| 5.0 THE EFFECT OF SCATTERING ON POLARIZATION | 53 |
| 5.1 The Stokes Formalism | 53 |
| 5.2 The Effect of Scattering on Polarization | 54 |
| 5.3 Results of Calculations of Polarization for Single Scattering | 59 |
| 5.4 Depolarization Due to Multiple Scattering | 60 |
| 6.0 RESULTS OF MONTE CARLO SIMULATION | 69 |
| 6.1 Phenomenological Theory of Depolarization | 69 |
| 6.2 Depolarization Calculation From Monte Carlo Results | 74 |
| APPENDIX A: RELATIONSHIP BETWEEN EXTINCTION, SCATTERING, AND ABSORPTION COEFFICIENTS AND THE MIE PARAMETERS | 81 |
| APPENDIX B: LISTINGS FOR MONTE CARLO ROUTINE | 82 |

TABLE OF CONTENTS (Concluded)

| | <u>Page</u> |
|---|-------------|
| APPENDIX C: LISTINGS FOR STOKES ROUTINE USED TO CALCULATE THE STOKES PARAMETERS OF THE BACKSCATTERED RADIANCE | 91 |
| APPENDIX D: LISTINGS FOR POLYMIE AND DBMIE ROUTINES USED TO CALCULATE THE VOLUME SCATTERING FUNCTIONS | 95 |
| APPENDIX E: PROGRAM LISTING FOR CURFIT ROUTINE USED TO FIT THE THEORETICAL SIZE DISTRIBUTIONS TO THE EMPERICAL DATA | 109 |
| REFERENCES | 123 |
| DISTRIBUTION LIST | 125 |

LIST OF ILLUSTRATIONS

| <u>Figure Number</u> | | <u>Page</u> |
|----------------------|---|-------------|
| 3-1 | Monte Carlo Simulation of Narrow Beam Transmission in Turbid Water | 12 |
| 4-1 | Cumulative Size Distribution of Feldspar Sample | 26 |
| 4-2 | Cumulative Size Distribution of Calvert Sample | 27 |
| 4-3 | Cumulative Size Distribution of Ball Sample | 28 |
| 4-4 | Cumulative Size Distribution of Jordan Sample | 29 |
| 4-5 | Particle Size Density Function for Feldspar (Modified Gamma Distribution) | 31 |
| 4-6 | Cumulative Size Distribution Fit of Feldspar Sample Using Modified Gamma Distribution | 32 |
| 4-7 | Particle Size Density Function for Ball Clay (Junges Distribution) | 33 |
| 4-8 | Cumulative Size Distribution for Ball Clay Sample Using Junge Distribution | 34 |
| 4-9 | Volume Scattering Functions For Feldspar ($\lambda = 500\text{NM}$) | 38 |
| 4-10 | Volume Scattering Functions For Ball Clay ($\lambda = 500\text{NM}$) | 39 |
| 4-11 | Volume Scattering Functions For Feldspar ($10\mu\text{M} = \text{Cutoff } \lambda = 500\text{NM}$) | 40 |
| 4-12 | Volume Scattering Functions For Ball Clay ($10\mu\text{M Cutoff } \lambda = 500\text{NM}$) | 41 |
| 4-13 | Volume Scattering Functions For Feldspar ($10\mu\text{M Cutoff } \lambda = 600\text{NM}$) | 42 |
| 4-14 | Volume Scattering Functions For Ball Clay ($10\mu\text{M Cutoff } \lambda = 600\text{NM}$) | 43 |
| 4-15 | Volume Scattering Distribution Functions for Feldspar ($\lambda = 500\text{NM}$) | 45 |
| 4-16 | Volume Scattering Distribution Functions For Ball Clay ($\lambda = 500\text{NM}$) | 46 |
| 4-17 | Volume Scattering Distribution Functions For Feldspar ($10\mu\text{M Cutoff } \lambda = 500\text{NM}$) | 47 |
| 4-18 | Volume Scattering Distribution Functions For Ball Clay ($10\mu\text{M Cutoff } \lambda = 500\text{NM}$) | 48 |
| 4-19 | Wavelength Dependence of Volume Scattering Distribution Functions For Feldspar ($10\mu\text{M Cutoff}$) | 50 |

LIST OF ILLUSTRATIONS (Concluded)

| <u>Figure Number</u> | | <u>Page</u> |
|----------------------|--|-------------|
| 4-20 | Wavelength Dependence of Volume Scattering Functions for Ball Clay ($10\mu\text{M}$ Cutoff) | 51 |
| 5-1 | Polarization for Feldspar ($\lambda = 500\text{NM}$) | 61 |
| 5-2 | Polarization for Ball Clay ($\lambda = 500\text{NM}$) | 62 |
| 5-3 | Polarization for Feldspar ($10\mu\text{M}$ Cutoff $\lambda = 500\text{NM}$) | 63 |
| 5-4 | Polarization for Ball Clay ($10\mu\text{M}$ Cutoff $\lambda = 500\text{NM}$) | 64 |
| 5-5 | Polarization for Feldspar ($10\mu\text{M}$ Cutoff $\lambda = 600\text{NM}$) | 65 |
| 5-6 | Polarization for Ball Clay ($10\mu\text{M}$ Cutoff $\lambda = 600\text{NM}$) | 66 |
| 6-1 | Relationship Between Spot Size, Density of Sediments and Number of Scattering Events | 71 |
| 6-2 | Mean Number of Scattering Events for Back-scattered Photons vs. Spot Size x Scattering Coefficient | 72 |
| 6-3 | Dependence of Polarization on Scattering Coefficient | 75 |
| 6-4 | Dependence of Polarization on A/S Ratio | 76 |
| 6-5 | Dependence of R-Factor on Scattering Coefficient | 77 |
| 6-6 | Dependence of R-Factor on A.S. Ratio | 79 |
| 6-7 | Comparison of Theoretical and Experimental Values for the R-Factor. Diamonds Represent Data Collected from the Chesapeake Bay Using a $2\frac{1}{2}$ Inch Radius Spot Size | 80 |

LIST OF TABLES

| <u>Table Number</u> | | <u>Page</u> |
|---------------------|---|-------------|
| 4.I | Chemical Composition and Index of Refraction of Clay Constituents | 24 |
| 4.II | Settling Velocities of Sand and Silt In Still Water | 36 |
| 5.I | Stokes Representation For Some Polarization Types ⁽¹⁴⁾ | 55 |

1.0 INTRODUCTION

Excessive amounts of suspended particles in the environmental waters lead to significant economical and ecological consequences. Economic losses are mostly due to expenditures for dredging operations and the reduction of the nation's reservoir capabilities. Less tangible, but probably more important are the adverse ecological effects. For example, organic debris and residues absorbed on the surface of particles increase biochemical oxygen demand (BOD) and chemical oxygen demand (COD) which cause a concomitant decrease in the concentrations of dissolved oxygen and the elimination or reduction of sensitive organisms. The introduction of sediments into an aquatic environment also may alter nutrient concentrations, especially total organic carbon (TOC), nitrogen, and phosphorus. Increases in nutrient loading may increase productivity in the absence of inhibitory factors. Although high productivity can be beneficial, it also may lead to serious eutrophication and nuisance algae blooms. As long as the concentration of suspended sediments remains high, primary productivity (photosynthesis) will be inhibited or much reduced due to a reduction in the penetration of light in the water column. Sediments also may transport toxic materials such as pesticides and certain heavy metals which may adversely affect the biota. In the light of the accumulated evidence, the knowledge of sediment concentration and composition seems of utmost

importance to the understanding of ecological processes in the aquatic environment.

Considering the dynamic character of the environmental waters monitoring procedures for measuring water quality parameters should be based on a timely data collection system, such as can be provided by applications of remote sensing technology. To develop appropriate remote sensing tools a laboratory field program is presently being pursued at the NASA/Langley Research Center (LaRC). The purpose of this program is to investigate the remote sensing of water quality parameters using information on the polarization properties of the backscattered radiance when a polarized laser beam is directed at turbid water. The present report describes a modeling effort which deals with variations in the polarization characteristics of the backscattered radiance as a function of water turbidity, suspended particulate type, and detector spot size. This investigation employs Monte Carlo simulation techniques to describe the radiative transfer processes in the turbid medium, and to determine the backscattered radiance. Specifically the polarization properties of the back-scattered beam is calculated based on the multiple scattering events and the optical properties of the water medium.

The organization of the report is as follows: Section 2.0 presents a summary of the investigation and the major conclusions; the details of the METREK Monte Carlo model are given in Section 3.0

while the details of the calculation of the scattering functions are presented in Section 4.0; Section 5.0 discusses the effect of scattering on polarization in an abstract, theoretical framework while Section 6.0 discusses the effect of scattering based on the Monte Carlo simulation and gives the results of the calculations.

2.0 SUMMARY AND CONCLUSIONS

This work has been done in support of an on-going laboratory and field experiment at the NASA/Langley Research Center (LaRC). The goal of this work is to investigate the effect of varying the amount and type of suspended particulates in water on the polarization of a backscattered beam of laser light. In addition, it is expected that the results of the study will provide some guidance to the experiment design.

The first step in performing this work is the calculation of the optical properties, represented by the Mie matrix, of selected soil types. Information concerning the size distributions of these soils was obtained from a previous LaRC study ⁽¹⁾. The calculated quantities are the Mie matrix and the associated volume scattering phase functions and volume scattering distribution functions. It is found in this portion of the study that the dominant source of variation in the scattering functions is the maximum size of the particles included in the size distribution. This has important implications for attempts to compare the laboratory results (where the water is constantly mixed) and the field test results (where the larger particles may have settled out).

A Monte Carlo simulation is next run using one of the calculated scattering functions. This simulation is done in such a way so as to follow each scattering event of each photon which emerged from the water. The results of the simulation are then analyzed using

a method which allows the calculation of the resultant intensity and polarization of the backscattered beam for different detector spot sizes (the size of the area on the surface of the water from which photons emerging from the water will enter the detector), different concentrations, and different optical properties (in terms of the ratio of the amount of absorption to the amount of scattering of the suspended sediments).

Based on the simulation study, the use of a polarization measurement of a backscattered beam of laser light for the determination of the concentration of suspended particulates appears feasible. The usefulness of the technique for discriminating between different types of suspended particulates is less certain. In this study a change in particulate type was represented by allowing the relative amount of scattering and absorption to vary over a limited range. It is found that there is a small dependence of the polarization on the relative amounts of absorption and scattering over the range of interest. In fact a change in particulate type will result in not only a change in the relative amounts of absorption and scattering but also in a change in the volume scattering distribution function. This effect has not been examined in this study. The results of this study suggest that a trade off exists between the detector spot size and signal-to-noise considerations. The ability to discriminate between different particulate concentrations is improved if the detector spot size is decreased. Thus the smallest detector spot

size commensurate with signal-to-noise requirements is indicated by this study.

While only a limited number of concentrations, optical properties and experiment configurations were considered in this study a simple phenomenological theory has been developed which should allow an extension of the results to other cases of interest. This theory relates the polarization of the backscattered beam to the detector spot size and the concentration of suspended particulates and gives excellent qualitative agreement with the results of the simulation.

Comparison of the theoretical predictions with data obtained from an experiment in the Chesapeake Bay area (see Figure 6-7) shows very good agreement.

3.0 METREK'S MONTE CARLO RADIATIVE TRANSFER MODEL

The important optical quantity which represents the scattering properties of a medium is the Mie Scattering Matrix, $S(m, \theta)$, which determines the intensity and polarization of the radiation scattered into an angle θ from a volume element containing particles with an index of refraction m (see Section 4.0 for a more thorough discussion of the Mie Matrix). A number of optical parameters of interest can be derived given knowledge of the Mie Matrix. These include the absorption coefficient, a , the scattering coefficient, s , and the total extinction coefficient, $\alpha = a + s$. (For a discussion of the relation between these parameters and the Mie Matrix see Appendix A). The physical importance of these quantities can be seen from Beer's law which states that, for a collimated beam of light passing through the medium, the intensity decreases exponentially as a function of distance traveled, r :

$$I \sim e^{-\alpha r} = e^{-ar} \cdot e^{-sr}. \quad (3-1)$$

That is, e^{-ar} measures the fraction of the beam intensity which is lost due to absorption and e^{-sr} measures the fraction of the beam intensity which is lost due to scattering out of the collimated beam.

Two other important optical parameters are the volume scattering phase function $\sigma(\theta)$ and the scattering distribution function $F(\theta)$.

The scattering phase function $\sigma(\theta)$ is related to the Mie Matrix through

$$\sigma(\theta) = S_{11}(m, \theta) + S_{22}(m, \theta) \quad (3-2)$$

and represents the total intensity scattered into an angle θ from a volume scattering element (properly normalized this is equivalent to the probability of scattering into an angle θ). The scattering distribution function is the cumulative probability of scattering between 0 and θ degrees and is given by

$$F(\theta) = \frac{\int_0^\theta \sigma(\theta') \sin \theta' d\theta'}{\int_0^\pi \sigma(\theta') \sin \theta' d\theta'} \quad (3-3)$$

The role of each of these parameters in the Monte Carlo simulation will be discussed in the next section.

3.1 Monte Carlo Simulation for Narrow Beam Transmission

The Monte Carlo simulation technique is based on the use of a random number generator to determine when each photon undergoes a scattering event and into which set of angles (θ, ϕ) . For this study the photons are assumed to strike the water surface at normal incidence in a narrow beam. In addition it is assumed that each photon is linearly polarized in the same sense and of the same wavelength ($\lambda = 500$ nm). Thus the simulation is that of a polarized laser beam.

The photons that are incident on the water surface are refracted at the air-water interface in accordance with Snell's law

(see Figure 3-1). To decide how far the photon travels before a scattering event occurs, a random number r_1 is chosen in the uniform interval (0,1) and the distance AB is set according to the formula

$$AB = - \ln(r_1) \quad (3-4)$$

AB is in units of scattering length, s^{-1} .

At point B two new random numbers, r_2 , r_3 , are chosen and used to determine the scattering angles θ_2 , and ϕ_2 (θ , ϕ are measured in a spherical coordinate system). The ϕ -angle is chosen to be uniformly distributed, i.e., $\phi_2 = 2\pi r_3$. The selection of θ_2 is accomplished from the relation $r_2 = F(\theta)$, where $F(\theta)$ is the scattering distribution function for polar angle. This is equivalent to choosing θ with a probability distribution identical to that given by the volume scattering phase function, $\sigma(\theta)$. After the selection of ϕ_2 and θ_2 a random number is chosen for computing the distance traveled, and the process will continue until the photon emerges from the water. Internal reflection from the water-air interface is also treated in the model.

At each step in the Monte Carlo process, the angles of scattering are chosen with respect to the previous incident photon direction, which is in general different from the direction of the original z-axis. In order to keep track of the photons with respect to the original coordinate system, (and be able to specify its coordinates as it leaves the water) coordinate transformations are applied after each scattering event. These transformation are: (1) a

12

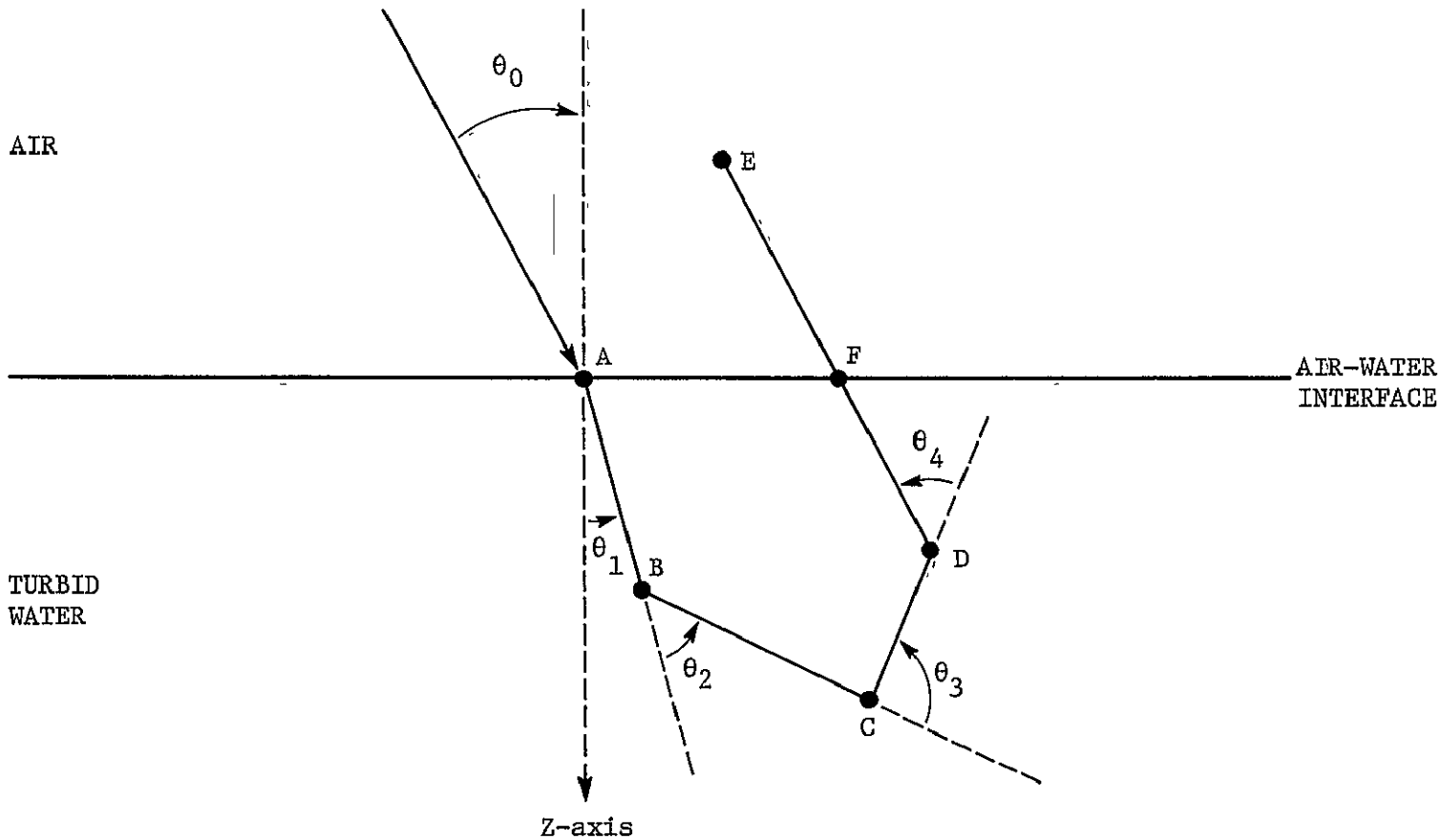


FIGURE 3-1
MONTE CARLO SIMULATION OF NARROW BEAM TRANSMISSION
IN TURBID WATER

rotational transformation to set the instantaneous system of the photon parallel to the original system, and (2) a translational transformation that takes into account the displacement of the instantaneous system with respect to the original system.

The procedure described so far takes into account only the scattering processes. In order to take absorption into account the probability weight associated with each photon emerging from the air-water interface is reduced by a factor of e^{-ay} , where y is the total path length traveled in the water by the photon, and a is the absorption coefficient.

For each photon that emerges from the water surface at an angle from the normal of less than 10° a record is kept of the θ and ϕ angles for each of the scattering events. Thus the statistics generated are applicable to the case of having a near nadir looking detector. In addition, the point of exit from the water is measured from the entry point in units of s^{-1} , the inverse scattering coefficient. Thus any detector spot size can be accommodated using the same set of statistics - all photons whose exit point is less than ($s \times$ detector's spot size) can be considered to have reached the detector. Clearly this allows the statistics generated from any simulation run to be used to analyze any combination of spot size and s values. The only parameter which is fixed in the Monte Carlo run is the scattering distribution function $F(\theta)$. The values for spot size, scattering coefficient and absorption coefficient, and

extinction coefficient, can all be varied after the initial simulation. For this reason, values for s , a , and α are chosen as adjustable parameters rather than being actually calculated from the Mie scattering formalism. By allowing s (or α) to vary while keeping the ratio a/s constant we can examine the effect of varying the concentration of a particular sediment. By the same token, holding s constant and varying the a/s ratio allows the investigation of the effect of changing the optical characteristics of the sediments. For each set of spot size, s value, and a/s value the photons which reach the detector are selected from the statistics of the Monte Carlo run and their Stokes vectors are computed using the set of angles (θ 's and ϕ 's) that each photon has been scattered. (For details see section 5.0). The resulting set of individual photon Stokes vectors are then averaged to yield a total Stokes vector for the backscattered beam which is received by the detector. Given this Stokes vector the total polarization and the degree of linear polarization can be calculated.

4.0 CALCULATION OF SCATTERING FUNCTIONS

This section is devoted to the theoretical treatment of scattering and absorption from suspended particulates. The Mie theory of light scattering from a single particle is treated in Sub-section 4.1. The extension of Mie theory to the case of polydisperse suspensions is then discussed along with the computational methods used to calculate the scattering function, in Sub-sections 4.2 and 4.3 (Appendix A discusses the relationships between the Mie parameters and the extinction, scattering and absorption coefficients). Sub-section 4.4 includes a discussion of the size distributions and optical properties of the clay sediments considered in the calculations. Finally, in Section 4.5 the results of the calculation of the scattering functions are presented.

The following discussion of the Mie theory of scattering and the computational methods is a brief summary. For more detailed discussions of Mie theory for single scattering, the reader is referred to References 2, 3, and 4. Reference 5 contains a discussion of Mie scattering from polydispersions and Reference 6 contains the details of the computational procedures and requirements.

4.1 Mie Theory for Single Particle Scattering

When light is incident on a particle, it undergoes both scattering and absorption (the inelastic scattering processes which result in a change in frequency are ignored in this study). The characteristics of the

scattered radiation depend on the wavelength, λ , of the incident light, the generally complex index of refraction, m , of the particle, and the size, r , and shape of the particle. In this report we will restrict the discussion to spherical particles; for the treatment of inorganic sediments in water this is probably not a serious restriction.

If a monochromatic beam of light, represented by the Stokes vector \vec{I}_o , is incident on a spherical particle at an angle $\theta = 0$, then the Stokes vector of the light scattered is given by

$$\vec{I}(x, m, \theta) = \frac{\lambda^2}{4\pi^2} S(x, m, \theta) \vec{I}_o , \quad (4-1)$$

where $S(x, m, \theta)$ is the single particle scattering matrix which depends in general, on the size parameter

$$x = \frac{2\pi r}{\lambda} \quad (4-2)$$

and the complex index of refraction, m . The calculation of $S(x, m, \theta)$ requires the solution of Maxwell's equation in spherical coordinates with a discontinuous change in the index of refraction across the spherical surface. This solution was originally derived by G. Mie⁽⁷⁾ in 1908, and independently by P. Debye⁽⁸⁾ in 1909.

The scattering matrix can be written as:

$$S(x, m, \theta) = \begin{pmatrix} M_1(x, m, \theta) & 0 & 0 & 0 \\ 0 & M_2(x, m, \theta) & 0 & 0 \\ 0 & 0 & S_{21}(x, m, \theta) & -D_{21}(x, m, \theta) \\ 0 & 0 & D_{21}(x, m, \theta) & S_{21}(x, m, \theta) \end{pmatrix} \quad (4-3)$$

and the Mie solution is

$$\begin{aligned} M_1(x, m, \theta) &= S_1(x, m, \theta) S_1^*(x, m, \theta) \\ M_2(x, m, \theta) &= S_2(x, m, \theta) S_2^*(x, m, \theta) \\ S_{21}(x, m, \theta) &= \frac{1}{2}(S_2(x, m, \theta) S_1^*(x, m, \theta) + S_1(x, m, \theta) S_2^*(x, m, \theta)) \\ D_{21}(x, m, \theta) &= \frac{1}{2}(S_2(x, m, \theta) S_1^*(x, m, \theta) - S_1(x, m, \theta) S_2^*(x, m, \theta)) \end{aligned} \quad (4-4)$$

Where $S_1(x, m, \theta)$ and $S_2(x, m, \theta)$ are the complex amplitudes for the scattered radiation (and * designates the complex conjugate),

$$\begin{aligned} S_1(x, m, \theta) &= \sum_{n=1}^{\infty} \frac{(2n+1)}{n(n+1)} \left\{ a_n(x, m) \pi_n(\mu) + b_n(x, m) \tau_n(\mu) \right\} \\ S_2(x, m, \theta) &= \sum_{n=1}^{\infty} \frac{(2n+1)}{n(n+1)} \left\{ b_n(x, m) \pi_n(\mu) + a_n(x, m) \tau_n(\mu) \right\}. \end{aligned} \quad (4-5)$$

In these expressions $\pi_n(\mu)$ and $\tau_n(\mu)$ are derivatives of the Legendre Polynomials:

$$\begin{aligned} \pi_n(\mu) &= \frac{dP_n(\mu)}{d\mu}, \\ \tau_n(\mu) &= \mu\pi_n(\mu) - (1-\mu^2) \frac{d\pi_n(\mu)}{d\mu} \end{aligned} \quad (4-6)$$

(where $\mu = \cos \theta$). Also

$$a_n(x, m) = \frac{\psi'_n(mx)\psi_n(x) - m\psi_n(mx)\psi'_n(x)}{\psi'_n(mx)\xi'_n(x) - m\psi_n(mx)\xi'_n(x)} \quad (4-7)$$

$$b_n(x, m) = \frac{m\psi'_n(mx)\psi_n(x) - \psi_n(mx)\psi'_n(x)}{m\psi'_n(mx)\xi'_n(x) - \psi_n(mx)\xi'_n(x)}$$

and the ψ 's and ξ 's are related to the spherical Bessel functions of the first and second kinds (j_n and y_n respectively):

$$\begin{aligned} \psi_n(z) &= zj_n(z) \\ \xi'_n(x) &= xj'_n(x) - iy_n(x) \\ \psi'_n(z) &= zj'_{n-1}(z) - nj_n(z) \\ \xi'_n(x) &= xj'_{n-1}(x) - iy_{n-1}(x) - nj_n(x) - iy_n(x) \end{aligned} \quad (4-8)$$

4.2 Mie Theory for Scattering from Polydispersions

A polydispersion is a suspension of scattering particles of uniform physical characteristics but of varying number concentration depending on particle size. Because of the existence of different particle sizes it makes little sense to talk of scattering from a single particle. Instead, it is useful to consider the scattering properties of a small volume element containing a number of particles. The size of this volume element is of some, at least theoretical, importance. Clearly, if it is to be used to represent the scattering properties of all similar volume elements then it must contain a representative set of particle sizes - this requires that the volume

element not be too small. On the other hand, since we are considering only single scattering from the volume element, it must not be too large. An additional condition that must be imposed is that the interparticle separation be large compared to the wavelength. The reason for this is that the interaction of light with a particle will be assumed independent of the interactions with all other particles. This condition requires that the particle density in the volume element not be too large. For our purposes, it will be assumed that all of the above conditions are satisfied.

The polydispersion can be completely specified, for our purposes, by an index of refraction m and a probability density function $n(r)$. The density function gives the relative concentration of each size contained in a volume element.

The characteristics of the scattered radiation due to the volume element can then be represented by a volume scattering matrix $\hat{S}(m, \theta)$ in a manner analogous to Equation (2-1):

$$\hat{I}(m, \theta) = \frac{\lambda^2}{4\pi^2} \hat{S}(m, \theta) \hat{I}_0 \quad (4-9)$$

This volume scattering matrix can be calculated from the set of particle scattering matrices:

$$\hat{S}(m, \theta) = \int_0^\infty \hat{S}(x, m, \theta) n(r) dr \quad (4-10)$$

where

$$\int_0^\infty n(r)dr = N \quad (4-11)$$

and N is the total number of particles per unit volume. In what follows, N will be assumed to be unity since $\tilde{S}(m, \theta)$ scales with N . The ability to represent $\tilde{S}(m, \theta)$ as a linear superposition of the individual scattering matrices is a direct consequence of our assumption that the interparticle separation is much greater than λ .

The calculation of $\tilde{S}(m, \theta)$ thus reduces to calculation of the individual $S(x, m, \theta)$ and then integration over all sizes with the proper weighting given by $n(r)$.

4.3 Computational Methods

The calculation of the scattering phase functions and the averaging over size distributions was carried out on an IBM 370/148. The program listings are reproduced in Appendix D.

In computing the sums in Equation (4-5), the major difficulty arises in the evaluation of the $a_n(x, m)$ and $b_n(x, m)$. Using the definitions of ψ_n , ψ'_n , ξ_n , and ξ'_n , and the standard recurrence relations for the Bessel functions, Equation (4-7) can be rewritten:

$$a_n(x, m) = \frac{\left\{ \frac{A_n(mx)}{m} + n/x \right\} \operatorname{Re} [\xi_n(x)] - \operatorname{Re} [\xi_{n-1}(x)]}{\left\{ \frac{A_n(mx)}{m} + n/x \right\} \xi_n(x) - \xi_{n-1}(x)} \quad (4-12)$$

$$b_n(x, m) = \frac{\left\{ mA_n(mx) + n/x \right\} \operatorname{Re} [\xi_n(x)] - \operatorname{Re} [\xi_{n-1}(x)]}{\left\{ mA_n(mx) + n/x \right\} \xi_n(x) - \xi_{n-1}(x)}$$

where

$$A_n(mx) = \frac{\psi'_n(mx)}{\psi_n(mx)} \quad (4-13)$$

the logarithmic derivative of $\psi_n(mx)$, and Re denotes the real part.

The natural approach to the evaluation of Equation (4-12) is to employ a standard (upward) recurrence procedure. Unfortunately, if the imaginary part of the index of refraction is not zero and n is large then the upward recurrence procedure results in large instabilities in the calculation of $A_n(mx)$. For this reason, the DBMIE subroutine employs a downward recurrence procedure to calculate the $A_n(mx)$ s. These values are then stored for use in the evaluation of Equation (4-12). Because of the large storage requirements resulting from this procedure ($n \sim 7000$), and the fact that double precision is employed in all of the calculations, a virtual machine with 512 K bytes of storage is required for the implementation of the DBMIE and POLYMIE routines.

The scattering phase functions are computed in the DBMIE subroutine, and the average, Equation (4-10), is computed in the calling routine POLYMIE. While analytic functions have been used for the size distributions, $n(r)$, the integral has been approximated by a summation over a discrete set of radii. Tests to determine the effect of using a summing procedure have shown that this results in no loss of accuracy. In addition, test runs were made to compare the results when $\Delta r = 0.1\mu$ and $\Delta r = 1\mu$ were used in the summing procedure. The use of $\Delta r = 1\mu$ resulted in no significant change in the

results from those obtained using $\Delta r = .1\mu$ over the range $0 < r < 100\mu$. Calculations were made using $r_{max} = 100\mu$ and $r_{min} = 10\mu$ ($\Delta r = 0.1\mu$). A discussion of the proper upper limit for r is given in Section 4.4.2.

The amount of virtual CPU time required for these calculations is significant and has been a major factor in determining r_{max} and Δr . As an example, the calculation of the volume scattering phase function for a polydispersion with $m = 1.144 - 0.0i$, $\lambda = 0.5\mu$, $r_{max} = 100\mu$ and $\Delta r = 1\mu$ requires approximately 26 minutes of virtual CPU time.

4.4 Properties of Clay Samples

Data on four different clay samples were provided by NASA/LaRC. This data consisted of empirical size distribution curves as well as brief descriptions of chemical composition. The physical characteristics of the clay are discussed in Section 4.4.1 while the size distributions are presented in Section 4.4.2.

4.4.1 Physical Characteristics of Clay Samples

Four types of clay were selected by NASA/LaRC. These were: Feldspar, Calvert, Ball and Jordan. According to the analysis of these clays performed by NASA/LaRC⁽¹⁾ the compositions are:

- Feldspar - Feldspar and Quartz Minerals
- Calvert and Jordan - Kaolinite and Illite
- Ball - Montmorilloite, Kaolinite and Illite

The real refractive index and chemical components of these minerals is shown in Table 4.1.⁽⁹⁾ For reasons which will be discussed in Section 4.4.2, Feldspar and Ball Clay were chosen to be included in this study.

To estimate the index of refraction of the clay samples, we take a simple average of the indices of refraction of the components. Thus, for both Feldspar and Ball Clay, the real part of the index of refraction is estimated as

$$\text{Re}(m_{\text{Air}}) = 1.53 .$$

This, of course, is the index of refraction with respect to air and we require the index of refraction with respect to water which can be obtained by dividing $\text{Re}(m_{\text{Air}})$ by the index of refraction of water 1.337 (for wavelengths of approximately 500 nm).

Thus

$$\text{Re}(m_{\text{water}}) = 1.144 .$$

Estimating the imaginary part of the index of refraction is not so straightforward, since direct measurements of $\text{Im}(m)$ have not been made. Since these minerals have very low conductivity, it is expected that the imaginary part of m will be quite small. The imaginary part of m has been measured for soil aerosols and has been found to be about .005 (with respect to air).⁽¹⁰⁾ For this study two values for

$\text{Im}(m)$ will be used:

$$\text{Im}(m_{\text{water}}) = \begin{cases} 0 & , \text{ Non-absorbing} \\ \frac{0.005}{1.337} = 0.004, & \text{Weakly-absorbing} \end{cases}$$

TABLE 4.1
CHEMICAL COMPOSITION AND INDEX OF REFRACTION
OF CLAY CONSTITUENTS

| <u>NAME</u> | <u>CHEMICAL COMPOSITION</u> | <u>INDEX OF REFRACTION</u> |
|-----------------|--|----------------------------|
| Kaolinite | $\text{Al}_2\text{O}_3 \cdot 2\text{SiO}_2 \cdot 2\text{H}_2\text{O}$ | 1.56 |
| Illite | $\text{K}_{1-1.5}\text{Al}_4\text{Si}_{7-6.5}\text{Al}_{1-1.5}\text{O}_2(\text{OH})_4$ | 1.54 |
| Montmorillonite | $(.5\text{Ca}, \text{Na})_{.7}(\text{Al, Mn, Fe})_4(\text{Si, Al})_8\text{O}_{20}(\text{HO})_4\text{nH}_2\text{O}$ | 1.48 |

Feldspars:

| | | |
|------------|---|------|
| Microcline | $\text{K}_2\text{O} \cdot \text{Al}_2\text{O}_3 \cdot 6\text{SiO}_2$ | 1.52 |
| Andesine | $(\text{CaO}_{.1}\text{Na}_2\text{O})\text{Al}_2\text{O}_3 \cdot 4\text{SiO}_2$ | 1.55 |
| Anthoclase | $(\text{Na, K})_2\text{O} \cdot \text{Al}_2\text{O}_3 \cdot 6\text{SiO}_2$ | 1.53 |

4.4.2 Particle Size Distributions

Empirical cumulative size distributions for the four samples were provided by NASA/LaRC and are shown in Figure 4-1, 4-2, 4-3 and 4-4. It is apparent from these figures that the size distributions for Ball, Jordan, and Calvert differ significantly from the size distribution for Feldspar. Since it was planned that two distributions would be employed, Feldspar and Ball Clay were chosen. This choice allows the investigation of the effect of radically different size distributions.

To utilize the size distribution information, it is necessary to determine the size distribution density function, $n(r)$, which specifies the relative number of particles with radius r per unit volume. If we denote the cumulative size distribution as provided by NASA/LaRC as $N(r_o)$ then the relationship between $N(r_o)$ and $n(r)$ is given by:

$$N(r_o) = 1 - \int_0^{r_o} n(r) dr, \quad (4-14)$$

or

$$n(r) = \frac{dN(r_o)}{dr_o} \quad | \quad r_o = r \quad (4-15)$$

A general curve fitting routine (See Appendix E) was used to determine the best distribution for both the Ball Clay and Feldspar.

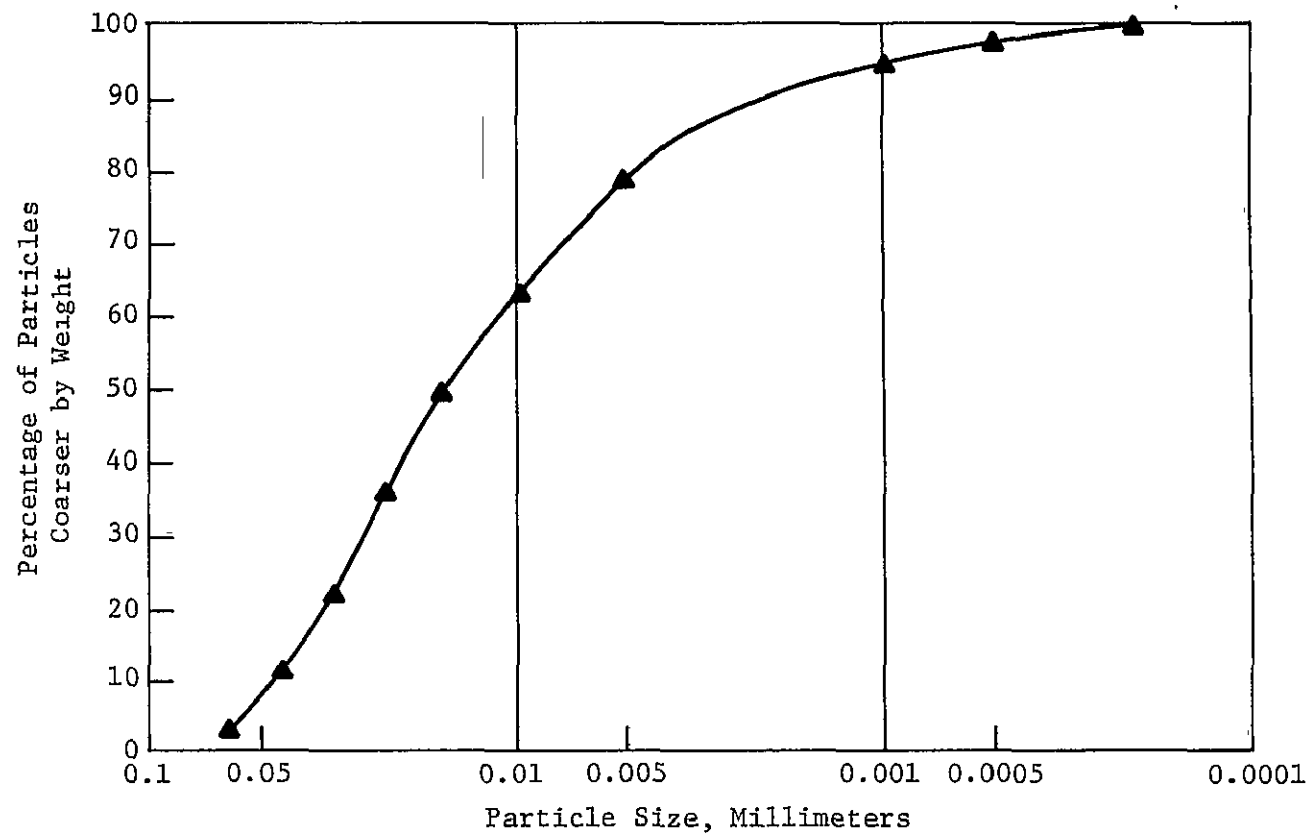


FIGURE 4-1
CUMULATIVE SIZE DISTRIBUTION OF FELDSPAR SAMPLE

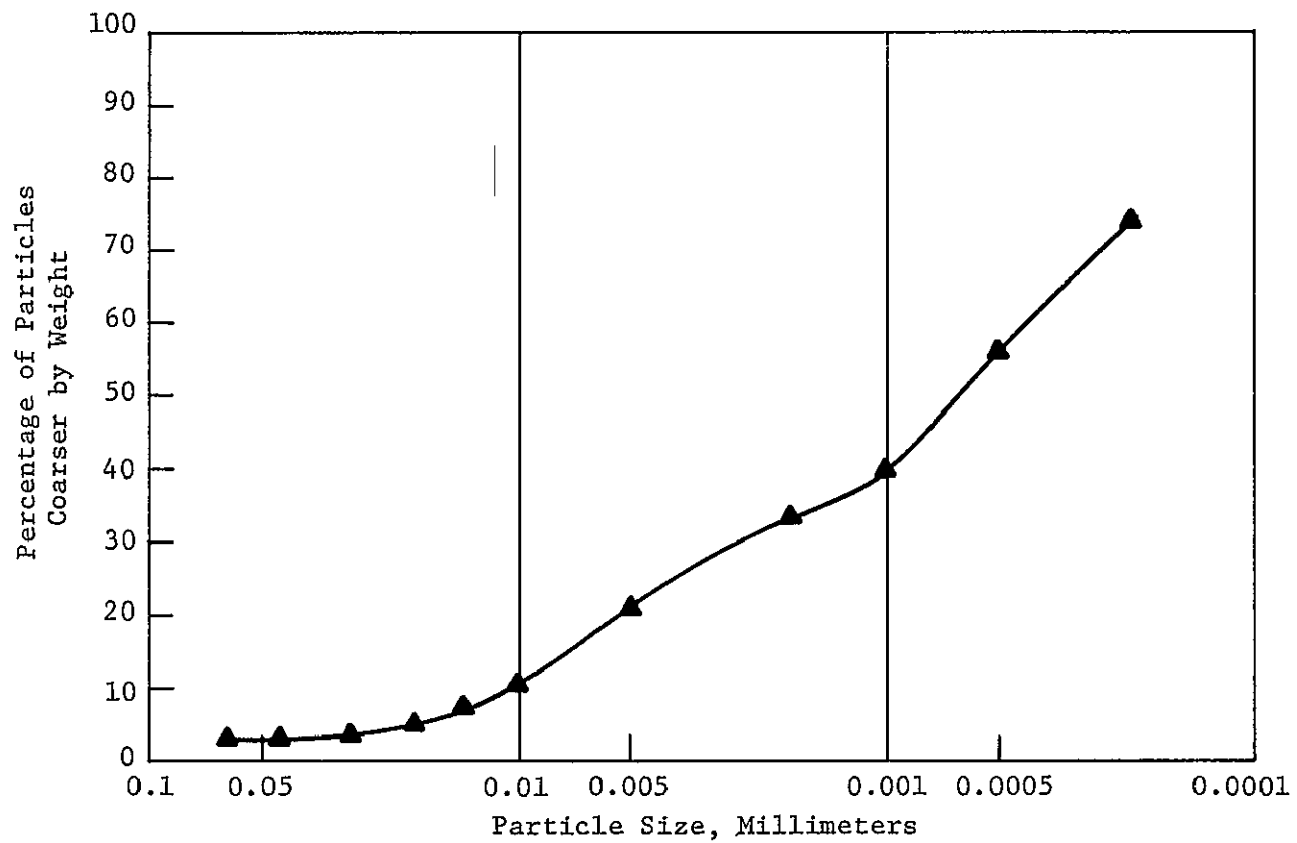


FIGURE 4-2
CUMULATIVE SIZE DISTRIBUTION OF CALVERT SAMPLE

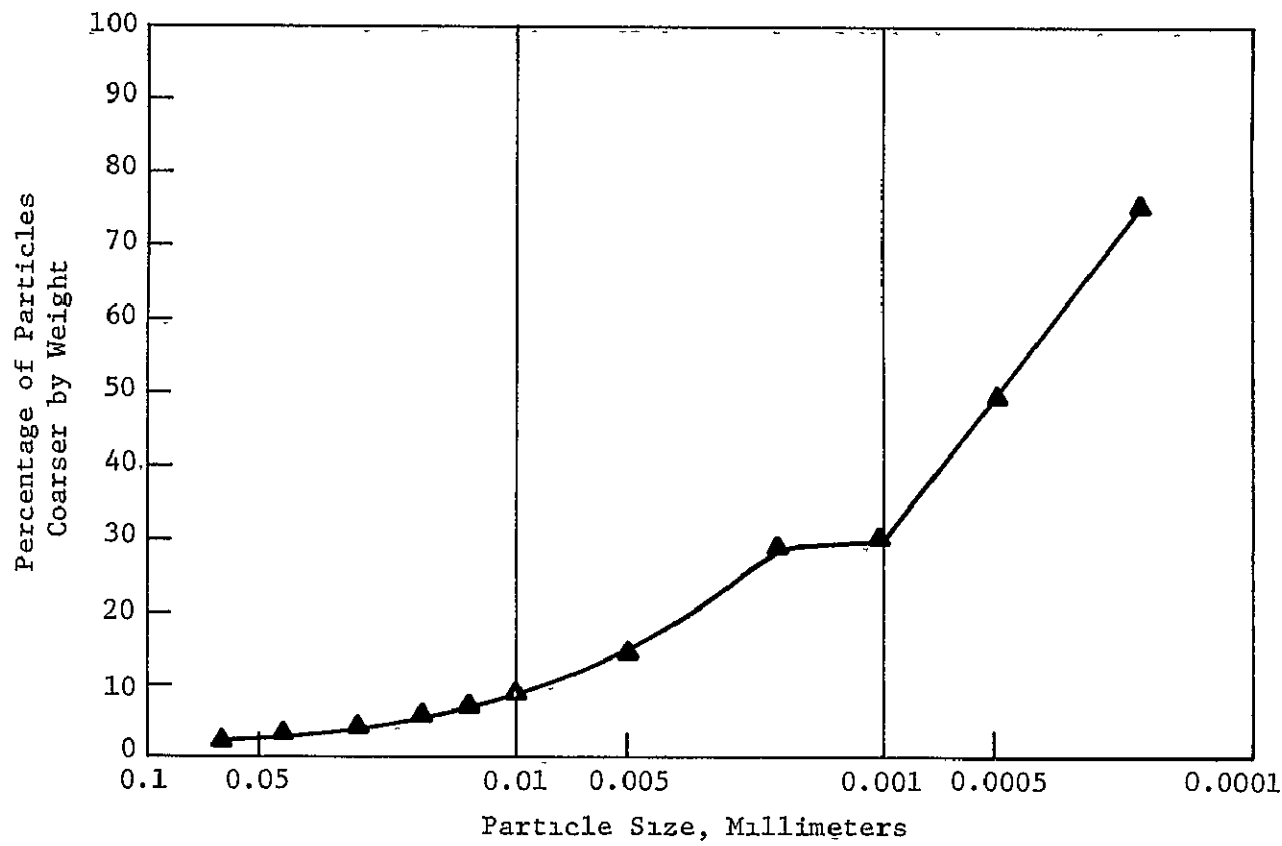


FIGURE 4-3
CUMULATIVE SIZE DISTRIBUTION OF BALL SAMPLE

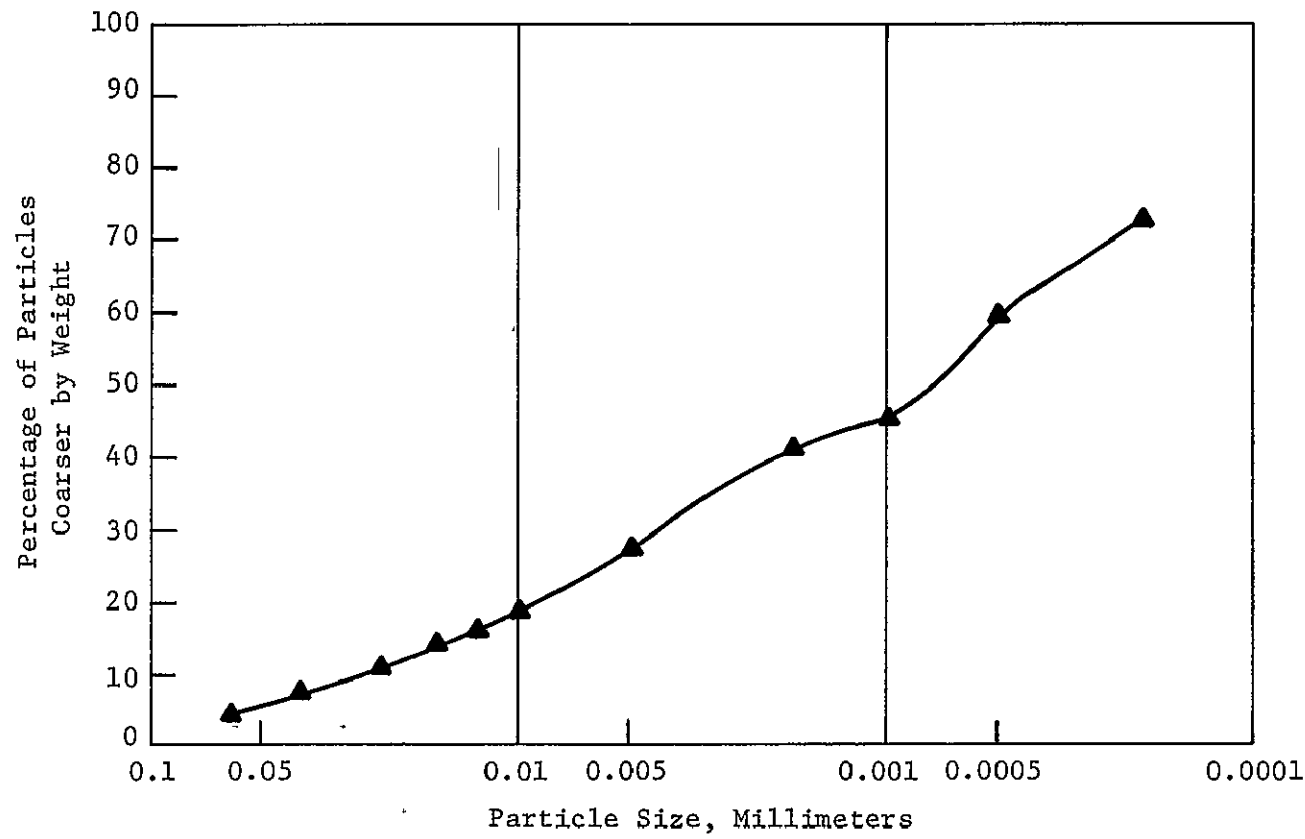


FIGURE 4-4
CUMULATIVE SIZE DISTRIBUTION OF JORDAN SAMPLE

For the Feldspar sample it was found that the data was well represented by a modified Gamma distribution:

$$n(r) = a_1 r^{a_2} \exp\left(-a_3 r^{a_4}\right) \quad (4-16)$$

The parameters were determined, using a minimum mean square error criterion, to be

$$a_1 = 2.05089$$

$$a_2 = 0.671066$$

$$a_3 = 3.58393$$

$$a_4 = 0.218499$$

A plot of this size distribution density function is shown in Figure 4-5, while a plot of the corresponding cumulative size distribution function (as obtained from Equation 4-16) is shown in Figure 4-6.

As can be seen in Figure 4-6, the modified Gamma distribution gives a good fit to the data points obtained in the NASA/LaRC analysis.

To fit the size distribution of the Ball Clay sample, Junge's distribution model was chosen:

$$n(r) = a_1 r^{-a_2} \quad (4-17)$$

with the parameters,

$$a_1 = 0.2006$$

$$a_2 = 1.624746$$

determined using the same curve fitting routine employed for Feldspar.

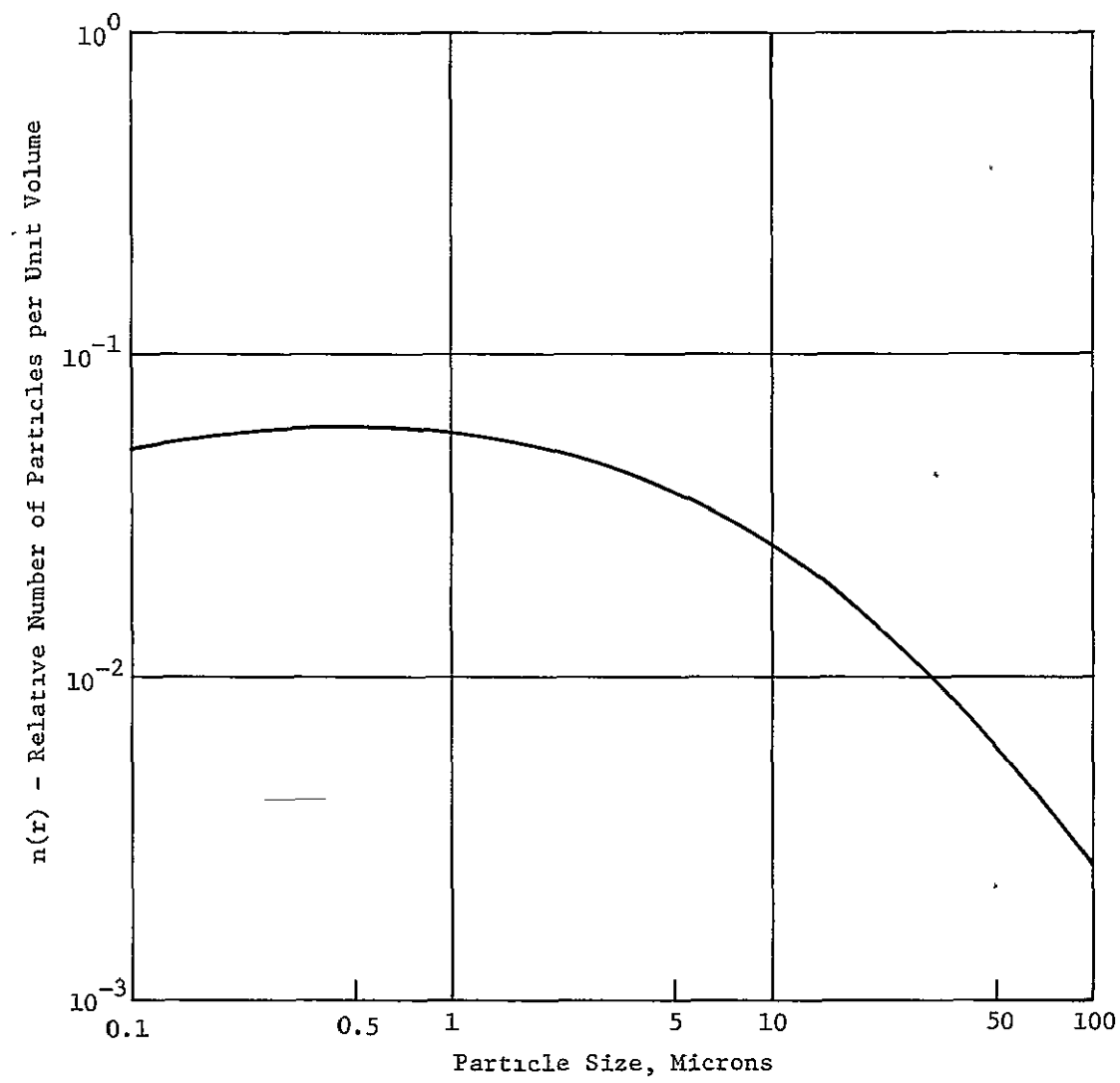


FIGURE 4-5
PARTICLE SIZE DENSITY FUNCTION FOR FELDSPAR (MODIFIED GAMMA DISTRIBUTION)

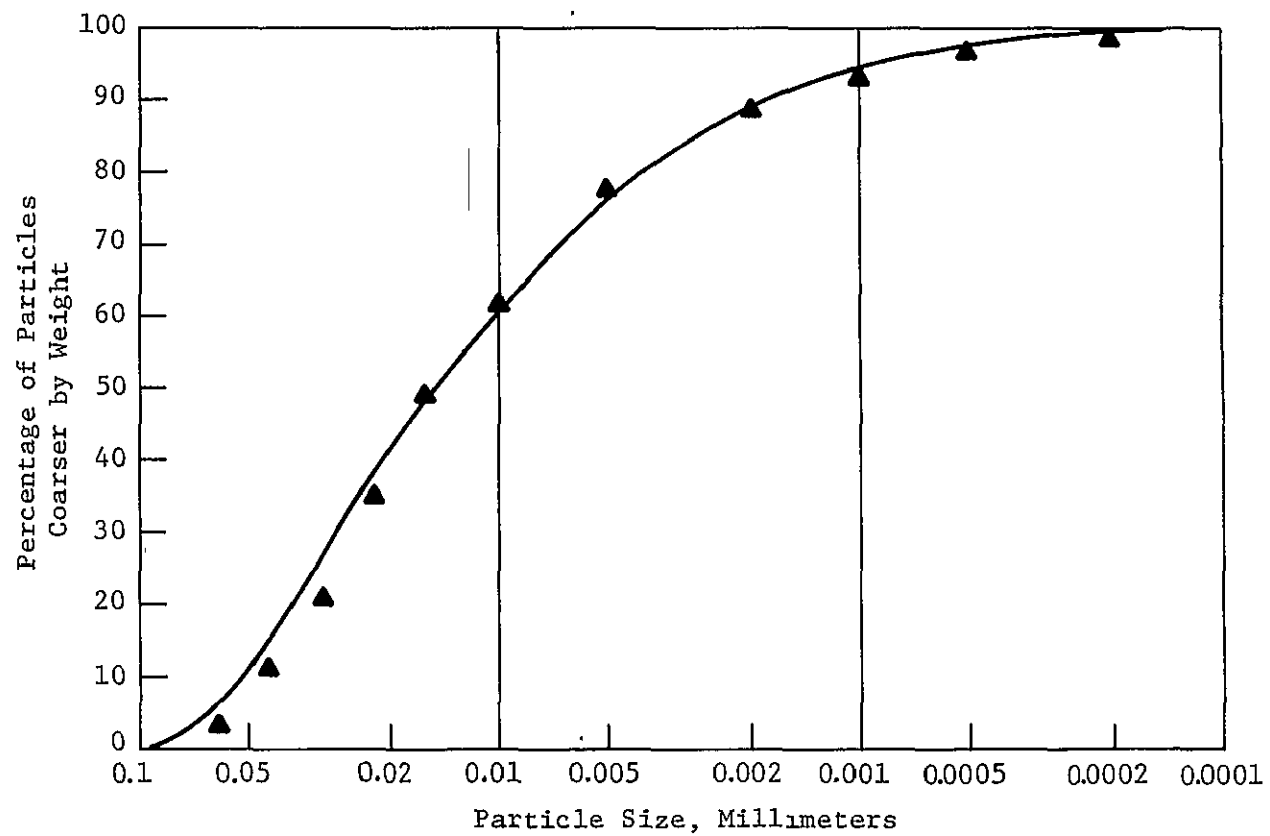


FIGURE 4-6
CUMULATIVE SIZE DISTRIBUTION FIT OF FELDSPAR SAMPLE USING MODIFIED GAMMA DISTRIBUTION

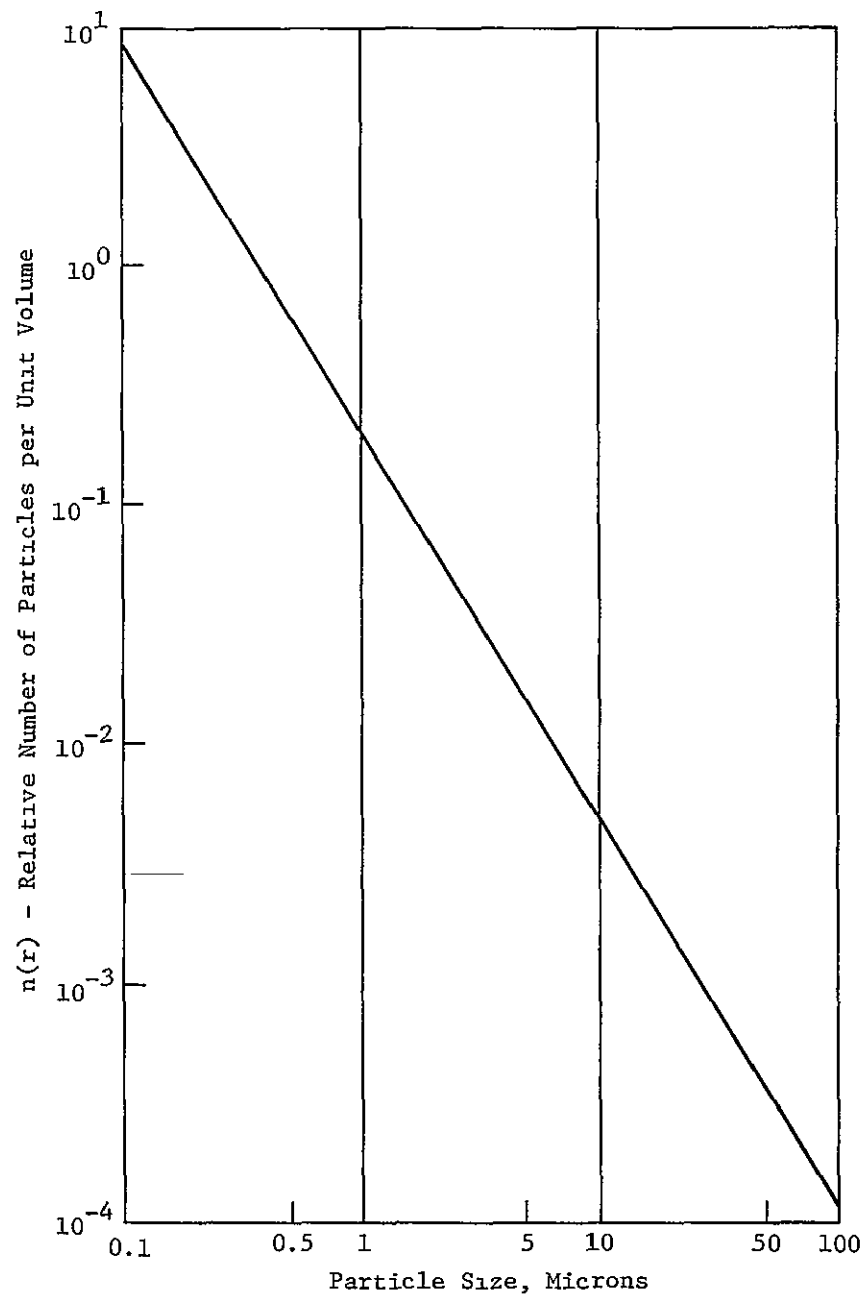


FIGURE 4-7
PARTICLE SIZE DENSITY FUNCTION FOR BALL CLAY (JUNGES DISTRIBUTION)

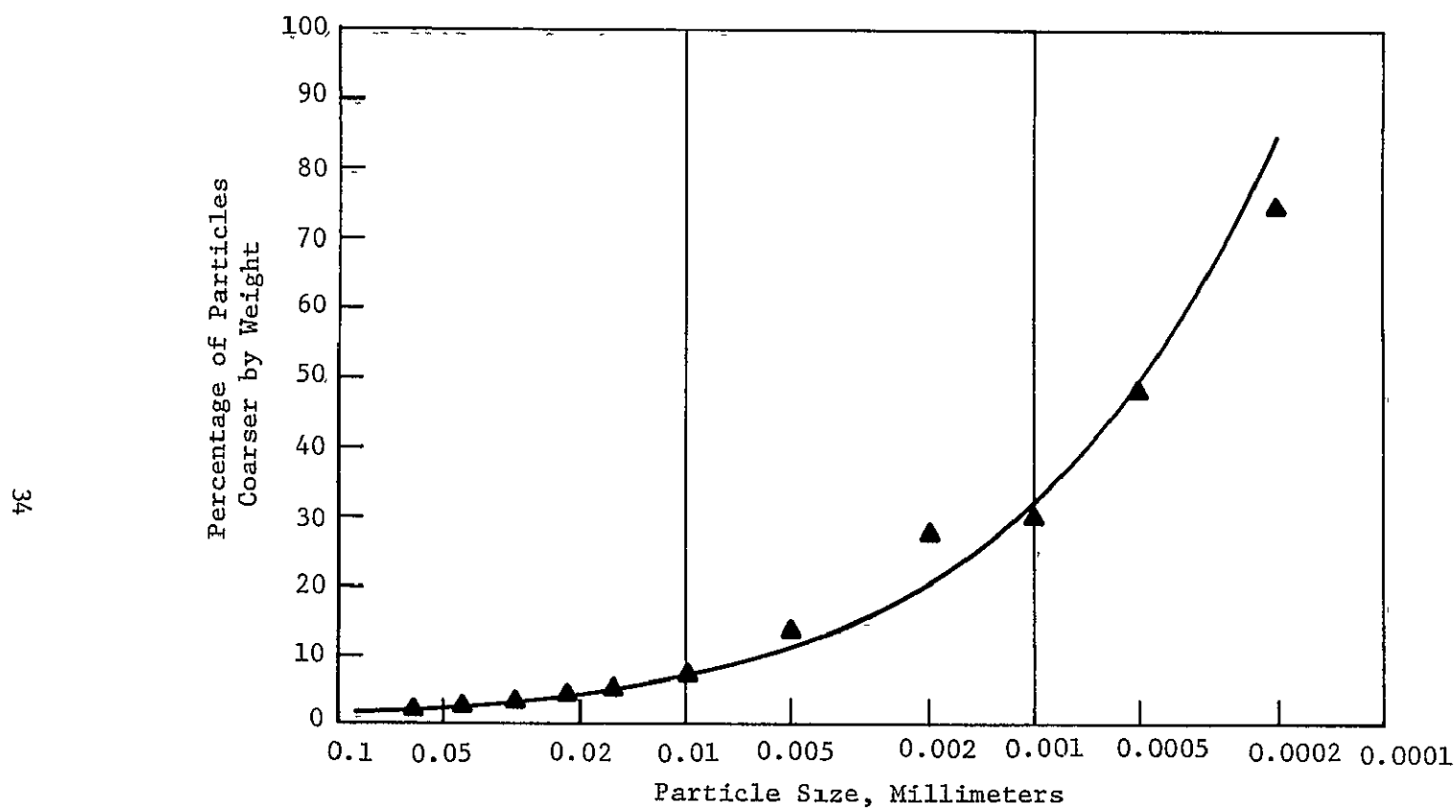


FIGURE 4-8
CUMULATIVE SIZE DISTRIBUTION FIT OF BALL CLAY SAMPLE USING JUNGE DISTRIBUTION

The size distribution density function and the cumulative size distribution function for Ball Clay using Junge's distribution are shown in Figure 4-7 and 4-8. It is apparent from Figure 4-7 that Junge's distribution function is not, strictly speaking, a probability distribution since the integral (Equation 4-11),

$$\int_0^{\infty} n(r) dr = N$$

can not be normalized, i.e., N is infinite. However, Junge's distribution has been found to accurately represent particle sizes of ocean sediments.⁽¹¹⁾ In addition, the lower and upper limits of integration in Equations (4-11) and (4-10) are not set equal to zero and infinity, in practice, allowing Equation (4-11) to be normalized.

The question of the proper upper limit for Equation (4-10) and Equation (4-11) is of more than theoretical interest. From the empirical size distributions provided by NASA/LaRC, it appears that an upper limit in Equation (4-10) should be chosen as 100 microns (μm). However, as can be seen in Table 4.2⁽¹²⁾ the settling rate for 100 μm particles is on the order of thirty seconds. Thus, the history of the particulates in the body of water is important. If the particulates have been allowed to settle, then the size distributions determined before the particles are introduced into the water are inappropriate. In order to investigate the effect of settling, two upper limits, 100 μm and 10 μm , were chosen for the integrals of

TABLE 4-II
SETTLING VELOCITIES OF SAND AND SILT IN STILL WATER

(Source: Amer. Water Works Assoc.)

[Temperature 50°F, all particles assumed to have a specific gravity of 2.65]

| Diameter of particle mm. | Order of Size | Settling Velocity mm./sec. | Time Required to Settle 1 Foot |
|-----------------------------|---------------------|-------------------------------|--------------------------------|
| 10.0 | Gravel | 1,000 | |
| 1.0 | | 100 | 0.3 seconds |
| 0.8 | | 83 | 3.0 seconds |
| 0.6 | | 63 | |
| 0.5 | | 53 | |
| 0.4 | Coarse Sand | 42 | |
| 0.3 | | 32 | |
| 0.2 | | 21 | |
| 0.15 | | 15 | |
| 0.10 | | 8 | 38.0 seconds |
| 0.08 | | 6 | |
| 0.06 | | 3.8 | |
| 0.05 | Fine Sand | 2.9 | |
| 0.04 | | 2.1 | |
| 0.03 | | 1.3 | |
| 0.02 | | 0.62 | |
| 0.015 | | 0.35 | |
| 0.010 | | 0.154 | 33.0 minutes |
| 0.008 | | 0.098 | |
| 0.006 | | 0.065 | |
| 0.005 | Silt | 0.0385 | |
| 0.004 | | 0.0247 | |
| 0.003 | | 0.0138 | |
| 0.002 | | 0.0062 | |
| 0.0015 | | 0.0035 | |
| 0.001 | Bacteria | 0.00154 | 55.0 hours |
| 0.0001 | Clay Particles | 0.0000154 | 230.0 days |
| 0.00001 | Colloidal Particles | 0.000000154 | 63.0 years |

Equations (4-10) and (4-11). Equation (4-11) was used to properly normalize Equation (4-10) with respect to the choice of upper limit.

4.5 Results of Computations

The results of the computation of the volume scattering phase functions (4.5.1) and the volume scattering distribution functions (4.5.2), using the size distributions of Section 4.4, are presented in this section. In addition to examining the effect of settling on the calculations, the wavelength dependence of the scattering functions are also investigated.

4.5.1 Volume Scattering Phase Functions

The computed volume scattering phase functions are shown in Figures 4.9 through 4.14.

Figures 4.9 and 4.14 display the extremely large forward scattering peak which is primarily the result of including the large ($\sim 100 \mu\text{m}$) particulates in the size distributions. Both the Feldspar and Ball Clay phase functions show considerable difference between the non-absorbing and absorbing cases at large angle. While it is not evident in the figures, the forward scattering peak is larger for the absorbing case at small but non-zero angles ($\theta \sim 0.5^\circ$).

Figures 4-11 and 4-12 demonstrate the effect of cutting the size distributions off at $10 \mu\text{m}$ instead of $100 \mu\text{m}$. The relative size of the forward peak is reduced and the difference between the absorbing and non-absorbing cases at large angles is reduced. It is interesting to note that, although the shape or the Feldspar and Ball

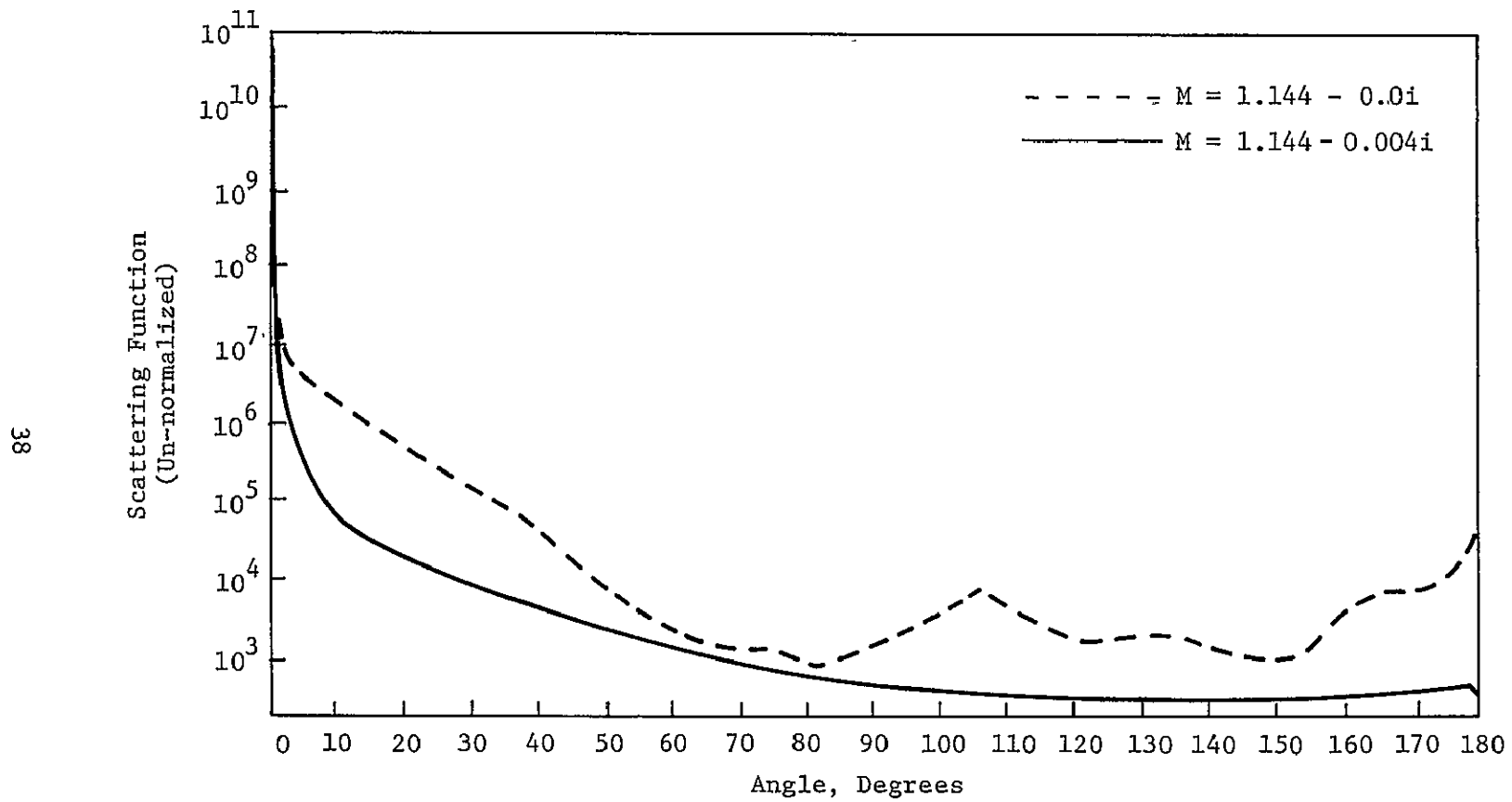


FIGURE 4-9
VOLUME SCATTERING FUNCTIONS FOR FELDSPAR ($\lambda = 500\text{NM}$)

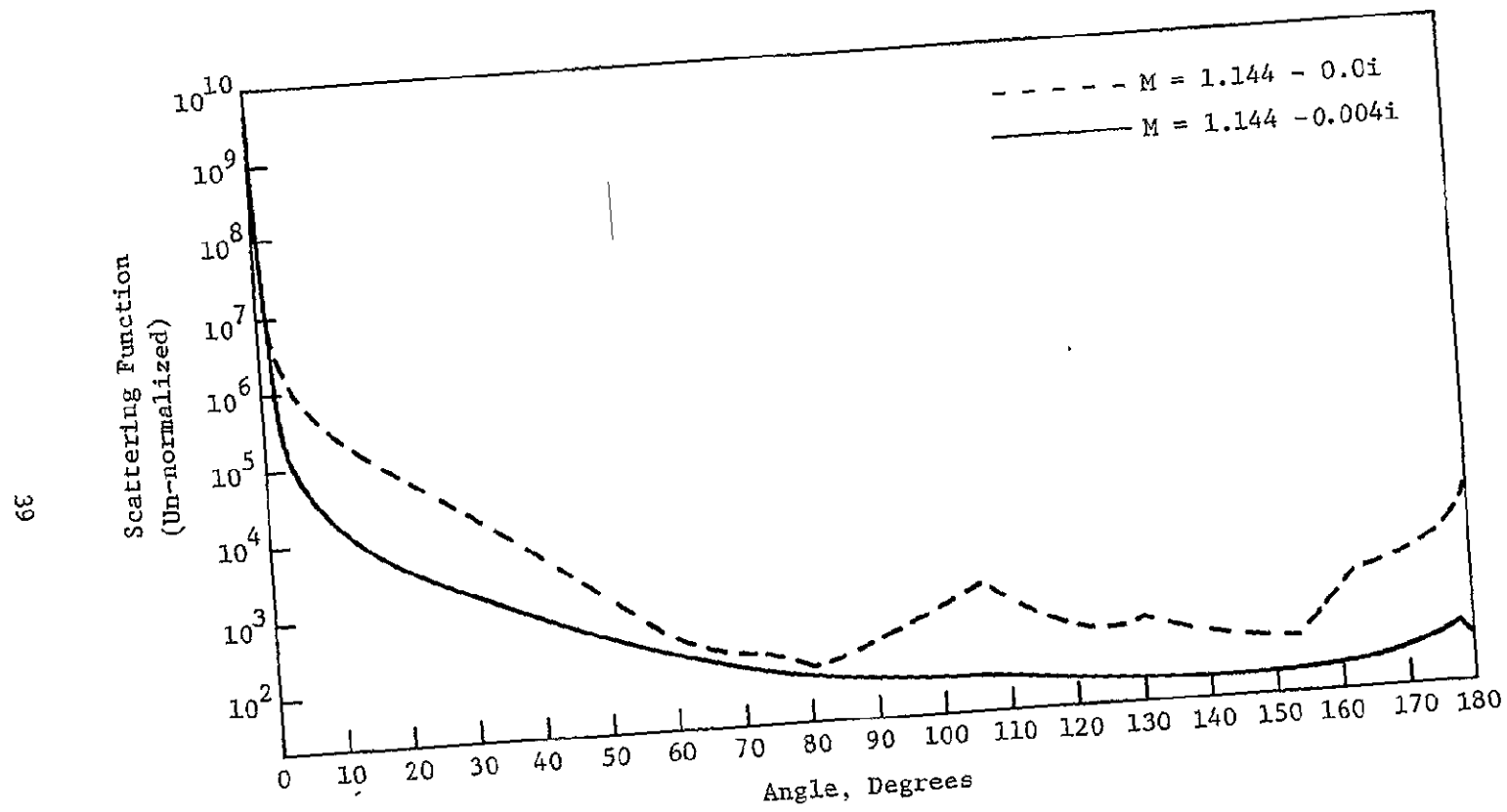


FIGURE 4-10
VOLUME SCATTERING FUNCTIONS FOR BALL CLAY ($\lambda = 500\text{NM}$)

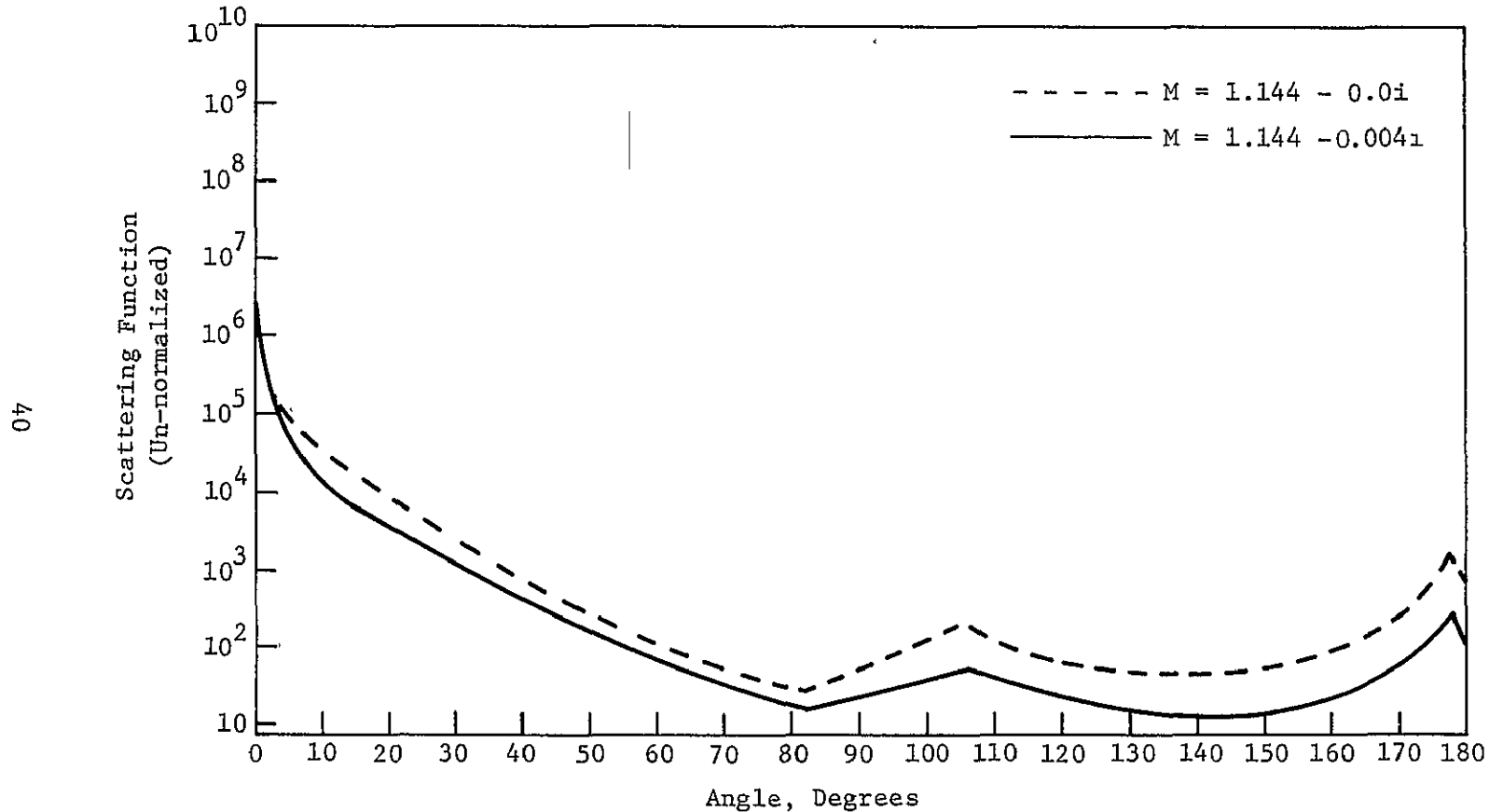


FIGURE 4-11
VOLUME SCATTERING FUNCTIONS FOR FELDSPAR ($10 \mu\text{m}$ CUTOFF $\lambda = 500\text{NM}$)

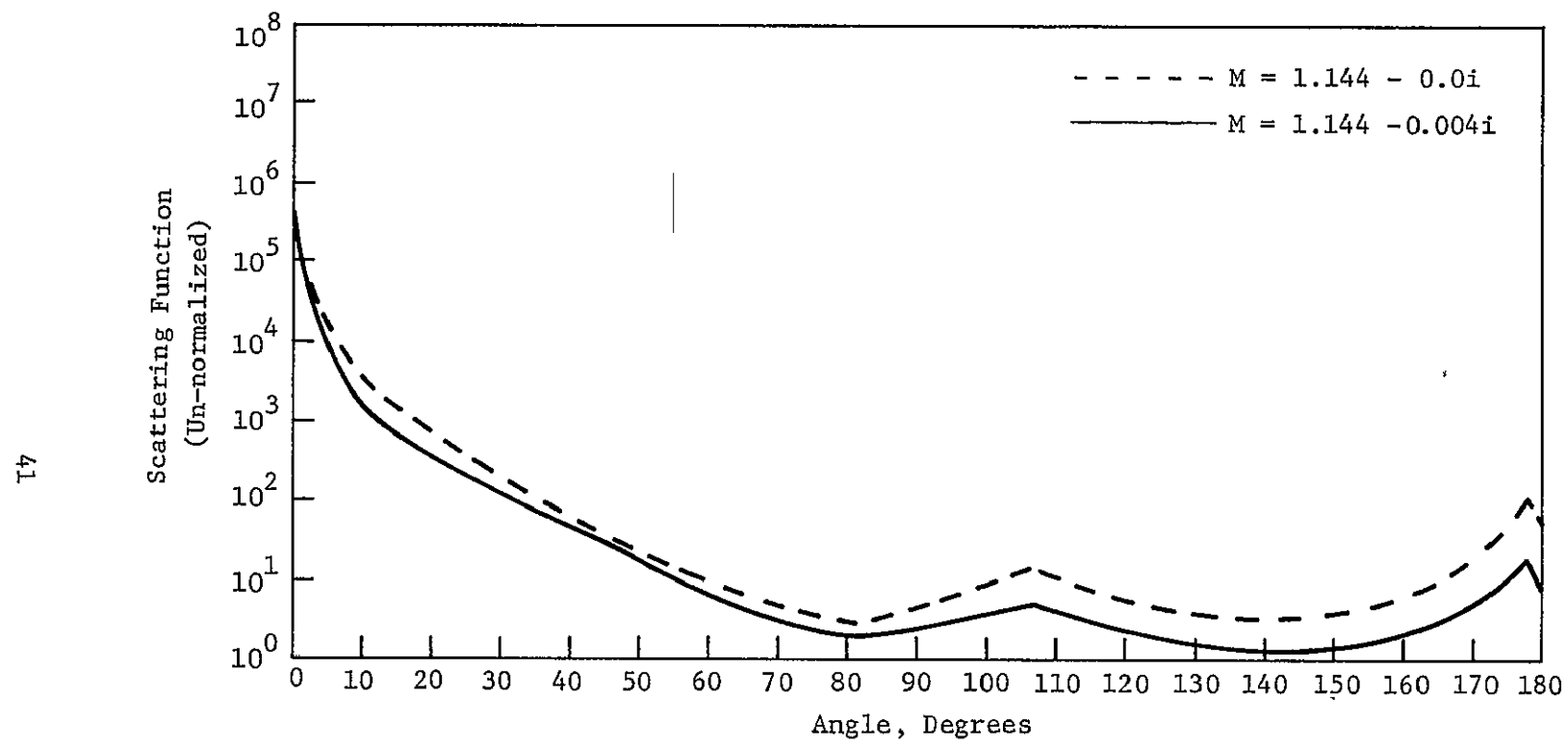


FIGURE 4-12
VOLUME SCATTERING FUNCTIONS FOR BALL CLAY ($10\mu\text{M}$ CUTOFF $\lambda = 500\text{NM}$)

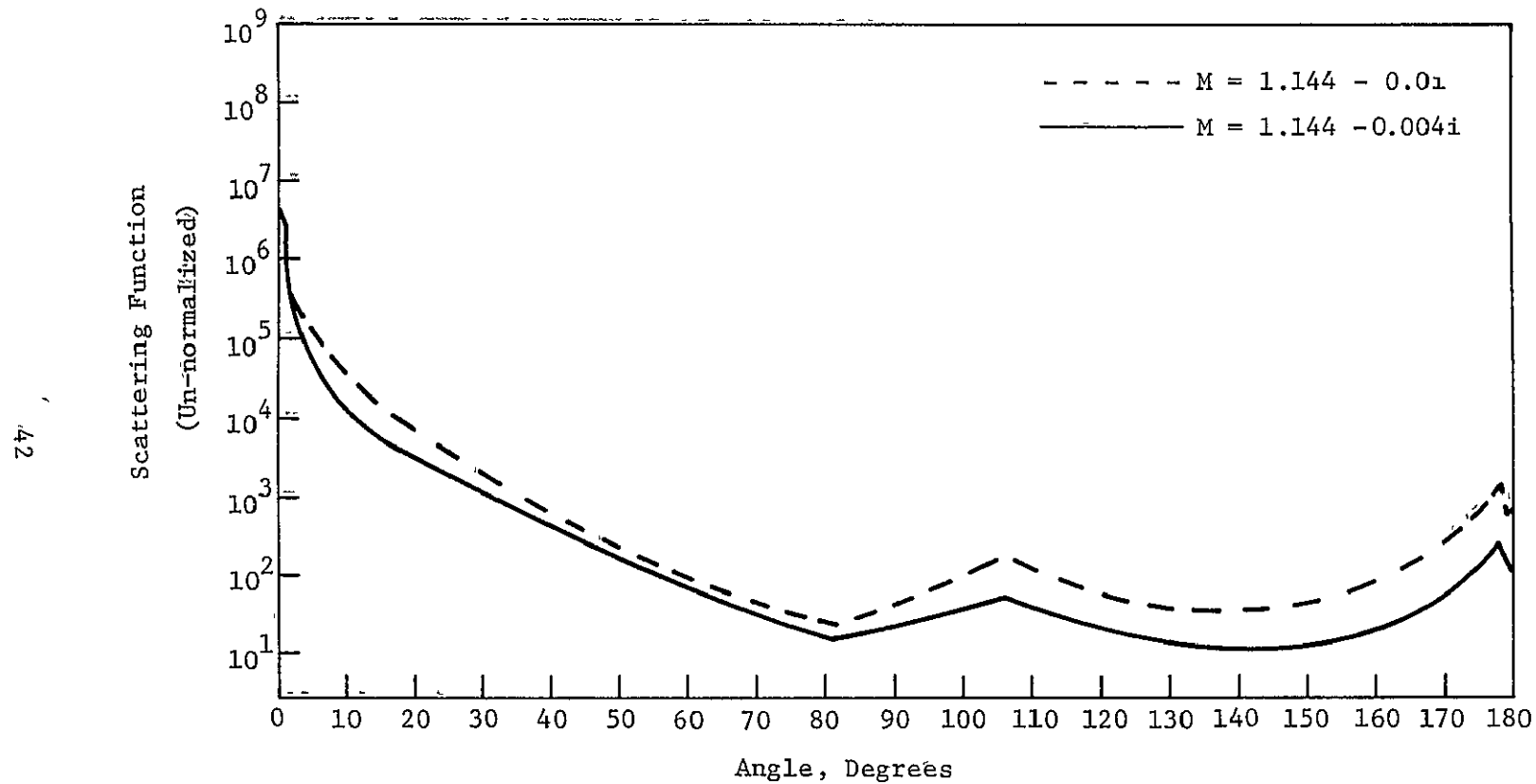


FIGURE 4-13
VOLUME SCATTERING FUNCTIONS FOR FELDSPAR ($10\mu\text{M}$ CUTOFF $\lambda = 600\text{NM}$)

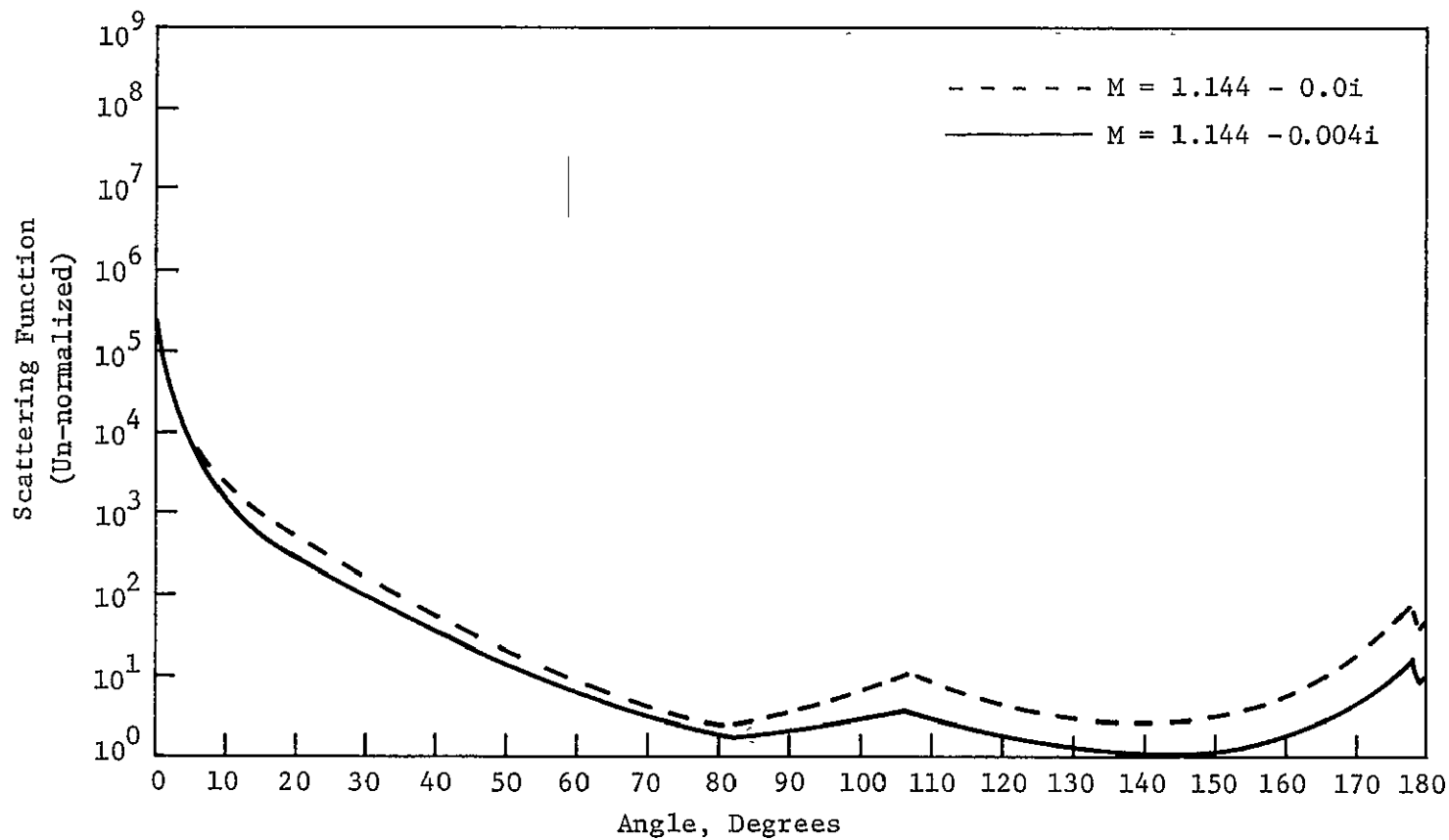


FIGURE 4-14
VOLUME SCATTERING FUNCTIONS FOR BALL CLAY ($10\mu\text{M}$ CUTOFF $\lambda = 600\text{NM}$)

Clay size distributions are very different, the upper limit on the size appears to be much more important in terms of the difference in phase functions.

Figure 4-13 and 4-14 show the scattering phase functions computed for $\lambda = 600$ nm (with a 10 μm cutoff) instead of $\lambda = 500$ nm as in Figures 4-11 and 4-12. It can be seen that the phase functions are not heavily wavelength dependent. In fact, it can be shown that for a uniform size distribution and upper and lower limits of zero and infinity in Equation (4-10), the volume scattering phase function will be strictly independent of wavelength.

4.5.2. Volume Scattering Distribution Functions

While the volume scattering phase function describes the angular dependence of scattered radiation, a more important function for use with the Monte Carlo simulation is the volume scattering distribution function, $F(\theta)$, defined by Equation (3-3). The distribution function gives the normalized cumulative probability that a photon is scattered in the range 0 to θ degrees. The volume scattering distribution functions for the cases considered in Section 4.5 are shown in Figures 4-15 through 4-20.

It is again apparent in Figures 4-15 and 4-16 that there is a considerable difference between the absorbing and non-absorbing case. The difference due to the Feldspar and Ball Clay size distributions is small.

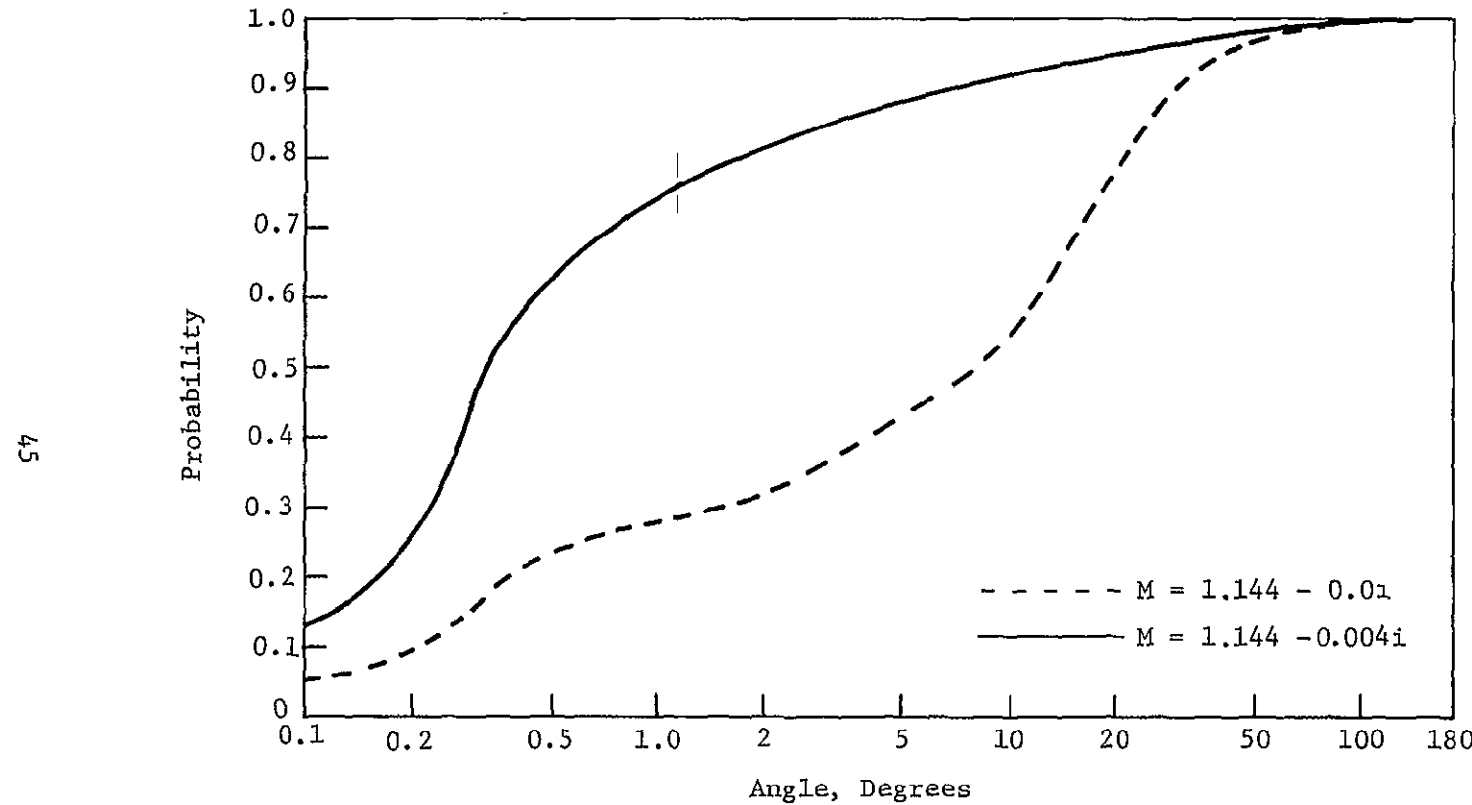


FIGURE 4-15
VOLUME SCATTERING DISTRIBUTION FUNCTIONS FOR FELDSPAR ($\lambda = 500\text{NM}$)

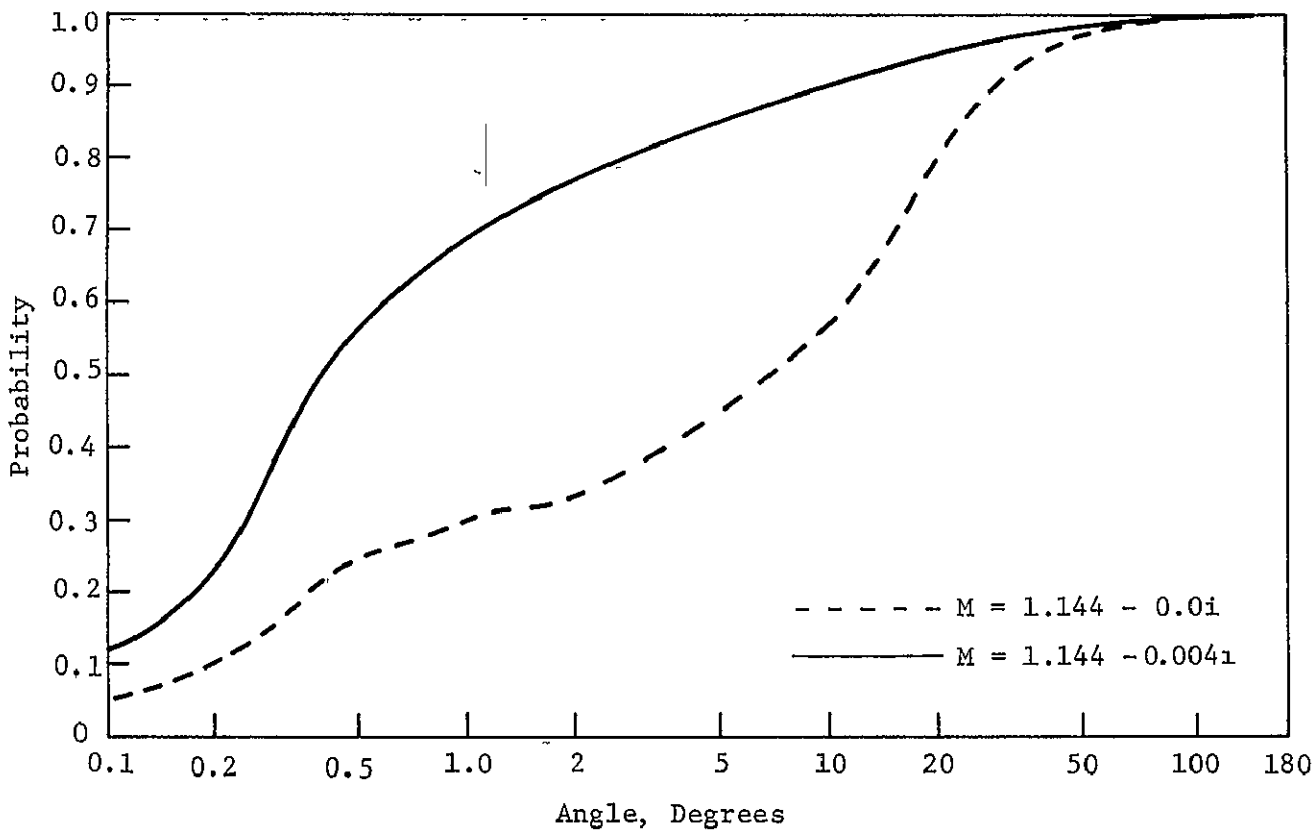


FIGURE 4-16
VOLUME SCATTERING DISTRIBUTION FUNCTIONS FOR BALL CLAY ($\lambda = 500\text{NM}$)

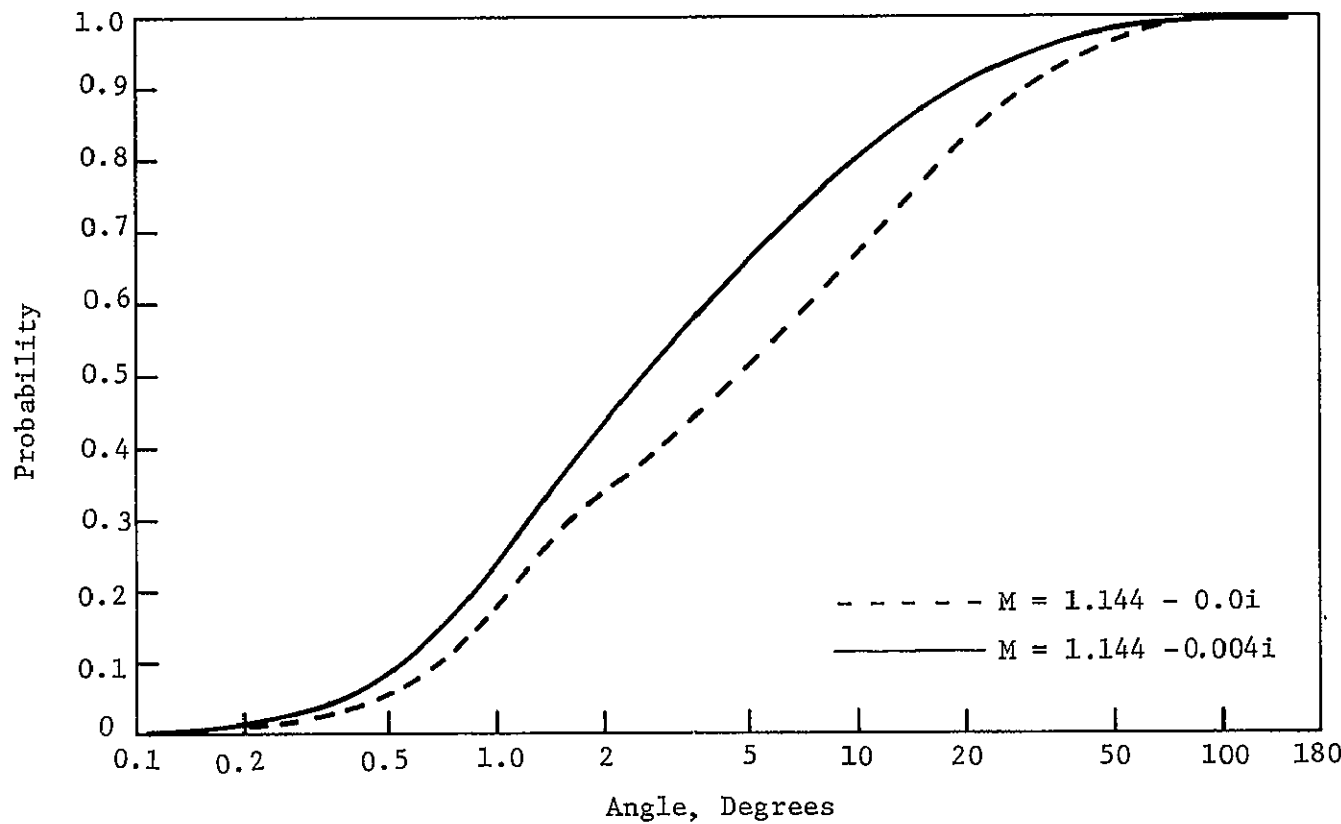


FIGURE 4-17
VOLUME SCATTERING DISTRIBUTION FUNCTIONS FOR FELDSPAR ($10\mu\text{M}$ CUTOFF $\lambda = 500\text{NM}$)

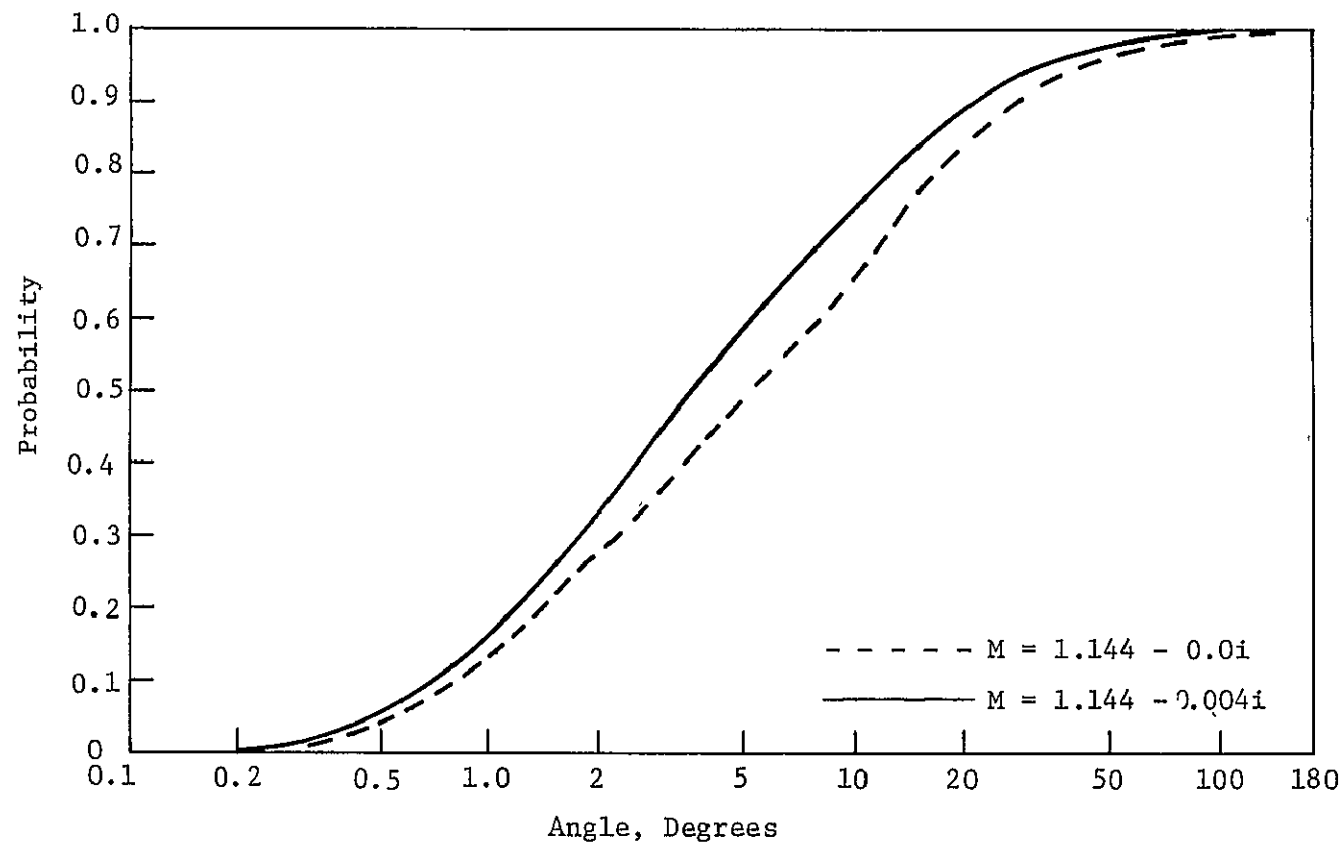


FIGURE 4-18
VOLUME SCATTERING DISTRIBUTION FUNCTIONS FOR BALL CLAY (10 μ M CUTOFF $\lambda = 500$ NM)

As with the scattering phase functions, the use of a 10 μm cutoff decreases the difference between the absorbing and non-absorbing cases. In addition, the volume scattering distribution functions are changed considerably when the 10 μm cutoff is imposed.

Figure 4-19 and 4-20 demonstrate the small change in the volume scattering distribution functions when the wavelength is changed.

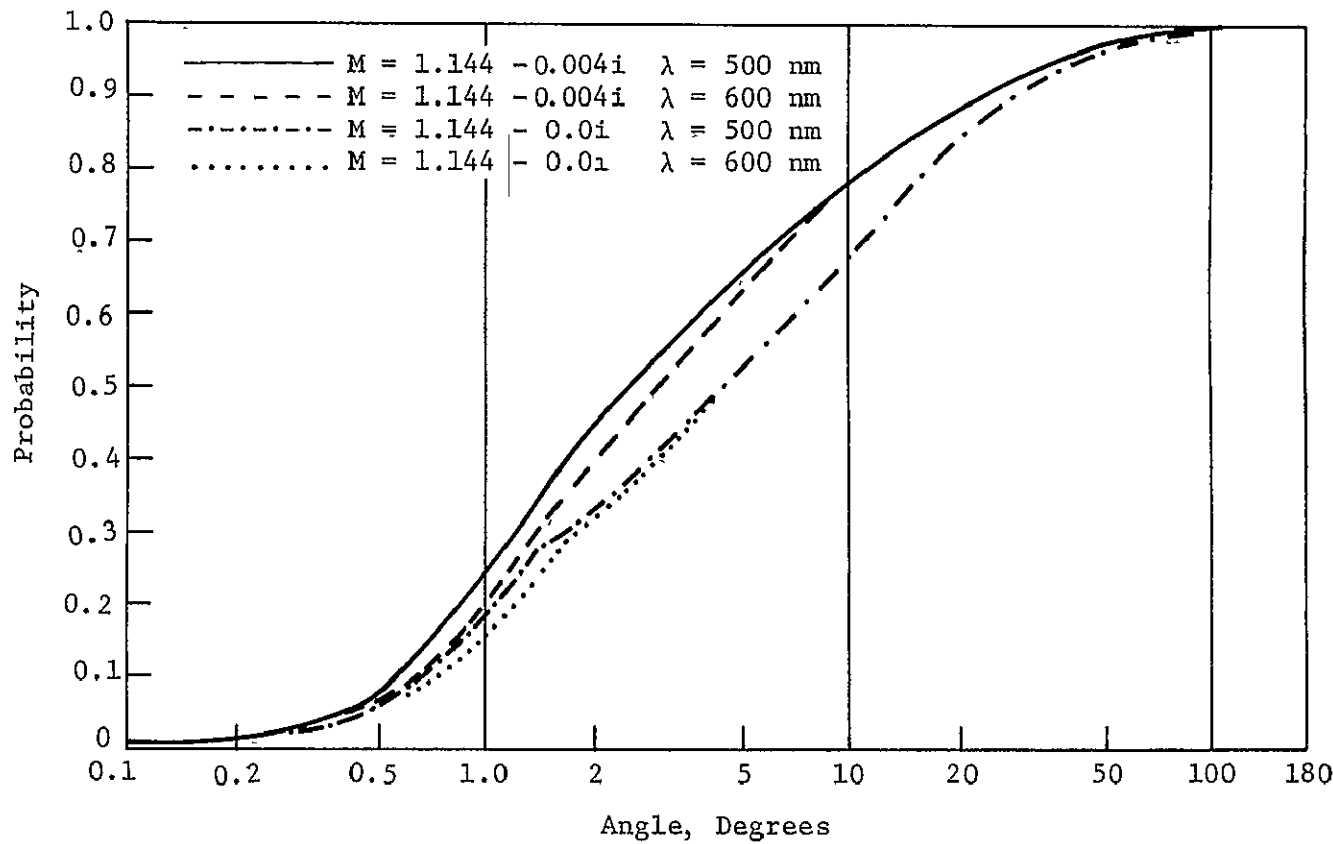


FIGURE 4-19
WAVELENGTH DEPENDENCE OF VOLUME SCATTERING DISTRIBUTION
FUNCTIONS FOR FELDSPAR ($10\mu\text{m}$ CUTOFF)

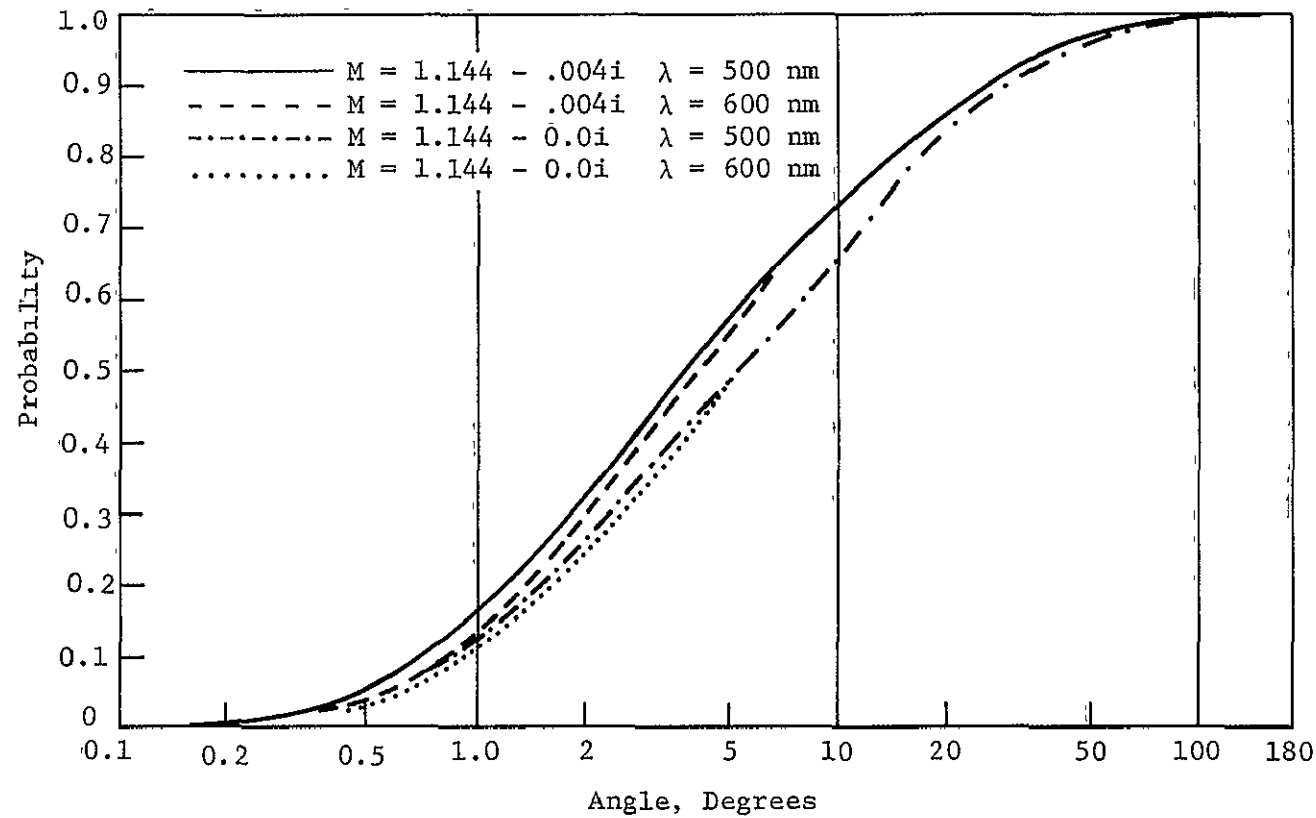


FIGURE 4-20
WAVELENGTH DEPENDENCE OF VOLUME SCATTERING FUNCTIONS
FOR BALL CLAY ($10\mu\text{m}$ CUTOFF)

5.0 THE EFFECT OF SCATTERING ON POLARIZATION

The description of a light wave in terms of its polarization properties requires the use of the Stokes formalism. In this section the Stokes formalism is developed and the effects of scattering on the polarization of a monochromatic light wave is investigated. The reader is referred to Reference 13 for a complete discussion of the Stokes formalism and polarization.

5.1 The Stokes Formalism

We consider a monochromatic, polarized electromagnetic wave propagating in the z-direction. The electric vector can then be written as

$$\begin{aligned} E_x &= A_1 \cos(\omega t) \\ E_y &= A_2 \cos(\omega t + \delta) \\ E_z &= 0 \end{aligned} \tag{5-1}$$

This wave can be represented using the Stokes formalism:

$$\vec{I} = \begin{pmatrix} I_1 \\ I_2 \\ U \\ V \end{pmatrix} \tag{5-2}$$

Where the Stoke parameters are given by

$$I_1 = A_1^2$$

$$I_2 = A_2^2$$

$$U = 2A_1 A_2 \cos\delta \quad (5-3)$$

$$V = 2A_1 A_2 \sin\delta$$

There are a number polarization "types" possible for a completely polarized beam of light; some examples are given in Table 5-I.

5.2 The Effect of Scattering on Polarization

If the light beam is not completely polarized then it can be broken into two components: a completely polarized component, I_p , and an unpolarized, or natural component, I_n . In terms of the Stokes vectors of a beam of light these components are

$$I_p = \begin{pmatrix} \frac{1}{2}(I_1 - I_2) + \frac{1}{2}((I_1 - I_2)^2 + U^2 + V^2)^{\frac{1}{2}} \\ \frac{1}{2}(I_2 - I_1) + \frac{1}{2}((I_1 - I_2)^2 + U^2 + V^2)^{\frac{1}{2}} \\ U \\ V \end{pmatrix} \quad (5-4)$$

$$I_n = \begin{pmatrix} \frac{1}{2}(I_1 + I_2) + \frac{1}{2}((I_1 - I_2)^2 + U^2 + V^2)^{\frac{1}{2}} \\ \frac{1}{2}(I_1 + I_2) + \frac{1}{2}((I_1 - I_2)^2 + U^2 + V^2)^{\frac{1}{2}} \\ 0 \\ 0 \end{pmatrix}$$

Note that if the beam is completely polarized then

$$(I_1 + I_2)^2 = (I_1 - I_2)^2 + U^2 + V^2 \quad (5-5)$$

TABLE 5.I
STOKES REPRESENTATION FOR SOME POLARIZATION TYPES⁽¹⁴⁾

| Type | I_1 | I_2 | U | V | δ | Description of Polarization |
|------|---------------|---------------|---------|---------|------------------|---|
| 1) | 1 | 0 | 0 | 0 | 0 | Linear, Vertical |
| 2) | 0 | 1 | 0 | 0 | 0 | Linear, Horizontal |
| 3) | $\frac{1}{2}$ | $\frac{1}{2}$ | 1 | 0 | 0 | Linear, 1st and 3rd Quadrants |
| 4) | $\frac{1}{2}$ | $\frac{1}{2}$ | -1 | 0 | 0 | Linear, 2nd and 4th Quadrants |
| 5) | $\frac{1}{2}$ | $\frac{1}{2}$ | 0 | 1 | $\pi/2$ | Circular, Right Handed |
| 6) | $\frac{1}{2}$ | $\frac{1}{2}$ | 0 | -1 | $-\pi/2$ | Circular, Left Handed |
| 7) | $5/8$ | $3/8$ | $3/4$ | $3/2$ | $\sin^{-1} 4/5$ | Elliptical, Right Handed, 1st and 3rd Quadrants |
| 8) | $3/8$ | $5/8$ | - $3/4$ | - $3/2$ | $-\sin^{-1} 4/5$ | Elliptical, Left Handed, 2nd and 4th Quadrants |

(as can be seen from Equation (5-3)) Equations (5-4) reduce to

$$I_p = \begin{pmatrix} I_1 \\ I_2 \\ U \\ V \end{pmatrix} \quad (5-6)$$

$$I_N = \begin{pmatrix} 0 \\ 0 \\ 0 \\ 0 \end{pmatrix}$$

The degree of polarization, P , is defined as the ratio of the intensity of the polarized component to the sum of the intensities of the polarized and unpolarized components,

$$P = \frac{I_p}{I_p + I_N} \quad (5-7)$$

which in terms of the Stokes parameters is

$$P = \frac{\sqrt{(I_1 - I_2)^2 + U^2 + V^2}}{I_1 + I_2} \quad (5-8)$$

For completely polarized light $P=1$ while for a light beam which contains a natural component $P < 1$.

Equation (5-8) can be inverted to give an alternate expression for determining if a wave is fully or partially polarized:

$$\pi = \frac{4I_1 I_2}{U^2 + V^2} \left\{ \begin{array}{l} = \\ > \end{array} \right\} 1 \left\{ \begin{array}{l} \text{fully polarized} \\ \text{partially polarized} \end{array} \right\} \quad (5-9)$$

This expression will be useful when examining the effect of scattering from a spherical particle, or a collection of spherical particles.

If an incident wave, represented by the Stokes vector

$$\vec{I}_i = \begin{pmatrix} I_1 \\ I_2 \\ U \\ V \end{pmatrix},$$

is scattered by a spherical particle whose scattering matrix is given by Equation (4-3) the scattered wave is given by (apart from a constant)

$$\vec{I}_s = \begin{pmatrix} I_{s,1} \\ I_{s,2} \\ U_s \\ V_s \end{pmatrix} = \begin{pmatrix} M_1(x, m, \theta) I_1 \\ M_2(x, m, \theta) I_2 \\ S_{21}(x, m, \theta) U - D_{21}(x, m, \theta) V \\ S_{21}(x, m, \theta) U + D_{21}(x, m, \theta) V \end{pmatrix} \quad (5-10)$$

Upon forming π_s for the scattered wave and simplifying it is found that

$$\pi_s = \frac{4I_{s,1} I_{s,2}}{U_s^2 + V_s^2} = \frac{M_1(x, m, \theta) M_2(x, m, \theta)}{S_{21}^2(x, m, \theta) + D_{21}^2(x, m, \theta)} \left(\frac{4I_1 I_2}{U^2 + V^2} \right) = \quad (5-11)$$

$$\frac{M_1(x, m, \theta) M_2(x, m, \theta)}{S_{21}^2(x, m, \theta) + D_{21}^2(x, m, \theta)} \pi.$$

If the wave incident on a spherical particle is completely polarized then $\pi=1$ and using the definitions of Equation (4-4) one finds

$$\pi_s = \frac{|S_1(x, m, \theta)|^2 |S_2(x, m, \theta)|^2}{|S_1(x, m, \theta)|^2 |S_2(x, m, \theta)|^2} = 1 \quad (5-12)$$

and the scattered wave is also completely polarized. This does not mean that the polarization type has not been changed. It can be seen from Equation (5-10) that the parameters of the Stokes vector are altered by the scattering matrix. For example, in general, linearly polarized light will be scattered as elliptically polarized light.

If, instead of scattering from a single particle, the light is scattered off of a volume element containing a collection of particles, then the parameters of the scattering matrix must be replaced by their averages (denoted by $\langle \dots \rangle$) over the volume element. Thus the polarization condition (Equation 5-11) becomes

$$\pi_s = \frac{\langle M_1(x, m, \theta) \rangle \langle M_2(x, m, \theta) \rangle}{\langle S_{21}(x, m, \theta) \rangle^2 + \langle D_{21}(x, m, \theta) \rangle^2} \quad \pi. \quad (5-13)$$

Again assuming that the incoming wave is completely polarized ($\pi=1$) and expanding the scattering parameters in terms of the scattering amplitudes as was done for Equation (5-12) we find

$$\pi_s = \frac{\langle S_1(x, m, \theta) \rangle^2 \langle S_2(x, m, \theta) \rangle^2}{\langle S_1^*(x, m, \theta) S_2(x, m, \theta) \times S_1(x, m, \theta) S_2^*(x, m, \theta) \rangle} \quad (5-14)$$

and using the Cauchy-Schwarz inequality results in

$$\pi_s \geq \frac{\langle s_1(x, m, \theta) \rangle^2 \langle s_2(x, m, \theta) \rangle^2}{\langle s_1(x, m, \theta) \rangle^2 + \langle s_2(x, m, \theta) \rangle^2} = 1 \quad (5-15)$$

or $\pi_s \leq 1$. The equality holds if all of the particles in the volume element are identical. For a polydispersion the scattered light will be depolarized, that is the degree of polarization will be reduced.

5.3 Results of Calculations of Polarization for Single Scattering

When computing the polarization of a beam of light which has been scattered from a particle (or collection of particles) it is necessary to first select a specific Stokes vector representation of the incoming light. For any type of polarization (i.e., linear, elliptical) there are an infinite number of Stokes vector representations. The representation which is appropriate for a particular scattering event depends on the plane of observation (PO) of that event. The PO is defined by the direction of the incoming wave and the direction of the observed scattered wave. The Stokes vector of the incoming wave is written in the representation for which E_x lies in the PO and E_y is perpendicular to the PO. For the purposes of calculating the depolarizing effects of single scattering from the clay sediments we will use an incoming wave represented by

$$\vec{I}_o = \begin{pmatrix} \frac{1}{2} \\ \frac{1}{2} \\ 1 \\ 0 \end{pmatrix} \quad (5-1)$$

This is a linearly polarized wave written in a representation which does not give a preference to the E_x and E_y components. In terms of the PO this Stokes vector represents a wave whose electric vector is at a 45° angle to the x and y coordinates.

The resulting polarization from the scattering of the wave from the Feldspar and Ball Clay polydispersions is shown in Figure 5-1 and 5-2. While the angular polarization properties of the two polydispersions differ there is a much more marked difference between the polarizations for the non-absorbing and weakly absorbing cases.

When a $10 \mu\text{m}$ cutoff is imposed on the size distributions the differences in the polarization for the non-absorbing and weakly absorbing cases are reduced (Figures 5-3 and 5-4). In addition the differences between the polarization curves of the Feldspar and Ball Clay samples are reduced.

A change in wavelength, from $\lambda=500 \text{ NM}$ to $\lambda=600 \text{ NM}$, results in only small changes in the polarization curves. (Compare Figures 5-3 and 5-5 and Figures 5-4 and 5-6).

5.4 Depolarization Due to Multiple Scattering

It is not possible to compute the depolarization due to multiple scattering without actually performing a Monte Carlo simulation.

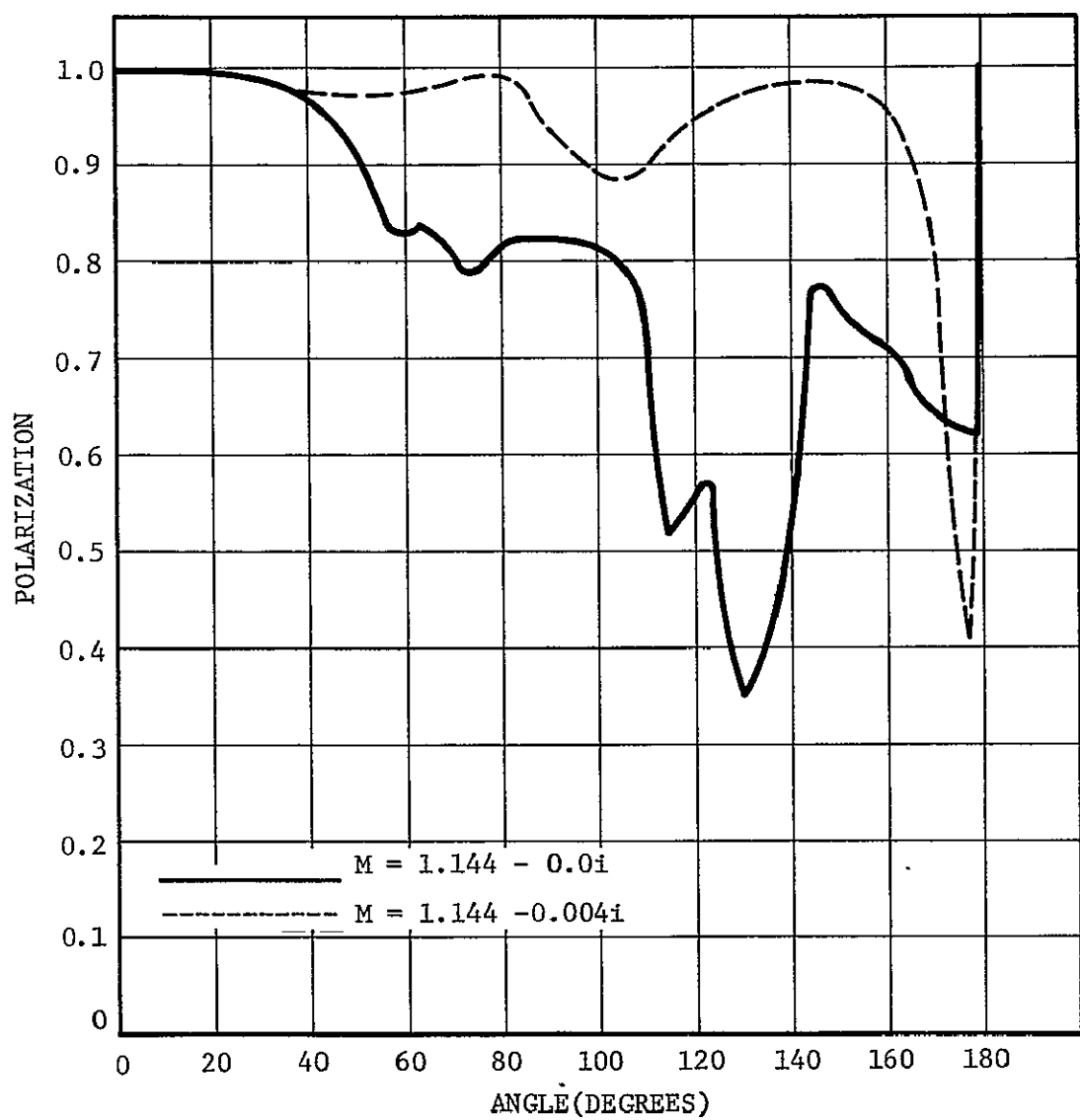


FIGURE 5-1
POLARIZATION FOR FELDSPAR ($\lambda = 500 \text{ NM}$)

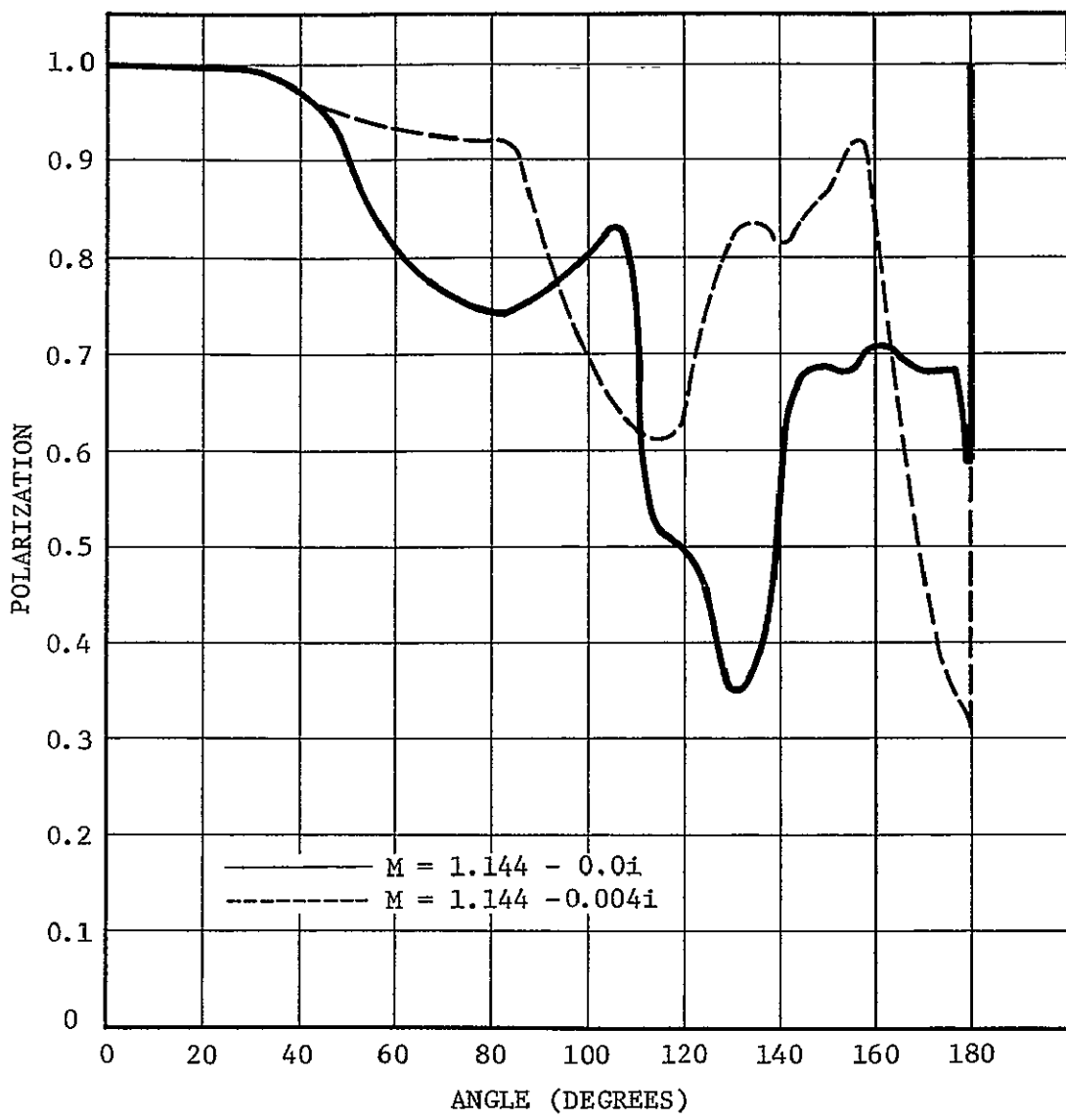


FIGURE 5-2
POLARIZATION FOR BALL CLAY ($\lambda = 500 \text{ NM}$)

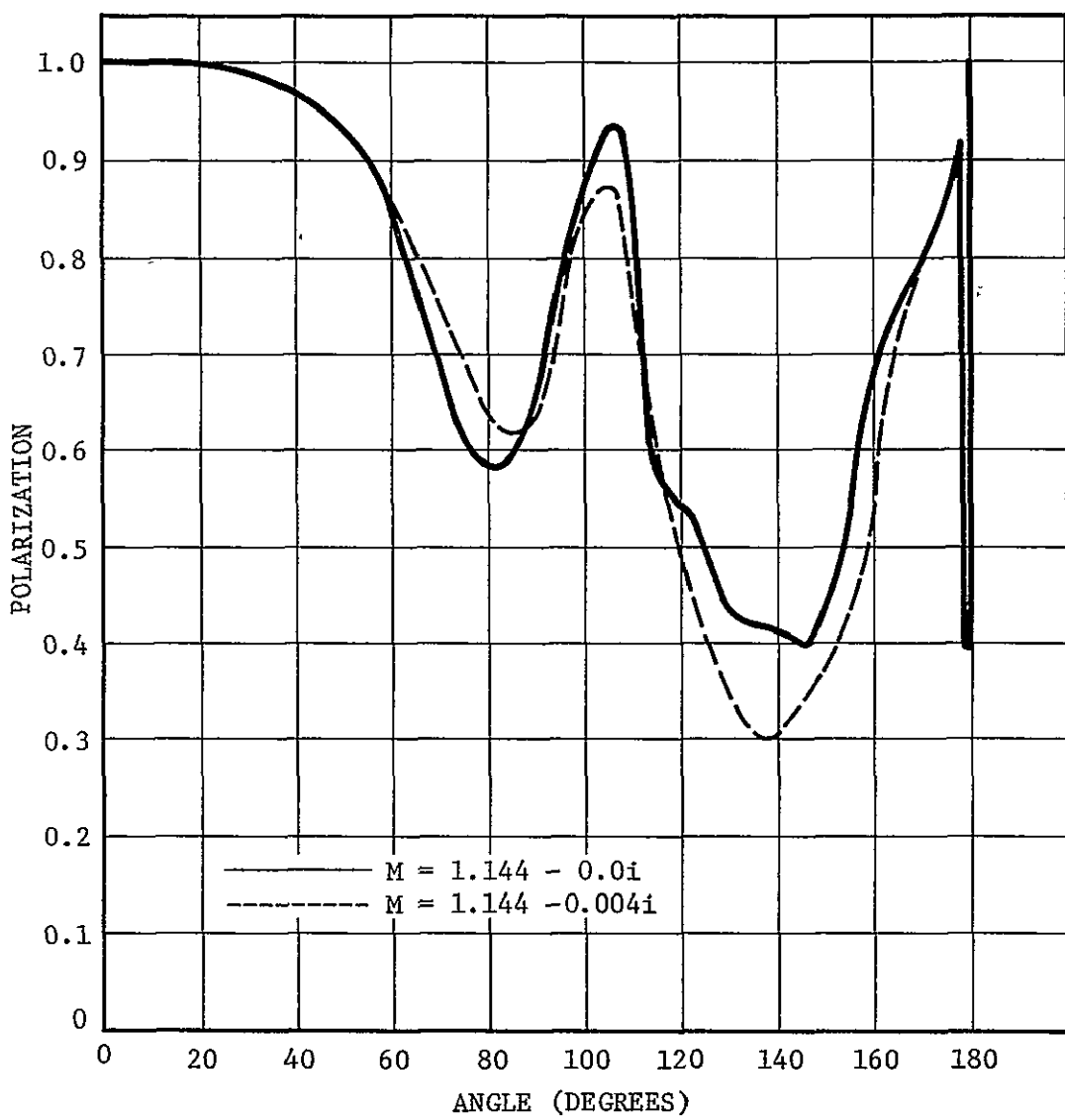


FIGURE 5-3
POLARIZATION FOR FELDSPAR (10 μ M CUTOFF $\lambda = 500$ NM)

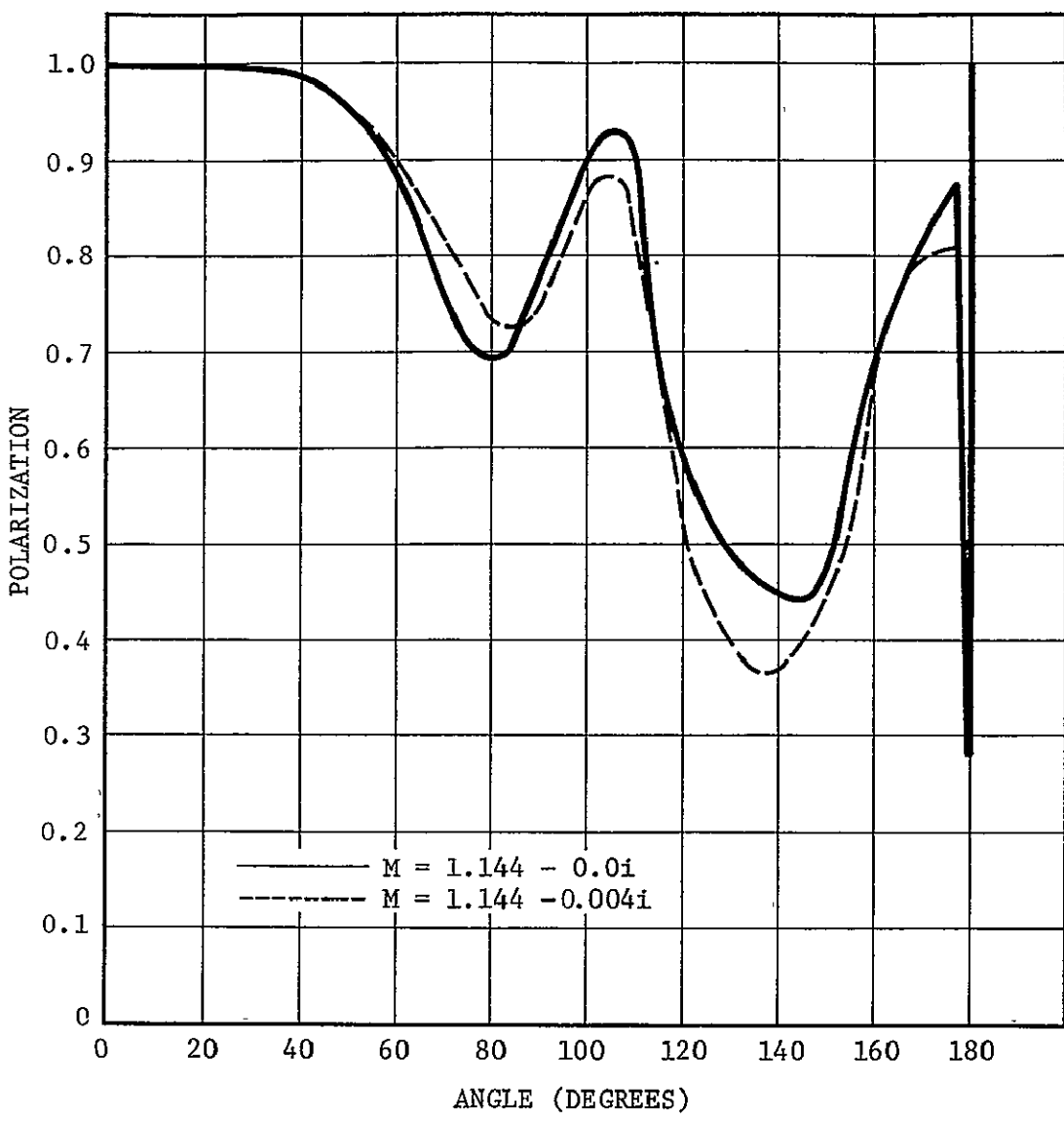


FIGURE 5-4
POLARIZATION FOR BALL CLAY (10 μ M CUTOFF $\lambda = 500$ NM)

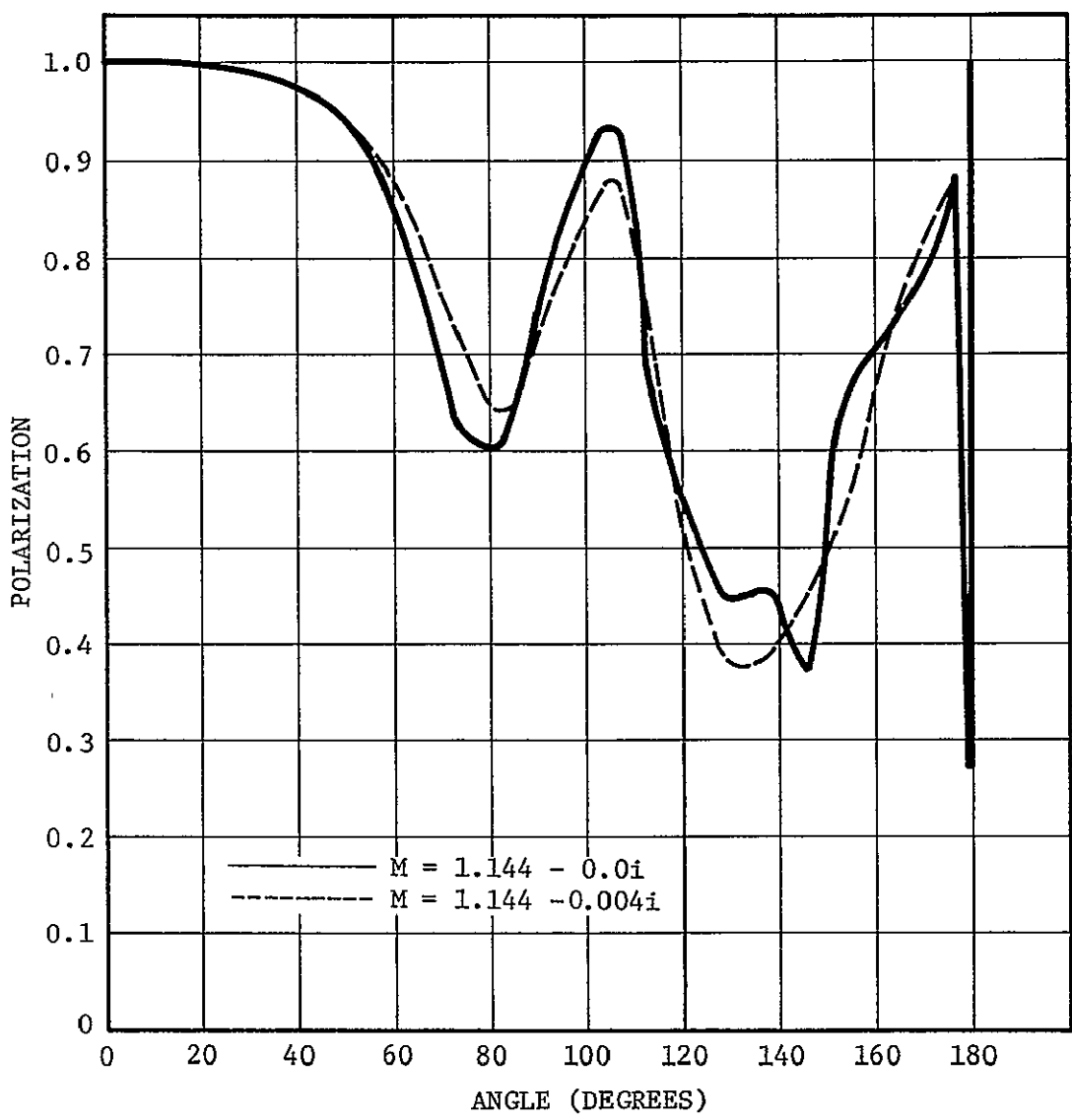


FIGURE 5-5
POLARIZATION FOR FELDSPAR (10 μ M CUTOFF $\lambda = 600$ NM)

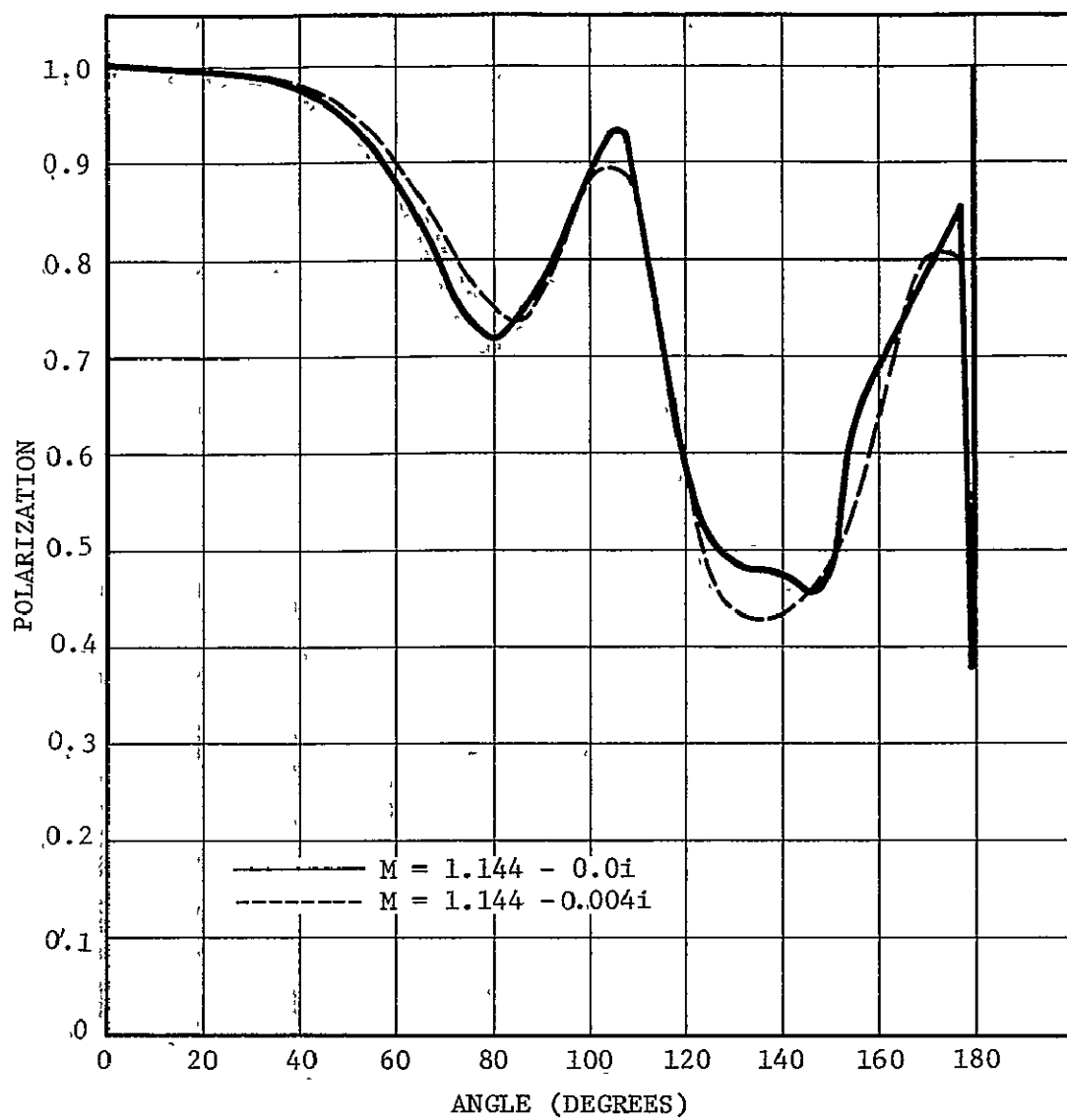


FIGURE 5-6
POLARIZATION FOR BALL CLAY ($10\mu\text{M}$ CUTOFF $\lambda = 600 \text{ NM}$)

One of the reasons for this is that the polarization of a wave represented by a Stokes vector, depends on the plane of observation (PO) which for multiple scattering is defined in terms of the incoming direction and the direction to the next scattering particle (or volume element). Thus, in general, for each scattering event the Stokes vector will have to be rotated into the representation of the new PO. For a clockwise rotation of the PO about the propagation direction, through an angle ϕ , the Stokes vector will have to be rotated by operating on it with a rotation matrix R :

$$\vec{I}' = R(\phi)\vec{I} \quad (5-16)$$

Where

$$R(\phi) = \begin{pmatrix} \cos^2\phi & \sin^2\phi & \frac{1}{2}\sin 2\phi & 0 \\ \sin^2\phi & \cos^2\phi & -\frac{1}{2}\sin 2\phi & 0 \\ -\sin 2\phi & \sin 2\phi & \cos 2\phi & 0 \\ 0 & 0 & 0 & 1 \end{pmatrix} \quad (5-17)$$

For the multiple scattering of a beam the product

$$\vec{I}_f = \prod_{i=1}^n S(\theta_i) R(\phi_i) \vec{I}_o \quad (5-18)$$

must be calculated. In Equation (5-18) \vec{I}_f is the final Stokes vector, \vec{I}_o is the initial Stokes vector, $S(\phi_i)$ is the Mie matrix for angle ϕ_i and the product is over all scattering events, $i=1, n$, that results in the beam being scattered into the detector.

In the next section we examine the results of using Monte Carlo simulation techniques to investigate the polarization effects due to multiple scattering

6.0 RESULTS OF MONTE CARLO SIMULATION

The Monte Carlo simulation was run for two cases, i.e., for two different volume scattering functions, $F(\theta)$. The cases chosen were for Ball Clay with a $10\mu\text{m}$ cutoff at a wavelength of 500 nm and with indices of refraction $M = 1.144 - 0.0i$ and $M = 1.144 - 0.004i$.

For the former ($\text{Im}(m) = 0$) the simulation was run in 10^4 photon increments until, after 3×10^4 photons had been run, 335 photons were found to have emerged from the water. When a small imaginary component is added to the index of refraction the forward scattering was increased and it was found that after 10^4 photons only 35 had emerged from the water. It was decided that too large a sample of photons would have to be run to obtain a significant number of photons and only the $M = 1.144 - 0.0i$ case was investigated in detail.

Before discussing the results of the simulation a phenomenological theory is developed which is useful in interpreting the simulation results.

6.1 Phenomenological Theory of Depolarization

As was discussed in Section 5, each scattering event from a volume element of a polydispersion results, in general, in a decrease in the degree of polarization. In addition, each scattering event results in a change in the type of polarization. Thus the more times a photon is scattered the more its degree of polarization is decreased. By the same token, if a photon starts out with a linear polarization, the more scattering events it undergoes the more it "loses its

"memory" of its polarization state. Thus, after a large number of scattering events, the degree of polarization should approach zero, and the ratio of the y- component of the electric vector to the x-component, $R = E_y/E_z$, should approach unity.

To develop an understanding of the relationship between depolarization and the parameters - spot size, s , and a values - a relationship between them and the average number of scattering events must be investigated. Assuming, for the present, that a/s is constant and that s is a variable parameter (i.e., the concentration of the sediments is variable) this relationship is shown in Figure 6-1. In a) the case of high concentration (large s) and small spot size is represented while b) illustrates the case for low concentration (small s) and large spot size. These two cases are equivalent because they will have the same average number of scattering events. In fact, the product (spot size $\times s$) is directly correlated with the average number of scattering events. Figure 6-2 shows the results of the Monte Carlo simulations in terms of the average number of scattering events vs. (spot size \times scattering coefficient). (Note that, for the $M = 1.144 - 0.0i$ case, the points lie along a smooth line and in addition the points are virtually identical for the 10^4 photon and 3×10^4 photon runs). For the $M = 1.144 - 0.004i$ case the points show significant scatter (thus indicating the lack of statistical significance for this run). Figure 6-1, c indicates that by decreasing the concentration (s value) while keeping the spot size

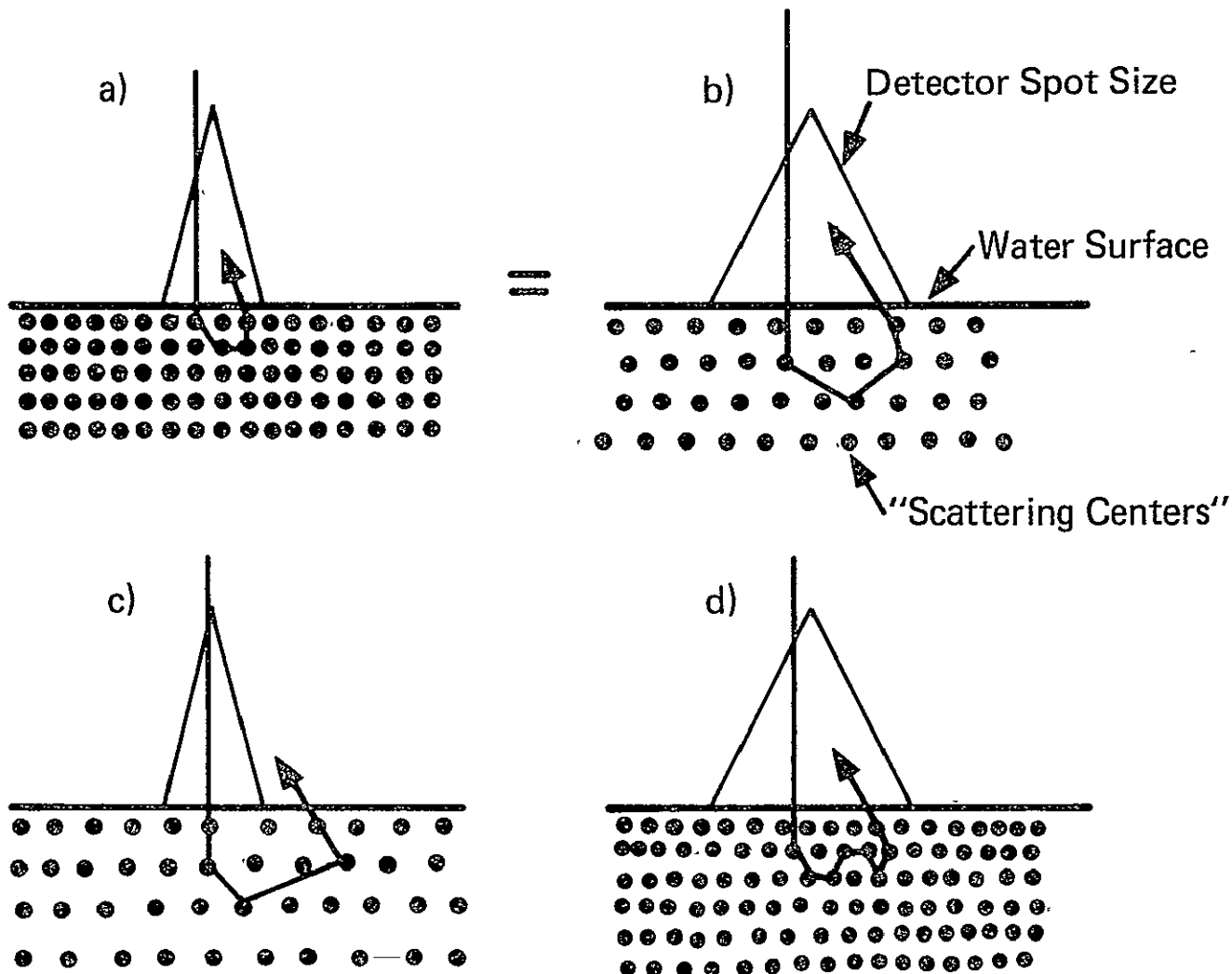


FIGURE 6-1
**RELATIONSHIP BETWEEN SPOT SIZE, DENSITY OF SEDIMENTS
AND NUMBER OF SCATTERING EVENTS**

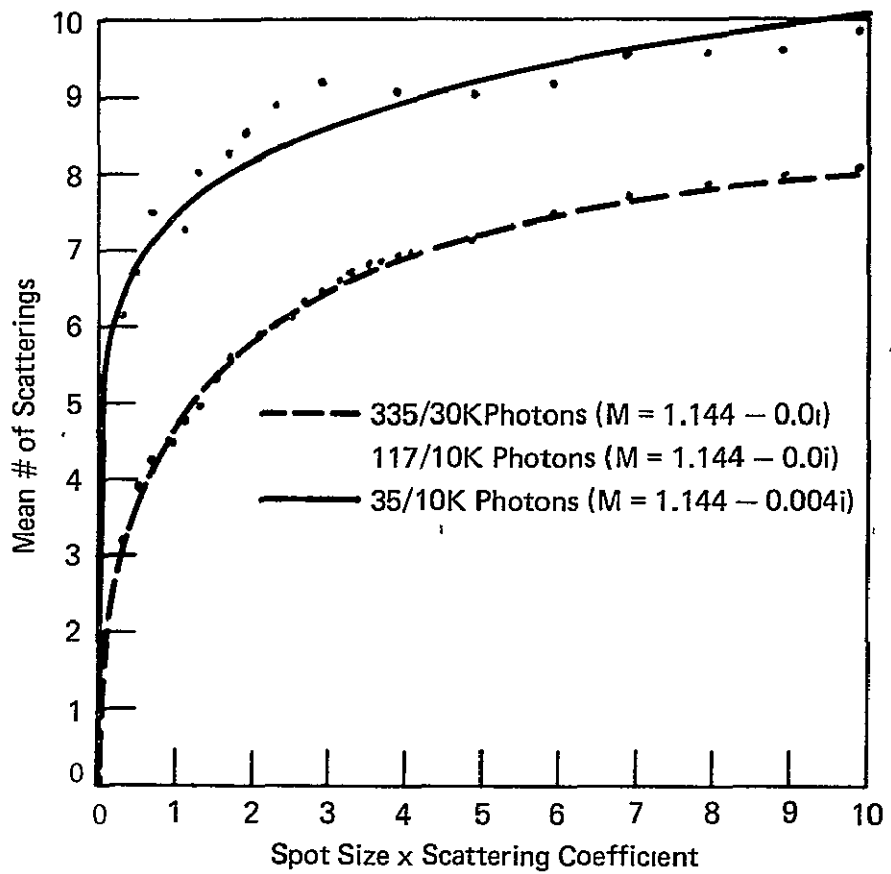


FIGURE 6-2
**MEAN NUMBER OF SCATTERING EVENTS FOR BACKSCATTERED
PHOTONS VS. SPOT SIZE x SCATTERING COEFFICIENT**

constant results in some of the photons which undergo a large number of scattering events being out of range of the detector when they emerge from the water surface. By the same token increasing the concentration (s value) while holding the spot size constant, results in a photon which undergoes a larger number of scattering events still being in the range of the detector when it emerges from the water (Figure 6-1, d).

Based on our previous discussion of the effect of increased scattering on depolarization we can now state the hypothesis:

As the s value (concentration) is increased (for a given spot size) the degree of polarization of the backscattered beam will decrease (the R-factor will approach unity); as the spot size is increased (for a given s value) the degree of polarization will decrease (the R-factor will increase towards unity).

If s is held constant and a/s is allowed to vary then those photons which travel a longer distance, and hence have been scattered more, will be weighted less as a/s is increased. Thus one would expect the degree of polarization would increase as the a/s ratio increases.

A word of caution concerning the phenomenological theory of this section is in order. An important factor has been ignored in this development, viz., the variation of the depolarization, due to single scattering, with the scattering angle. However, based on the fact that most of the scattering is in the forward direction, where there is little difference in Figures 5-1 through 5-6 it may be reasonable to expect any differences at angles greater than

40 degrees to have little impact. As will be seen in the next section, the results of the depolarization calculations seem to fit the hypothesis concerning the relationship between depolarization, spot size, s-value and a/s-ratio.

6.2 Depolarization Calculation From Monte Carlo Results

The results of the degree of polarization calculations for the backscattered beam from the Ball Clay, $M = 1.144 - 0.0i$ case are shown in Figure 6-3. It is found that the degree of polarization does decrease asymptotically as the scattering coefficient is increased. It is also found that the degree of polarization is approximately the same for combinations of spot size and scattering coefficient which yield the same product. Another result of the simulation is that small spot size will provide better discrimination at high levels of scattering coefficient. For discrimination between different a/s ratios it is found that a large spot size is necessary. From Figure 6-4 it can be seen that there is virtually no dependence of the degree of polarization on the a/s ratio for the 1 inch radius spot size.

The results of the calculations of the R-factor are shown in Figure 6-5. Here again it is found that the results agree with the hypothesis of Section 6.1. That is, for all spot sizes the R-factor increases for large s-values. In addition it is found that the R-factor has approximately the same value for corresponding pairs of spot size and s-value. As with the degree of polarization it is

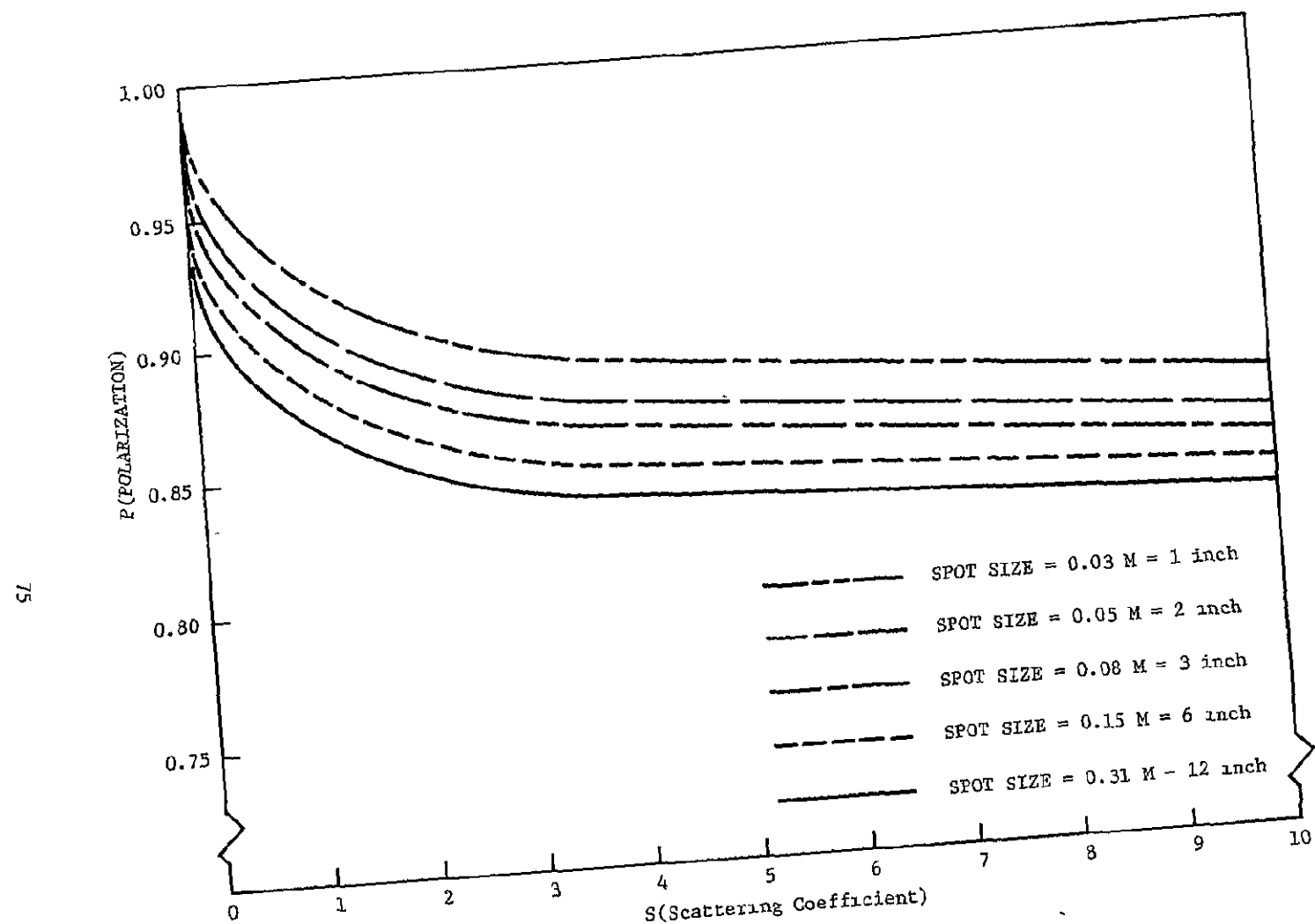


FIGURE 6-3
DEPENDENCE OF POLARIZATION ON SCATTERING COEFFICIENT

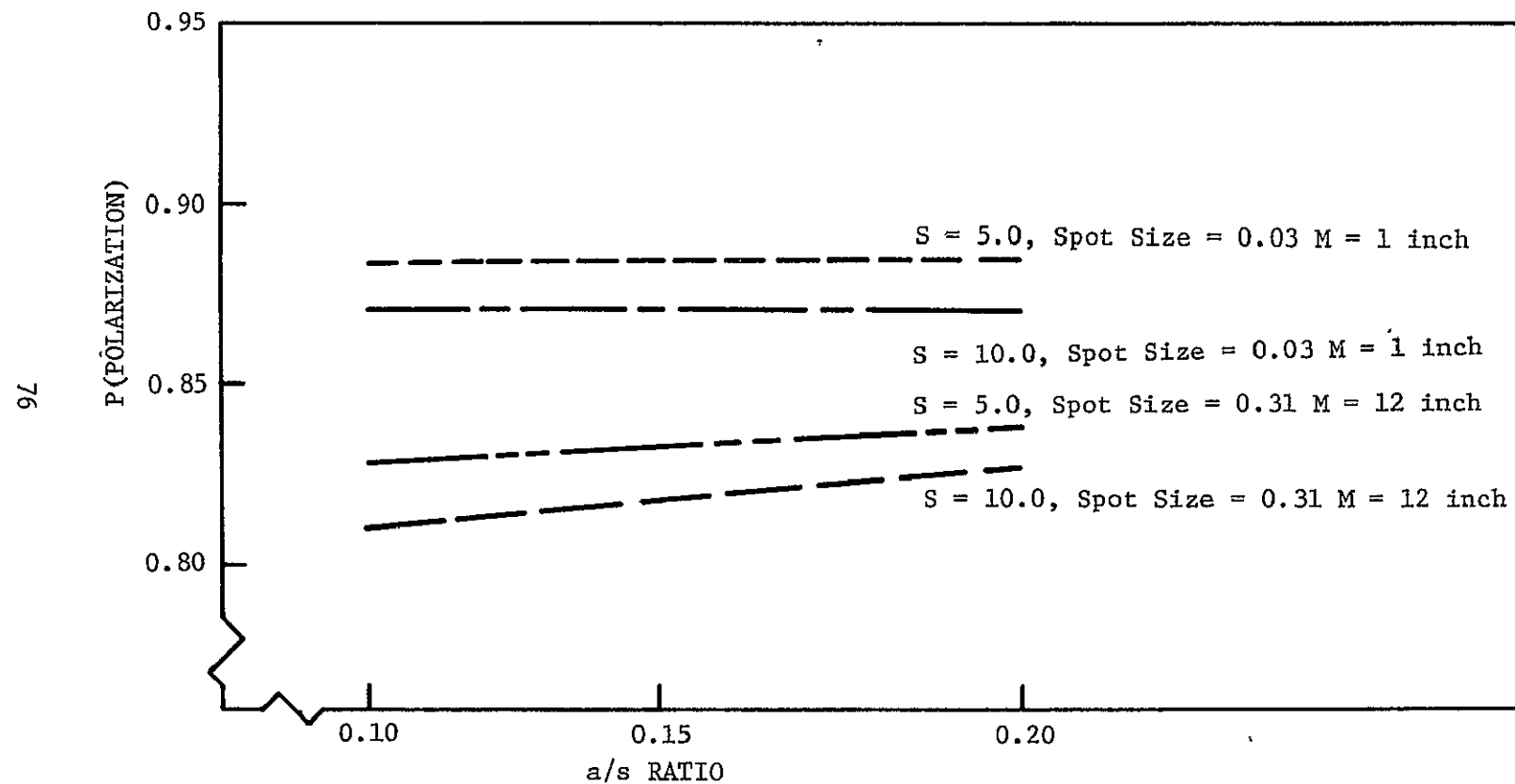


FIGURE 6-4
DEPENDENCE OF POLARIZATION ON a/s RATIO

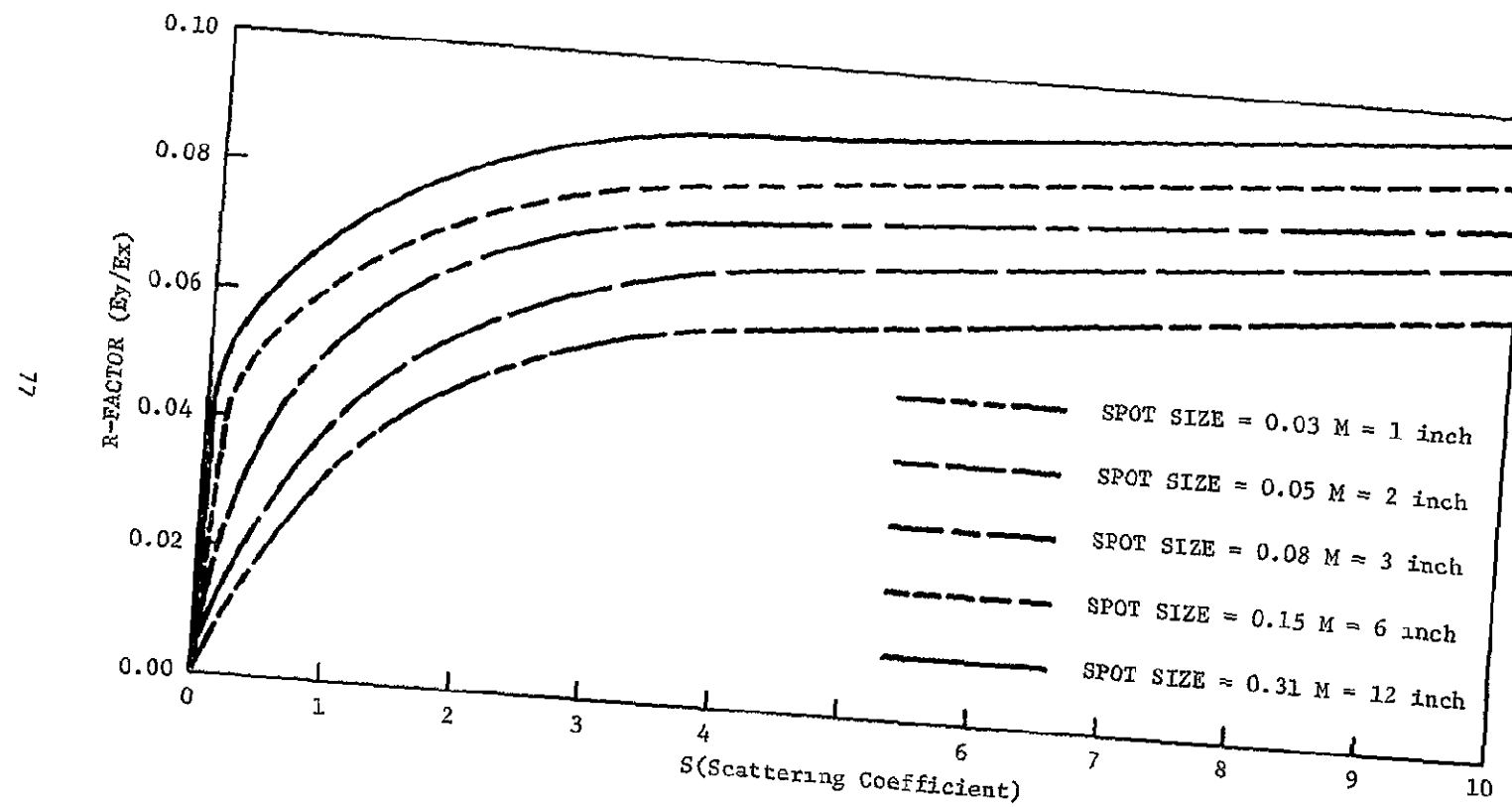


FIGURE 6-5
DEPENDENCE OF R-FACTOR ON SCATTERING COEFFICIENT

found that small spot size gives the best results for discrimination at high values of s . The R-Factor is also found to be relatively insensitive to variations in the a/s ratio (from .1 to .2) for constant s -value and small spot size (Figure 6-6).

Recently data on the depolarization of a backscattered beam of laser light has been collected from a portion of the Chesapeake Bay⁽¹⁶⁾. The results of that experiment, which used a 2.5 inch radius spot size, is compared with the theoretical curves in Figure 6-7. The agreement is obviously quite good.

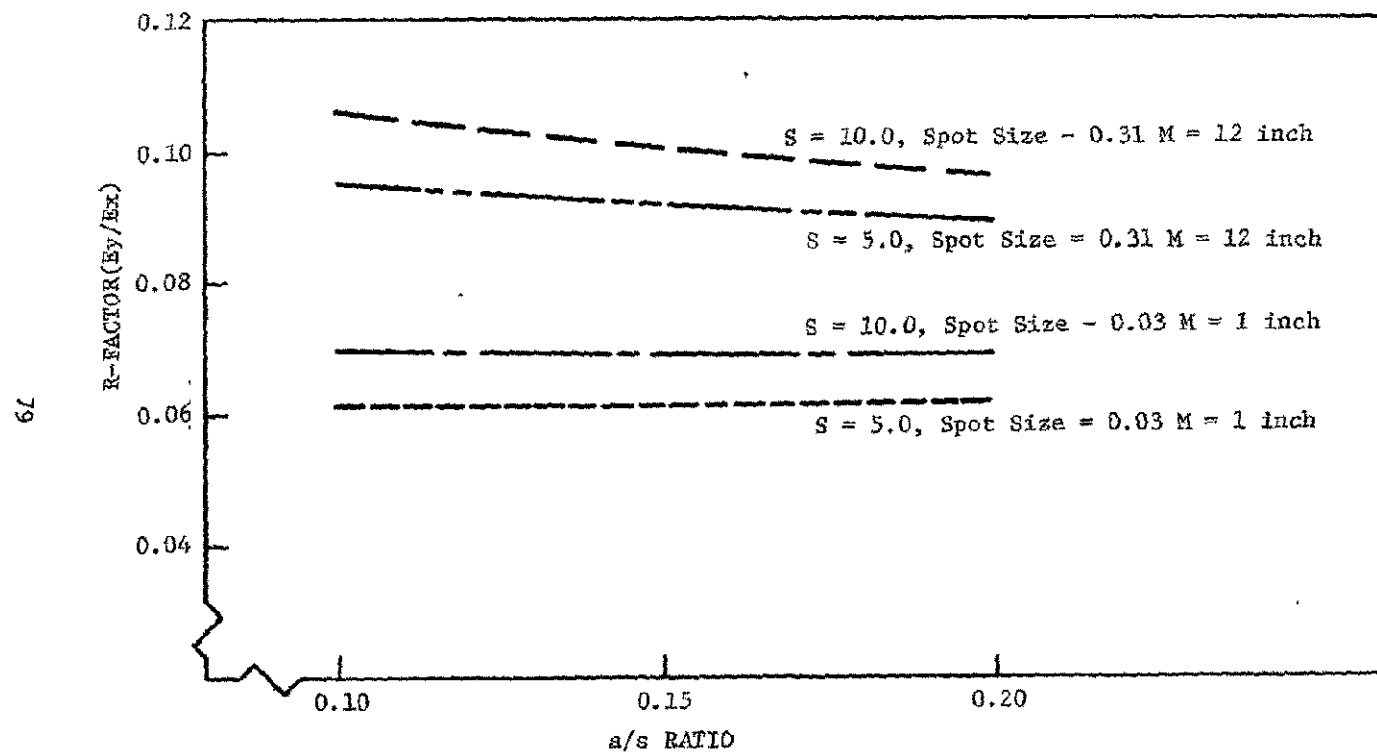


FIGURE 6-6
DEPENDENCE OF R-FACTOR ON a/s RATIO

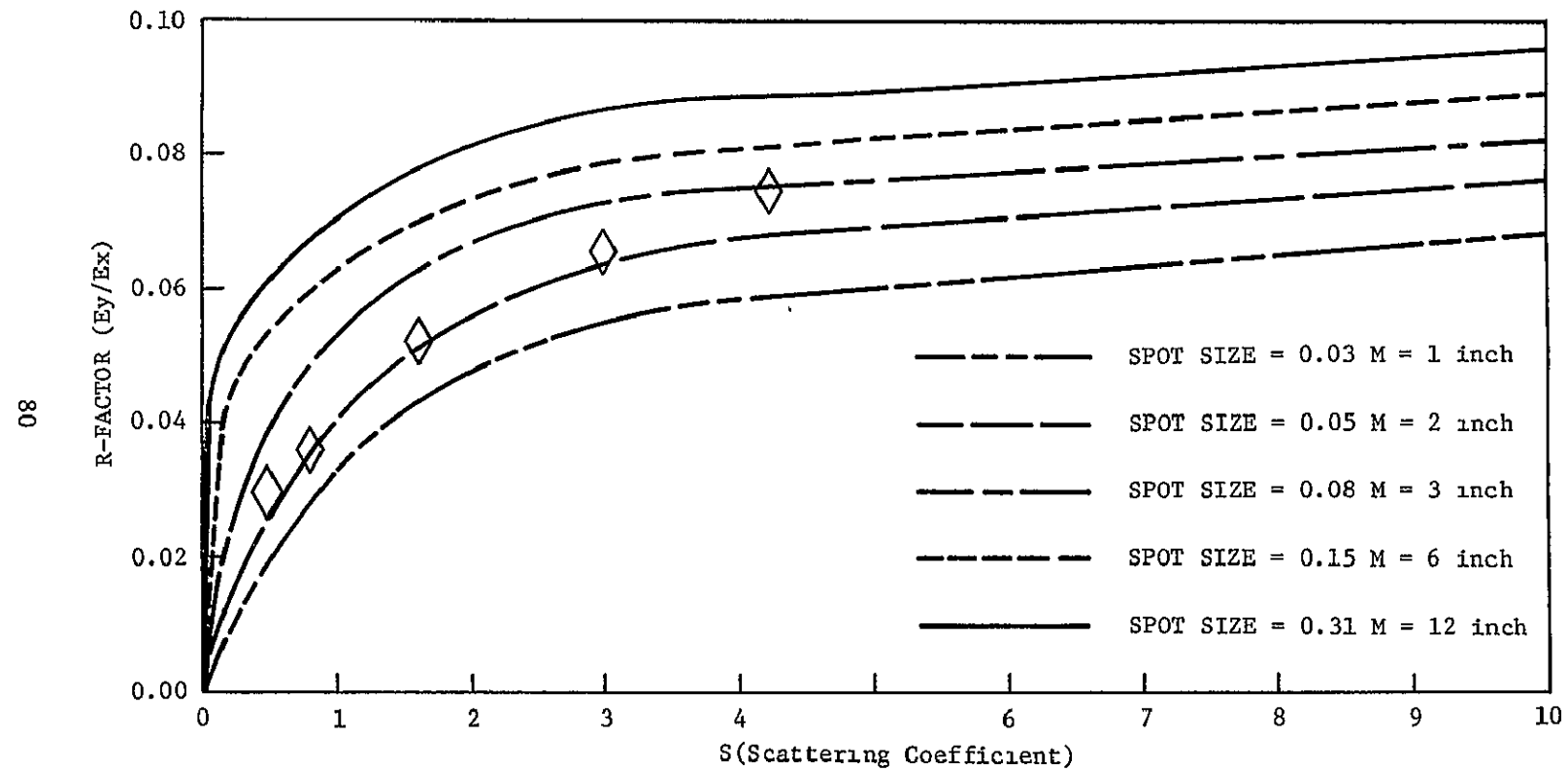


FIGURE 6-7
COMPARISON OF THEORETICAL AND EXPERIMENTAL VALUES FOR THE R-FACTOR.
DIAMONDS REPRESENT DATA COLLECTED FROM THE CHESAPEAKE BAY USING
A 2½ INCH RADIUS SPOT SIZE.

APPENDIX A

RELATIONSHIP BETWEEN EXTINCTION, SCATTERING, AND
ABSORPTION COEFFICIENTS AND THE MIE PARAMETERS

The extinction (α), scattering (s), and absorption (a) coefficients for suspended particulates can be calculated using the Mie formalism. Using the Mie parameters, $a_n(x,m)$ and $b_n(x,m)$ of equations (3-7) the extinction coefficient is given by:

$$\alpha = \frac{\lambda^2}{2\pi} \int \sum_{n=1}^{\infty} (2n+1) \left\{ \operatorname{Re}(a_n(x,m)) + \operatorname{Re}(b_n(x,m)) \right\} n(r) dr$$

where $n(r)$ is the particle size distribution function and $x = 2\pi r/\lambda$.

The expression for the scattering coefficient is:

$$s = \frac{\lambda^2}{2\pi} \int \sum_{n=1}^{\infty} (2n+1) \left\{ |a_n(x,m)|^2 + |b_n(x,m)|^2 \right\} n(r) dr$$

The absorption coefficient is the difference between α and s , thus

$$a = \frac{\lambda^2}{2\pi} \int \sum_{n=1}^{\infty} (2n+1) \left\{ \operatorname{Re}(a_n(x,m)) + \operatorname{Re}(b_n(x,m)) - |a_n(x,m)|^2 - |b_n(x,m)|^2 \right\} n(r) dr.$$

The values for α , s , and a used in the Monte Carlo routine were not calculated in this way because the values explicitly depend on the concentration through $n(r)$. Instead α , s , and a were chosen to correspond to physically observed values.

The absorption coefficient depends on the imaginary part of the index of refraction, but in a non-trivial way. If $\operatorname{Im}(m) = 0$ then it can be shown ⁽²⁵⁾ that

$$\left| a_n(x, m) - \frac{1}{2} \right|^2 = \frac{1}{4}$$

$$\left| b_n(x, m) - \frac{1}{2} \right|^2 = \frac{1}{4}$$

Expanding equation (A-4) leads to

$$[\operatorname{Re}(a_n(x, m))]^2 - \operatorname{Re}(a_n(x, m)) + [\operatorname{Im}(a_n(x, m))]^2 + \frac{1}{4} = \frac{1}{4}$$

or

$$\begin{aligned} \operatorname{Re}(a_n(x, m)) &= [\operatorname{Re}(a_n(x, m))]^2 + [\operatorname{Im}(a_n(x, m))]^2 \\ &= \left| a_n(x, m) \right|^2 \end{aligned}$$

with a similar result holding for $b_n(x, m)$. Using these results in equation (A-3) leads to $a=0$. Thus if the imaginary part of the index of refraction is zero the absorption coefficient is also zero.

If $\operatorname{Im}(m) \neq 0$ then (15)

$$\left| a_n(x, m) - \frac{1}{2} \right|^2 < \frac{1}{4}$$

$$\left| b_n(x, m) - \frac{1}{2} \right|^2 < \frac{1}{4}$$

Which, after expansion, leads to

$$\operatorname{Re}(a_n(x, m)) > \left| a_n(x, m) \right|^2$$

$$\operatorname{Re}(b_n(x, m)) > \left| b_n(x, m) \right|^2,$$

so that, by equation (A-3), $a>0$ for a non-zero imaginary component in the index of refraction.

APPENDIX B

LISTINGS FOR MONTE' CARLO ROUTINE

PRECEDING PAGE BLANK NOT FILED

IV G1 RELEASE 2.0

" MAIN

DATE = 77264

13/25/51

```
C
C
C      MONTECARLO PROGRAM WITH DOCUMENTATION
      DIMENSION FIS(100),TES(100),VALU(50),ANGL(50)
      READ (5,25) MAXNPH,NMAX,IS
      25 FORMAT (3(2X,I8))
      READ(5,30) TETAI,FII
      30 FORMAT(2(5X,F8.3))
      WRITE (6,26) MAXNPH
      26 FORMAT ('0','MAXIMUM NO. OF PHOTONS TRACED=',I8)
      WRITE (6,27)NMAX
      27 FORMAT ('0','MAXIMUM NO. OF EVENTS FOR EACH PHOTON=',I8)
      WRITE (6,29) IS
      29 FORMAT ('0','INITIAL SEED FOR RANDOM NO GENERATOR=',I8)
      WRITE (6,31) TETAI,FII
      31 FORMAT('0','INITIAL TETA IN D=',F8.3,'INITIAL FI IN DEG=',1F8.3)
C      MAXNPH IS THE MAXIMUM NO OF PHOTONS TRACED
C      NMAX IS THE MAXIMUM NO OF EVENTS FOR EACH PHOTON
      PI=3.141592654
      RNW=1.334
C      RNW IS THE REFRACTION INDEX OF WATER
      DTRE=PI/180.0
C      DTRE IS DEGREES TO RADIANS CONVERSION.
      TETAI=TETAI*DTRE
      FII = FII * DTRE
C      START THE CALCULATION
C      NPH IS DEFINED AS THE NO OF PHOTONS AT A GIVEN TIME
      NPH=0
      READ(9,5004) (ANGL(I),VALU(I),I=1,41)
      5004 FORMAT(F10.4,E15.6)
C      RECORDS NO OF PHOTONS TRACED
      10 IF (NPH.EQ.MAXNPH )GO TO 2000
C      TEST FOR END OF COMPUTATIONS
C      PHOTON ENTERS THE MEDIUM AT X=Y=Z=0
C      PHOTON ENTERS AT ANGLS TETAI, FII
      TETA=TETAI
      FI=FII
      X=0.
      Y=0.
      Z=0.000001
C      DECIDE HOW FAR PHOTON TRAVELS BEFORE AN EVENT OCCURS
      RHOD=RANDNO(IS)
      T=-ALGG(RHOD)
      GAMA=T
C      T IS THE DISTANCE IN S - 1 UNITS PHOTON TRAVELS TO THE EVENT
C      PHOTON IS AT
```

ORIGINAL PAGE IS
OF POOR QUALITY

N IV G1 RELEASE 2.0

MAIN

DATE = 77264

13/25/51

```
X = X+T*SIN(TETA)*COS(FI)
Y = Y+T*SIN(TETA)*SIN(FI)
Z = Z+T*COS(TETA)
GO TO 150
100 NPH=NPH+1
C      ABSORPTION HAS OCCURED, OR PHOTON HAS COME OUT OF WATER
C      START A NEW PHOTON
GO TO 10
150 CONTINUE
IF (Z) 400,500,500
400 XINT=X-Z*TAN(TETA)*COS(FI)
YINT=Y-Z*TAN(TETA)*SIN(FI)
WRITE(6,108) J
108 FORMAT(' ', 'J= ', 18)
DINT=SQRT(XINT**2+YINT**2)
IF (RNW*SIN(TETA).GT.1.0) GO TO 100
TETAAR=ARSIN(RNW*SIN(TETA))
IF(TETAAR .GT. 0.4)GO TO 100
WRITE (6,410) DINT,TETAAR
410 FORMAT(' ','DISTANCE FROM AXIS=',F8.5,5X,'POLAR ANGLE=',F8.5)
WRITE (6,420) FI,XINT,YINT
420 FORMAT (' ','AZIMUTH ANGLE=',F8.5,5X,'XINT=',F8.5,5X,'YINT=',F8.5
CTA=COS(TETA)
ACT=ABS(CTA)
TCUT=(ABS(ZR)-ABS(Z))/ACT
GAMA=GAMA+TCUT
WRITE(6,109) GAMA
WRITE(4,6002) GAMA
WRITE(8,6002) GAMA
WRITE(4,6002) DINT
WRITE(8,6002) DINT
6002 FORMAT(E12.6)
109  FORMAT('0','GAMA = ',F8.5)
WRITE(6,101) NPH
101  FORMAT('0','NO. OF PHOTONS TRACED = ',18)
JJ=J-1
WRITE(4,6001) JJ
WRITE(8,6001) JJ
6001 FORMAT(I5)
DO 5001 III=2,J
TES(III)=TES(III)/DTRC
WRITE(4,5003) FIS(III),TES(III)
WRITE(8,5003) FIS(III),TES(III)
5003 FORMAT(2F12.6)
5001 WRITE(6,5002) III,FIS(III),TES(III)
5002 FORMAT(5X,I3,5X,'FI=',F8.3,5X,'TETA=',F8.3)
      GO TO 100
500  CONTINUE
```

I IV G1 RELEASE 2.0

MAIN

DATE = 77264

13/25/51

```
C      Z>0 THIS MEANS PHOTON STILL IN WATER
C      DO 1290 J=2,NMAX
C      WHAT ARE THE COORDINATE OF THE END POINT IN THE NON-ROTATED SYSTEM
C      FIRST STEP IS TO ROTATE THE SYSTEM USING TETA AND FI
C      ROTATION MATRIX IS AIJ, FOR I=J=1-3.
C      GENERATION OF THE ROTATION MATRIX, WITH THE CONSTRAINT THAT Y-
C      AXIS LIES IN A PLANE PARALLEL TO THE YZ-PLANE
CT=CCS(TETA)
CF=CLS(FI)
CT2=CT*CT
CF2=CF*CF
ST=SIN(TETA)
SF=SIN(FI)
ST2=ST*ST
SF2=SF*SF
SS1=CT2+SF2*ST2
SS=SQRT(SS1)
SSD=1./SS
A11=SQRT(1.-CF2*ST2)
A12=-SF*CF*ST2*SSD
A13=-CT*ST*CF*SSD
A22=CT*SSD
A23=-SF*ST*SSD
A31=CF*ST
A33=CT
A32=SF*ST
C      ROTATION MATRIX HAS BEEN GENERATED
C      SCATTERING HAS OCCURED
C      CALL ANGELS FIP,TETAP TO DISTINGUISH FROM FI,TETA
C      FIP,TETAP ARE DETERMINED IN SYSTEM WITH Z-AXIS
C      PARALLEL TO THE INCIDENT DIRECTION
RHOF=RANDNO(IS)
FIP=2.*PI*RHOF
RHOT=RANDNO(IS)
C      PROBABILITY SCATTERING FUNCTION FOR POLAR ANGELS FOLLOWS
DC 1001 I=1,41
IF (RHOT .GE. VALU(I) .AND. RHOT .LE. VALU(I+1)) GOTO 1002
1001 CONTINUE
GO TO 2000
1002 TETA=ANGL(I)+(ANGL(I+1)-ANGL(I))*(RHOT-VALU(I))/(VALU(I+1)-VALU(I))
C      CONVERT TETA TO RADIANS
1011 TETA=TETA*DTRC
TETAP=TETA
C      HOW FAR BEFORE AN EVENT OCCURS, IN THE ROTATED SYSTEM
FIS(J)=FIP
TES(JJ)=TETAP
RHOD=RANDNO(IS)
```

ORIGINAL PAGE IS
OF POOR QUALITY

N IV G1 RELEASE 2.0

MAIN

DATE = 77264

13/25/51

```
T=-ALOG(RHOD)
C      CALCULATE COORDINATE OF END POINTS IN ROTATED SYSTEM
XSTAR=T*SIN(TETAP)*CCS(FIP)
YSTAR=T*SIN(TETAP)*SIN(FIP)
ZSTAR=T*COS(TETAP)
C      APPLY ROTATION MATRIX TO DETERMINE THE COORDINATE OF THE
C      END POINT IN A SYSTEM PARALLEL TO THE ORIGINAL ONE BUT
C      DISPLACED
XR=A11*XSTAR+A31*ZSTAR
YR=A12*XSTAR+A22*YSTAR+A32*ZSTAR
ZR=A13*XSTAR+A23*YSTAR+A33*ZSTAR
C      CALCULATE TETA AND FI IN THE PRESENT SYSTEM, WHICH IS
C      PARALLEL TO THE ORIGINAL ONE.
FI=ATAN(ABS(YR)/ABS(XR))
IF (XR.LT.0.0) GO TO 133
IF(YR) 333,333,633
333   FI=2.*PI-FI
GO TO 533
633   FI=FI
GO TO 533
133  IF(YR) 233,233,433
233  FI=FI+PI
GO TO 533
433  FI=PI-FI
533  CONTINUE
Xk2=XR*XR
YR2=YR*YR
ZR2=ZR*ZR
DT=XR2+YR2+ZR2
SQDT=SQRT(DT)
TETA=ARCCOS(ZR/SQDT)
C      CALCULATE X,Y,Z OF THE END POINT OF THE PHOTON IN RESPECT TO THE
C      ORIGINAL AXES
X=X+XR
Y=Y+YR
Z=Z+ZR
IF (Z) 400,400,700
700   GAMA=GAMA+T
1290  CONTINUE
GO TO 100
2000  WRITE (6,5000) IS
5000  FORMAT (' ', 'LAST RANDNO USED=', I10)
CALL EXIT
END
```

N IV G1 RELEASE 2.0

MAIN

DATE = 77264

13/25/51

```
C
C
      FUNCTION RANDNC(IX)
      IY=IX*65539
      IF(IY) 5,6,6
      5  IY=IY+2147483647+1
      6  XANDNO=IY
      RANDNC=RANDNO*.4656613E-9
      IX=IY
      RETURN
      END
```

APPENDIX C

LISTINGS FOR STOKES ROUTINE USED TO
CALCULATE THE STOKES PARAMETERS OF THE
BACKSCATTERED RADIANCE

N IV G1 RELEASE 2.0

MAIN

DATE = 77270

13/59/45

```
100 FORMAT(I5)
101 FORMAT(4F5.2)
104 FORMAT(2F12.6)
110 FORMAT(//T10,'STOKES VECTOR FOR PHOTON NO.',I5)
111 FORMAT(4E12.6)
113 FORMAT(//T10,'FINAL STOKES VECTOR')
114 FORMAT(4E12.6)
99 FORMAT(//T10,'POLARIZATION = ',F7.4)
REAL*8 THETA(4,4),SFINT(500,4),FINT(4),ROT(4,4),DINT(4),PHI(500),
1TETA(20),SMAT(50,6),STETA(42),SSFIN(4),SSIFI(4),GAMA,S(20),SRA(20)
1,RAD(500)
READ(4,150) AS
READ(4,100) NS
READ(4,100) NRAD
READ(4,150) (S(I),I=1,NS)
READ(4,150) (SRA(I),I=1,NRAD)
150 FORMAT(D12.6)
DG 120 J=1,41
READ(8,121) STETA(J),(SMAT(J,K),K=1,6)
120 CONTINUE
121 FORMAT(F10.4,5D12.6,F10.4)
READ(4,101) (DINT(I),I=1,4)
WRITE(6,130)
130 FORMAT(//T10,'INITIAL STOKES VECTOR')
WRITE(6,101) (DINT(I),I=1,4)
WRITE(6,131) AS
131 FORMAT(//T10,'A/S VALUE = ',F6.3)
DG 124 I=1,4
DC 125 J=1,4
THETA(1,J)=0.000
125 CONTINUE
FINT(I)=0.000
124 CONTINUE
L=1
102 READ(5,150,END=501) GAMA
READ(5,150) RAD(L)
READ(5,100) NSC
READ(5,104) (PHI(J),TETA(J),J=1,NSC)
DC 105 I=1,4
SFINT(L,I)=DINT(I)
105 CONTINUE
J=1
106 CONTINUE
RCT(1,1)=(DCOS(PHI(J)))**2
RCT(1,2)=(DSIN(PHI(J)))**2
RCT(1,3)=.5*DSIN(2*PHI(J))
ROT(1,4)=0.000
ROT(2,1)=ROT(1,2)
```

ORIGINAL PAGE IS
OF POOR QUALITY

c-2

IN IV G1 RELEASE 2.0

MAIN

DATE = 77270

13/59/45

```
      RCT(2,2)=ROT(1,1)
      RCT(2,3)=-ROT(1,3)
      RCT(2,4)=ROT(1,4)
      ROT(3,1)=2*ROT(2,3)
      ROT(3,2)=2*ROT(1,3)
      ROT(3,3)=DCOS(2*PHI(J))
      RCT(3,4)=ROT(1,4)
      ROT(4,1)=ROT(1,4)
      RLT(4,2)=ROT(1,4)
      ROT(4,3)=ROT(1,4)
      ROT(4,4)=1.000
      DC 122 K=1,41
      IF (TETA(J) .GE. STETA(K) .AND. TETA(J) .LE. STETA(K+1)) GOTO 123
122  CONTINUE
      GOTG 500
123  THETA(1,1)= SMAT(K,1)+(SMAT(K+1,1)-SMAT(K,1))*(TETA(J)-STETA(K))/1
     (STETA(K+1)-STETA(K))
      THETA(2,2)= SMAT(K,2)+(SMAT(K+1,2)-SMAT(K,2))*(TETA(J)-STETA(K))/1
     (STETA(K+1)-STETA(K))
      THETA(3,3)= SMAT(K,3)+(SMAT(K+1,3)-SMAT(K,3))*(TETA(J)-STETA(K))/1
     (STETA(K+1)-STETA(K))
      THETA(4,4)=THETA(3,3)
      THETA(4,3)= SMAT(K,4)+(SMAT(K+1,4)-SMAT(K,4))*(TETA(J)-STETA(K))/1
     (STETA(K+1)-STETA(K))
      THETA(3,4)=-THETA(4,3)
      THETN=.5*(THETA(1,1)+THETA(2,2))
      DC 160 I=1,4
      DC 161 JJ=1,4
      THETA(I,JJ)=THETA(I,JJ)/THETN
161  CONTINUE
160  CONTINUE
      DG 107 I=1,4
      SSFIN(I)=0.000
      DC 147 K=1,4
      SSFIN(I)=SSFIN(I)+ROT(I,K)*SFINT(L,K)
      SSSFI(I)=SSFIN(I)
147  CONTINUE
107  CONTINUE
      DG 170 I=1,4
      SFINT(L,I)=SSSFI(I)
170  CONTINUE
      DC 108 I=1,4
      SSFIN(I)=0.000
      DG 148 K=1,4
      SSFIN(I)=SSFIN(I)+THETA(I,K)*SFINT(L,K)
      SSSFI(I)=SSFIN(I)
148  CONTINUE
108  CONTINUE
```

ORIGINAL PAGE IS
OF POOR QUALITY

N IV GL RELEASE 2.0

MAIN

DATE = 77270

13/59/45

```
      DC 171 I=1,4
      SFINT(L,I)=SSSFI(I)
171  CGTINUE
      NSC=NSC-1
      J=J+1
      IF (NSC.GT.0) GOTO 106
      DC 109 I=1,4
      SFINT(L,I)=SFINT(L,I)*(DEXP(-AS*GAMA))
109  CGTINUE
      WRITE(6,110) L
      WRITE(6,111)(SFINT(L,I),I=1,4)
      NTGT=L
      L=L+1
      GOTC 102
501  DO 4002 N=1,NS
      DO 4003 M=1,NRAD
      SRAD=SRA(M)*S(N)
      NTOTT=0
      DG 5000 I=1,4
5000 FINT(I)=0.0D0
      DC 3999 L=1,NTOT
      IF(RAD(L).LE. SRAD) GO TO 4000
      GCTC 3999
4000 NTOTT=NTOTT+1
      DG 4001 I=1,4
4001 FINT(I)=FINT(I)+SFINT(L,I)
3999 CGTINUE
      WRITE(6,4004) S(N),SRA(M)
      WRITE(6,98) NTOTT
      98 FORMAT(//T10,'NUMBER OF PHOTONS USED = ',I5)
4004 FORMAT(//T10,'S VALUE=',E5.2,5X,'SPOT SIZE = ',F5.2)
      DC 112 I=1,4
112  FINT(I)=FINT(I)/NTOTT
      WRITE(6,113)
      WRITE(6,114) (FINT(I),I=1,4)
      PCLR=(FINT(1)-FINT(2))**2
      POLR=POLR+FINT(3)**2
      POLR=POLR+FINT(4)**2
      PCLR=SQRT(PCLR)
      POLR=POLR/(FINT(1)+FINT(2))
      WRITE(6,99) POLR
      RFAC=FINT(2)/FINT(1)
      WRITE(6,97) RFAC
      97 FORMAT(//T10,'R-FACTOR(EY/EX) = ',F7.4,/)
4003 CGTINUE
4002 CGTINUE
500  STOP
END
```

APPENDIX D

LISTINGS FOR POLYMIE AND DBMIE ROUTINES USED TO
CALCULATE THE VOLUME SCATTERING FUNCTIONS

ORIGINAL PAGE IS
OF POOR QUALITY

MAIN

```
C MAIN PROG POLYMIE(VECTOR)
C THE FOLLOWING DOUBLE PRECISION INPUTS ARE REQUIRED:
C RFR=REAL PART OF REFRACTIVE INDEX
C RFI=IMAGINARY PART OF REFRACTIVE INDEX
C RADU=UPPERBOUND ON RADIUS(MICRONS)
C WAVE=WAVELENGTH IN MICRONS
C A(I)=PARAMETERS FOR DISTRIBUTION ONE
C B(I)=PARAMETERS FOR DISTIBUTION TWO
C THETD(J)=VECTOR OF ANGLES FROM 0-90 (COMPLIMENTS ARE ALSO CALC)
C OTHER INPUTS ARE:
C JX=NUMBER OF ANGLES FROM 0-90
C NRAD=NUMBER OF RADII BETWEEN 0-RADU
C NPARA=NUMBER OF PARAMETERS IN DISTRIBUTION ONE
C NPARA2=NUMBER OF PARAMETERS IN DISTRIBUTION TWO
C TWO=LOGICAL VARIABLE TO ENABLE THE USE OF TWO DISTRIBUTIONS
C
C
C TWO FUNCTION SUBPROGRAMS DIST(RAD,A) AND DIST2(RAD,B) ARE REQUIRED
C IN ADDITION TO PD8MIE SUBROUTINE
C
C
C TWO DATA SETS (6 AND 8) ARE USED FOR OUTPUT; NORMALLY 6=PRINTER
C AND 8=TAPE
C
C
C
10 FORMAT(3D15.5)
11 FORMAT(2D15.5)
12 FORMAT(D15.5)
13 FORMAT(D15.5,15)
14 FORMAT(2I5)
15 FORMAT(L5)
16 FORMAT(I5)
17 FORMAT(D15.5)
20 FORMAT(1H1)
25 FORMAT(//T10,'ELEMENTS OF THE TRANSFORMATION MATRIX FOR A SPHERE
1WITH SIZE PARAMETER = ',F15.5)
30 FORMAT(//T10,'REFRACTIVE INDEX. REAL = ',D15.5,T60,'IMAGINARY',D15
1.5,/)
35 FORMAT(T3,'ANGLE',T17,'SIGMA1',T31,'SIGMA2',T46,'SIGMA3',T61,'SIGM
1A4',T76,'INTENSITY',T91,'POLARIZATION'//)
40 FORMAT(F10.4,5E15.6,F15.4)
45 FORMAT(//T10,' EFFICIENCY FACTOR FOR EXTINCTION',E15.6)
50 FORMAT(//T10,' EFFICIENCY FACTOR FOR SCATTERING',E15.6)
55 FORMAT(//T10,' EFFICIENCY FACTOR FOR ABSORPTION',E15.6)
60 FORMAT(//T10,' ASYMMETRY FACTOR',E15.6//)
70 FORMAT(//T10,' TOTAL TIME FOR THIS CASE IN SECONDS= ',F15.3//)
```

MAIN

```
2 FORMAT(//T10,'PROBABILITY FOR THIS SIZE PARAMETER = ',D15.5,/)
3 FORMAT(//T10,'NORMALIZATION FACTOR FOR THIS SET OF SIZE PARA=',
1D15.5,/)
  REAL*8 RFR,RFI,X,QEXT,QSCAT,QABS,THETD(100),PQEXT,PQSCAT,PQABS
80 FORMAT(//T10,'SCATTERING CROSS SECTION',E15.6)
  REAL*8 ELTRMX(4,100,2),ALAM,CON,CTBRQS,AVCSTH,PELTMX(4,100,2)
  REAL*8 PAVCTH,THE(100),PBSCAT
  REAL*4 AIN(100,2),POLR(100,2)
  REAL*4 PAIN(100,2),PPOLR(100,2)
  REAL*4 PAI(100,2),PPOL(100,2)
  REAL*8 PROB2,PNORM2
  REAL*8 PQEX,PQSCA,PQAB,PBSCA,PAVCT,PELTM(4,100,2)
  REAL*8 RADU,DRAD,WAVE,GAMMA,A(20),PROB,B(20)
  LOGICAL WRN,TWO
  WRN=.FALSE.
  CON=3.1415926535897932D+0
  INTEGER NPARA,NPARA2
90 READ (5,10) RFR,RFI,WAVE
  READ (5,14) JX,NPARA
  READ (5,12) (THETD(I),I=1,JX)
  READ (5,13) RADU,NRAD
1 FORMATT (D15.5)
  DO 5 I=1,NPARA
  READ (5,1) A(I)
5 CONTINUE
  READ(5,15) TWO
  DO 95 I=1,JX
95 THE(I)=THETD(I)
  IF (TWO) GO TO 61
  GO TO 62
61 READ(5,16) NPARA2
  DO 62 I=1,NPARA2
  READ(5,17) B(I)
62 CONTINUE
  PQEXT=0.0D0
  PQEX=0.0D0
  PQSCA=0.0D0
  PQAB=0.0D0
  PBSCA=0.0D0
  PAVCT=0.0D0
  PQSCAT=0.0D0
  PQABS=0.0D0
  PBSCAT=0.0D0
  PAVCTH=0.0D0
  DRAD=RADU/NRAD
  DO 1000 J=1,JX
  DO 1000 K=1,2
  DO 999 I=1,4
```

MAIN

```
PELTMX(I,J,K)=0.000
PELM(I,J,K)=0.000
999 CONTINUE
PAIN(J,K)=0.000
PAI(J,K)=0.000
PPOL(J,K)=0.000
PPOLR(J,K)=0.000
1000 CONTINUE
RAD=0.0
PNORM2=0.000
IF (TWO) GO TO 91
PNORM2=1.000
91 CONTINUE
PNORM=0.000
TIME1=0.0
DO 3000 L=1,NRAD
RAD=RAD+DRAD
DO 100 J=1,JX
100 THETD(J)=THE(J)
X=2.000*CON*RAD/WAVE
PROB=DIST(RAD,A)
IF (TWO) GO TO 63
PROB2=0.000
GO TO 64
63 PROB2=DIST2(RAD,B)
64 CALL SETCLK
CALL PDBMIE ( X,RFR,RFI,THETD,JX,QEXT,QSCAT,CTBRQS,ELTRMX,WRN)
CALL READCL(TIME)
IF (WRN) GO TO 1001
PNORM=PNORM+PROB
PNORM2=PNORM2+PROB2
TIME1=TIME1+TIME
QABS=QEXT-QSCAT
AVCSTH=CTBRQS/QSCAT
DO 150 K=1,2
DO 150 J=1,JX
AIN(J,K)= ELTRMX(1,J,K)+ELTRMX(2,J,K)
POLR(J,K)= (ELTRMX(2,J,K)-ELTRMX(1,J,K))/AIN(J,K)
AIN(J,K)= .5*AIN(J,K)
PAIN(J,K)=AIN(J,K)*PROB+PAIN(J,K)
PAI(J,K)=AIN(J,K)*PROB2+PAI(J,K)
PPOL(J,K)=POLR(J,K)*PROB2+PPOL(J,K)
PPOLR(J,K)=PPOLR(J,K)+POLR(J,K)*PROB
150 CONTINUE
DO 2000 I=1,4
DO 2000 J=1,JX
DO 2000 K=1,2
PELTMX(I,J,K)=PELTMX(I,J,K)+ELTRMX(I,J,K)*PROB
```

ORIGINAL PAGE IS
OF POOR QUALITY

MAIN

```
PELTM(I,J,K)=PELTM(I,J,K)+ELTRMX(I,J,K)*PROB2
2000 CONTINUE
      WRITE(6,20)
      WRITE(6,25) X
      WRITE(6,30) RFR,RFI
      WRITE(6,35)
      WRITE(6,40) ((THETD(J),(ELTRMX(I,J,1),I=1,4),AIN(J,1),POLR(J,1)),
      1J=1,JX)
C      WRITE(8,40) ((THETD(J),(ELTRMX(I,J,1),I=1,4),AIN(J,1),POLR(J,1)),
C      1J=1,JX)
      DO 200 J=1,JX
      THETD(J)= 180.0D0-THETD(J)
200 CONTINUE
      JMX=JX-1
      DO 210 J=1,JMX
      JJ=JX-J
      WRITE(6,40)(THETD(JJ),(ELTRMX(I,JJ,2),I=1,4),AIN(JJ,2),POLR(JJ,2))
C      WRITE(8,40)(THETD(JJ),(ELTRMX(I,JJ,2),I=1,4),AIN(JJ,2),POLR(JJ,2))
210 CONTINUE
      WRITE(6,45) QEXT
      WRITE(6,50) QSCAT
      WRITE(6,55) QABS
      WRITE(6,60) AVCSTH
      WRITE(6,2) PROB
      WRITE(6,2) PROB2
      WRITE(6,20)
      WRITE(6,70) TIME
      PQSCAT=PQSCAT+QSCAT*PROB
      PQSCA=PQSCA+QSCAT*PROB2
      PQEX=PQEX+QEXT*PROB2
      PQAB=PQAB+QABS*PROB2
      PBSCA=PBSCA+QSCAT*(RAD**2)*PROB2
      PAVCT=PAVCT+AVCSTH*PROB2
      PQEXT=PQEXT+QEXT*PROB
      PQABS=PQABS+QABS*PROB
      PBSCAT=PBSCAT+QSCAT*(RAD**2)*PROB
      PAVCTH=PAVCTH+AVCSTH*PROB
1001 WRN=.FALSE.
3000 CONTINUE
      DO 4000 J=1,JX
      DO 4000 K=1,2
      DO 4001 I=1,4
      PELEMX(I,J,K)=PELEMX(I,J,K)/PNORM
      PELEM(I,J,K)=PELEM(I,J,K)/PNORM2
4001 CONTINUE
      PAIN(J,K)=PAIN(J,K)/PNORM
      PAI(J,K)=PAI(J,K)/PNORM2
      PPOL(J,K)=PPOL(J,K)/PNORM2
```

```

      ' MAIN

      PPOLR(J,K)=PPOLR(J,K)/PNORM
4000 CONTINUE
C     END FILE 8
      PQSCAT=PQSCAT/PNORM
      PQEXT=PQEXT/PNORM
      PQABS=PQABS/PNORM
      PBSCAT=PBSCAT*CON/PNORM
      PAVCTH=PAVCTH/PNORM
      PQSCA=PQSCA/PNORM2
      PQEX=PQEX/PNORM2
      PQAB=PQAB/PNORM2
      PBSCA=PBSCA*CON/PNORM2
      PAVCT=PAVCT/PNORM2
      DO 6000 J=1,JX
6000 THETD(J)=THE(J)
      WRITE(6,20)
65 FORMAT(//T10,'ELEMENTS OF TRANFORMATION MATRIX FOR POLYDISPERSION'
1,/)
      WRITE(6,65)
      WRITE(6,30) RFR,RFI
      WRITE(6,35)
      WRITE(6,40) ((THETD(J),(PELTMX(I,J,1),I=1,4),PAIN(J,1),PPOLR(J,1)
1),J=1,JX)
C      WRITE(8,40) ((THETD(J),(PELTMX(I,J,1),I=1,4),PAIN(J,1),PPOLR(J,1)
C 1),J=1,JX)
      DO 5000 J=1,JX
      THETD(J)=180.000-THETD(J)
5000 CONTINUE
      JMX=JX-1
      DO 5001 J=1,JMX
      JJ=JX-J
      WRITE(6,40) (THETD(JJ),(PELTMX(I,JJ,2),I=1,4),PAIN(JJ,2),PPOLR
1(JJ,2))
C      WRITE(8,40) (THETD(JJ),(PELTMX(I,JJ,2),I=1,4),PAIN(JJ,2),PPOLR
C 1(JJ,2))
5001 CONTINUE
C     END FILE 8
      WRITE(6,45) PQEXT
      WRITE(6,50) PQSCAT
      WRITE(6,55) PQABS
      WRITE(6,80) PBSCAT
      WRITE(6,60) PAVCTH
      WRITE(6,3) PNORM
      WRITE(6,70) TIME1
      WRITE(6,20)
      DO 5010 J=1,JX
5010 THETD(J)=THE(J)
      IF (TWO) GOTO 5002

```

MAIN

ORIGINAL PAGE IS
OF POOR QUALITY

```

5002 GO TO 5003
      WRITE(6,20)
      WRITE(6,65)
      WRITE(6,30) RFR,RFI
      WRITE(6,35)
      WRITE(6,40) ((THETD(J),(PELTM(I,J,1),I=1,4),PAI(J,1),PPOL(J,1)
      I),J=1,JX)
C      WRITE(8,40) ((THETD(J),(PELTM(I,J,1),I=1,4),PAI(J,1),PPOL(J,1)
C      I),J=1,JX)
      DO 5004 J=1,JX
      THETD(J)=180.0D0-THETD(J)
5004 CONTINUE
      JMX=JX-1
      DO 5005 J=1,JMX
      JJ=JX-J
      WRITE(6,40) (THETD(JJ),(PELTM(I,JJ,2),I=1,4),PAI(JJ,2),PPOL
      I(JJ,2))
C      WRITE(8,40) (THETD(JJ),(PELTM(I,JJ,2),I=1,4),PAI(JJ,2),PPOL
C      I(JJ,2))
5005 CONTINUE
C      END FILE 8
      WRITE(6,45) PQEX
      WRITE(6,50) PQSCA
      WRITE(6,55) PQAB
      WRITE(6,80) PBSCA
      WRITE(6,60) PAVCT
      WRITE(6,3) PNORM2
      WRITE(6,70) TIME1
      WRITE(6,20)
5003 STOP
      END

```

PDBMIE

```

SUBROUTINE PDBMIE (X,RFR,RFI,THETD,JX,QEXT,QSCAT,CTBRQS,ELTRMX,WRN)
1) RADIATION SCATTERED BY A SPHERE. THIS SUBROUTINE CARRIES OUT ALL
C SUBROUTINE FOR COMPUTING THE PARAMETERS OF THE ELECTROMAGNETIC
C COMPUTATIONS IN SINGLE PRECISION ARITHMETIC.
C THIS SUBROUTINE COMPUTES THE CAPITAL A FUNCTION BY MAKING USE OF
C DOWNWARD RECURRENCE RELATIONSHIP.
C X O SIZE PARAMETER OF THE SPHERE,( 2 * PI * RADIUS OF THE SPHERE)/
C WAVELENGTH OF THE INCIDENT RADIATION).
C RFO REFRACTIVE INDEX OF THE MATERIAL OF THE SPHERE. COMPLEX
C QUANTITY..FORMO (RFR - I + RFI )
C THETD(J) O ANGLE IN DEGREES BETWEEN THE DIRECTIONS OF THE INCIDENT
C AND THE SCATTERED RADIATION. THETD(J) IS > OR = 90.0.
C IF THETD(J) SHOULD HAPPEN TO BE GREATER THAN 90.0, ENTER WITH
C SUPPLEMENTARY VALUEO SEE COMMENTS BELOW ON ELTRMX..
C JXO TOTAL NUMBER OF THETD FOR WHICH THE COMPUTATION AREREQUIRED.
C JX SHOULD NOT EXCEED 200 UNLESS THE DIMENSIONS STATEMENTS
C ARE APPROPRIATELY MODIFIED.
C MAIN PROGRAM SHOULD ALSO HAVE REAL THETD(200),ELTRMX(4,200,2).
C DEFINITIONS FOR THE FOLLOWING SYMBOLS CAN BE FOUND IN ' LIGHT
C SCATTERING BY SMALL PARTICLES, H. C. VAN DE HULST, JOHN WILEY +
C SONS, INC., NEW YORK, 1957 '.
C QEXT82 EFFICIENCY FACTOR FOR EXTINCTION, VAN DE HULST, P.14 + 127
C QSCAT82 EFFICIENCY FACTOR FOR SCATTERING,VAN DE HULST,P.14 + 127.
C CTBRQSJ AVERAGE(COSINE THETA) * QSCAT,VAN DE HULST, P. 128.
C ELTRMX(I,J,K) O ELEMENTS OF THE TRANSFORMATION MATRIX F,VAN DE HUL
C ST,P.34,45 + 125. I = 10 ELEMENT M SUB 2..I = 20ELEMENT M SUB 1..
C I = 30 ELEMENT S SUB 21.. I = 40 ELEMENT D SUB 21...
C ELTRMX(I,J,1) REPRESENTS THE ITH ELEMENT OF THE MATRIX FOR
C THE ANGLE THETD(J).. ELTRMX(I,J,2) REPRESENTS THE ITH ELEMENT
C OF THE MATRIX FOR THE ANGLE 180.0 - THETD(J) ..
5 FORMAT(10X' THE VALUE OF THE SCATTERING ANGLE IS GREATER THAN 90.0
$ DEGREES. IT IS ',E15.4)
6 FORMAT(//10X' PLEASE READ THE COMMENTS'//)
7 FORMAT(//10X' THE VALUE OF THE ARGUMENT JX IS GREATER THE 100'')
8 FORMAT(//10X' THE UPPER LIMIT FOR ACAP IS NOT ENOUGH. SUGGEST GET
1DETAILED OUTPUT AND MODIFY SUBROUTINE'//)
REAL*8 X,RX,RFR,RFI,QEXT,QSCAT,T(5),TA(4),TB(2),TC(2),TD(2),TE(2),
2 CTBRQS,ELTRMX(4,100,2),PI(3,100),TAU(3,100),
3 CSTHT(100),SI2THT(100),THETD(100)
COMPLEX*16 RF,RRF,RRFX,WM1,FNA,FNB,TC1,TC2,WFN(2),ACAP(8000),
2 FNAP,FNBP
LOGICAL WRN
9 FORMAT(//T10,'WARNING,ACCURACY NOT ACHIEVED'//)
C TA(1)O REAL PART OF WFN(1).. TA(2)O IMAGINARY PART OF WFN(1)..
C TA(3)O REAL PART OF WFN(2).. TA(4)O IMAGINARY PART OF WFN(2)..
C TB(1)O REAL PART OF FNA...TB(2)O IMAGINARY PART OF FNA...
C TC(1)O REAL PART OF FNB...TC(2)O IMAGINARY PART OF FNB...

```

ORIGINAL PAGE IS
OF POOR QUALITY

PDBMIE

```
C TD(1)0 REAL PART OF FNAP.. TD(2) IMAGINARY PART OF FNAP...
C TE(1)0 REAL PART OF FNBP... TE(2)0 IMAGINARY PART OF FNBP...
C FNAP + FNBP ARE THE PRECEDING VALUES OF FNA + FNB RESPECTIVELY.
C EQUIVALENCE (WFN(1), TA(1)), (FNA, TB(1)), (FNB, TC(1))
C EQUIVALENCE (FNAP, TD(1)), (FNBP, TE(1))
C IF ( JX .LT. 101 ) GO TO 20
C WRITE (6, 7)
C WRITE(6, 6)
C STOP 1
20 RF=DCMPLX(RFR,-RFI)
  RRF = 1.0D0/RF
  RX = 1.0D0/X
  RRFX = RRF * RX
  T(1)=(X**2)*(RRF**2+RFI**2)
  T(1)=DSQRT(T(1))
  NMX1 = 1.10D0 * T(1)
  IF (NMX1 .LT. 7999) GO TO 21
  WRITE(6, 8)
  STOP 2
21 NMX2 = T(1)
  IF (NMX1 .GT. 150) GO TO 22
  NMX1 = 150
  NMX2 = 135
22 ACAP(NMX1 + 1) = ( 0.0D0, 0.0D0 )
  DO 23 N = 1, NMX1
  NN = NMX1 - N + 1
  ACAP(NN) = (NN+1) * RRFX - 1.0D0/((NN+1)*RRFX + ACAP(NN+1))
23 CONTINUE
  DO 30 J = 1, JX
  IF ( THETD(J) .LT. 0.0D0 ) THETD(J) = DABS(THETD(J))
  IF ( THETD(J) .GT. 0.0D0 ) GO TO 24
  CSTHT(J) = 1.0D0
  SI2THT(J) = 0.0D0
  GO TO 30
24 IF ( THETD(J) .GE. 90.0D0 ) GO TO 25
  T(1) = ( 3.1415926535897932D+0 * THETD(J))/180.D0
  CSTHT(J) = DCOS(T(1))
  SI2THT(J) = 1.0D0 - CSTHT(J)**2
  GO TO 30
25 IF ( THETD(J) .GT. 90.0D0 ) GO TO 28
  CSTHT(J) = 0.0D0
  SI2THT(J) = 1.0D0
  GO TO 30
28 WRITE (6, 5) THETD(J)
  WRITE(6,6)
  STOP 3
30 CONTINUE
  DO 35 J = 1, JX
```

PDBMIE

```

PI(1,J) = 0.000
PI(2,J) = 1.000
.
TAU(1,J) = 0.000
300 TAU(2,J) = CSTHT(J)
35 CONTINUE
T(1) = DCOS(X)
T(2) = DSIN(X)
WM1=DCMPLX(T(1),-T(2))
WFN(1)=DCMPLX(T(2),T(1))
WFN(2) = RX * WFN(1) - WM1
TC1 = ACAP(1) * RRF + RX
TC2 = ACAP(1) * RF + RX
FNA = (TC1 * TA(3) - TA(1)) / (TC1 * WFN(2) - WFN(1))
FNB = (TC2 * TA(3) - TA(1)) / (TC2 * WFN(2) - WFN(1))
FNAP = FNA
FNBP = FNB
T(1) = 1.50D0
TB(1) = T(1) * TB(1)
TB(2) = T(1) * TB(2)
TC(1) = T(1) * TC(1)
TC(2) = T(1) * TC(2)
DO 60 J =1,JX
ELTRMX(1,J,1) = TB(1) * PI(2,J) + TC(1) * TAU(2,J)
ELTRMX(2,J,1) = TB(2) * PI(2,J) + TC(2) * TAU(2,J)
ELTRMX(3,J,1) = TC(1) * PI(2,J) + TB(1) * TAU(2,J)
ELTRMX(4,J,1) = TC(2) * PI(2,J) + TB(2) * TAU(2,J)
ELTRMX(1,J,2) = TB(1) * PI(2,J) - TC(1) * TAU(2,J)
ELTRMX(2,J,2) = TB(2) * PI(2,J) - TC(2) * TAU(2,J)
ELTRMX(3,J,2) = TC(1) * PI(2,J) - TB(1) * TAU(2,J)
ELTRMX(4,J,2) = TC(2) * PI(2,J) - TB(2) * TAU(2,J)
60 CONTINUE
QEXT = 2.000 * ( TB(1) + TC(1) )
QSCAT =(TB(1)**2 + TB(2)**2 + TC(1)**2 + TC(2)**2)/0.75D0
CTBRQS = 0.000
N = 2
65 T(1) = 2 * N - 1
T(2) = N - 1
T(3) = 2 * N + 1
D070J=1,JX
PI(3,J)=(T(1)*PI(2,J)*CSTHT(J)-N*PI(1,J))/T(2)
TAU(3,J)=CSTHT(J)*(PI(3,J)-PI(1,J))-T(1)*SI2THT(J)*PI(2,J)+TAU(1,J)
1)
70 CONTINUE
WM1 = WFN(1)
WFN(1) = WFN(2)
WFN(2) = T(1) * RX * WFN(1) - WM1
TC1 = ACAP(N) * RRF + N * RX
TC2 = ACAP(N) * RF + N * RX

```

PDBMIE

ORIGINAL PAGE
IF POOR QUALITY

```
FNA = (TC1 * TA(3) - TA(1)) / (TC1 * WFN(2) - WFN(1))
FNB = (TC2 * TA(3) - TA(1)) / (TC2 * WFN(2) - WFN(1))
T(5) = N
T(4) = T(1) / (T(5) + T(2))
T(2) = (T(2)*(T(5) + 1.0D0))/T(5)
CTBRQS = CTBRQS + T(2) + (TD(1) * TB(1) + TD(2) * TB(2) + TE(1) +
$TC(1) + TE(2) * TC(2)) + T(4) * (TD(1) * TE(1) + TD(2) + TE(2))
QEXT = QEXT + T(3) * (TB(1) + TC(1))
T(4) = TB(1)**2 + TB(2)**2 + TC(1)**2 + TC(2)**2
QSCAT = QSCAT + T(3) + T(4)
T(2) = N + (N + 1)
T(1) = T(3) / T(2)
K = (N / 2) + 2
DO 80 J = 1, JX
ELTRMX(1,J,1)=ELTRMX(1,J,1)+T(1)*(TB(1)*PI(3,J)+TC(1)*TAU(3,J))
ELTRMX(2,J,1)=ELTRMX(2,J,1)+T(1)*(TB(2)*PI(3,J)+TC(2)*TAU(3,J))
ELTRMX(3,J,1)=ELTRMX(3,J,1)+T(1)*(TC(1)*PI(3,J)+TB(1)*TAU(3,J))
ELTRMX(4,J,1)=ELTRMX(4,J,1)+T(1)*(TC(2)*PI(3,J)+TB(2)*TAU(3,J))
IF(K.EQ.N) GO TO 75
ELTRMX(1,J,2)=ELTRMX(1,J,2)+T(1)*(TB(1)*PI(3,J)-TC(1)*TAU(3,J))
ELTRMX(2,J,2)=ELTRMX(2,J,2)+T(1)*(TB(2)*PI(3,J)-TC(2)*TAU(3,J))
ELTRMX(3,J,2)=ELTRMX(3,J,2)+T(1)*(TC(1)*PI(3,J)-TB(1)*TAU(3,J))
ELTRMX(4,J,2)=ELTRMX(4,J,2)+T(1)*(TC(2)*PI(3,J)-TB(2)*TAU(3,J))
GOTO80
75 ELTRMX(1,J,2)=ELTRMX(1,J,2)+T(1)*(-TB(1)*PI(3,J)+TC(1)*TAU(3,J))
ELTRMX(2,J,2)=ELTRMX(2,J,2)+T(1)*(-TB(2)*PI(3,J)+TC(2)*TAU(3,J))
ELTRMX(3,J,2)=ELTRMX(3,J,2)+T(1)*(-TC(1)*PI(3,J)+TB(1)*TAU(3,J))
ELTRMX(4,J,2)=ELTRMX(4,J,2)+T(1)*(-TC(2)*PI(3,J)+TB(2)*TAU(3,J))
80 CONTINUE
IF( T(4) .LT. 1.0D-14 ) GO TO 100
N = N + 1
DO 90 J = 1, JX
PI(1, J) = PI(2, J)
PI(2, J) = PI(3, J)
TAU(1, J) = TAU(2, J)
TAU(2, J) = TAU(3, J)
90 CONTINUE
FNAP = FNA
FNBP = FNB
IF (N .LE. NMIX2) GO TO 65
WRITE(6, 9)
WRN = .TRUE.
RETURN
100 DO120J=1,JX
DO120K=1,2
DO115I=1,4
T(I)=ELTRMX(I,J,K)
115 CONTINUE
```

PDBMIE

```
ELTRMX(2,J,K) = T(1)**2 + T(2)**2
ELTRMX(1,J,K) = T(3)**2 + T(4)**2
ELTRMX(3,J,K) = T(1)*T(3) + T(2)*T(4)
ELTRMX(4,J,K) = T(2)*T(3) - T(4)*T(1)
120 CONTINUE .
T(1) = 2.0D0 * RX**2
QEXT = QEXT * T(1)
QSCAT = QSCAT * T(1)
CTBRQS = 2.0D0 * CTBRQS * T(1)
RETURN
END
```

DIST

```
FUNCTION DIST(RAD,A)
REAL*8 A(20),RAD
REAL*8 DIST,B,C
B=-A(3)
C=RAD**A(4)
C=B*C
DIST=A(1)*(RAD**A(2))*DEXP(C)
RETURN
END
```

ORIGINAL PAGE IS
OF POOR QUALITY

DIST2

```
FUNCTION DIST2(RAD,B)
REAL*8 B(20),RAD
REAL*8 DIST2,A
A=-(B(2)+1)
DIST2=B(1)*B(2)*(RAD**A)
RETURN
END
```

ORIGINAL PAGE IS
IF POOR QUALITY

APPENDIX E

PROGRAM LISTING FOR CURFIT ROUTINE USED TO FIT THE
THEORETICAL SIZE DISTRIBUTIONS TO THE EMPERICAL DATA

```

MAIN

C SUBROUTINE CURFIT
C
C MAKES A LEAST SQUARES FIT TO A NON-LINEAR FUNCTION
C
C DESCRIPTION OF PARAMETERS
C X      -ARRAY OF IND. VARIABLE DATA POINTS
C Y      -ARRAY OF DEP. VARIABLE DATA POINTS
C SIGMAY -ARRAY OF STANDARD DEVIATIONS FOR Y DATA POINTS
C NPTS   -NUMBER OF DATA POINTS
C NTERMS -NUMBER OF PARAMETERS
C MODE   -DETERMINES WEIGHTING FOR LEAST SQUARES FIT
C           +1(INSTRUMENTAL) W(I)=1./SIGMAY(I)**2
C           0(NO WEIGHTING) W(I)=1.
C           -1(STATISTICAL) W(I)=1./Y(I)
C A      -ARRAY OF PARAMETERS
C DELTAA -ARRAY OF INCREMENTS FOR PARAMETERS
C FLAMDA -PROPORTION OF GRADIENT SEARCH INCLUDED
C YFIT   -ARRAY OF CALCULATED VALUES OF Y
C CHISQR -REDUCED CHI SQUARE FOR FIT
C
C SUBROUTINES AND FUNCTION SUBPROGRAMS REQUIRED
C FUNCTN(X,I,A)
C     EVALUATES THE FITTING FUNCTION FOR THE ITH TERM
C SSP ROUTINE DSINV
C     INVERTS CURVATURE MATRIX
C
C COMMENTS
C DATA FORMAT
C     NPTS,NTERMS,MODE(3I5)
C     X(I),Y(I),(SIGMAY(I)),(2{3}E12.6)
C     DIMENSION X(100),Y(100),SIGMAY(100),A(20),DELTAA(20),SIGMAA(20),
C     1YFIT(100),YFITI(100)
C     LOGICAL GRAD,CUR,GRID
21 FORMAT(3L5)
    READ(5,21) GRAD,CUR,GRID
    READ(5,1) NPTS,NTERMS,MODE
1 FORMAT(3I5)
    IF (MODE) 2,2,4
2 READ(5,3) (X(I),Y(I),I=1,NPTS)
3 FORMAT(2E12.6)
    GO TO 6
4 READ(5,5) (X(I),Y(I),SIGMAY(I),I=1,NPTS)
5 FORMAT(3E12.6)
6 READ(5,7) (A(J),DELTAA(J),J=1,NTERMS)
7 FORMAT(2E12.6)
    ISUM=0
    CHISQ1=1.0
14 FLAMDA=.001

```

ORIGINAL PAGE IS
OF POOR QUALITY

ORIGINAL PAGE IS
OF POOR QUALITY

MAIN

```
IF(CUR) GO TO 22
IF(GRID) GO TO 23
CALL GRADLS(X,Y,SIGMAY,NPTS,NTERMS,MODE,A,DELTA,
1YFIT,CHISQR)
GO TO 24
22 CALL CURFIT(X,Y,SIGMAY,NPTS,NTERMS,MODE,A,DELTA,
1YFIT,CHISQR)
GO TO 24
23 CALL GRIDLS(X,Y,SIGMAY,NPTS,NTERMS,MODE,A,DELTA,
1SIGMAA,YFIT,CHISQR)
GO TO 24
24 PRINT 8, {A(J),J=1,NTERMS}
8 FORMAT(' ',E12.6)
PRINT 9,CHISQR
9 FORMAT(' ','CHISQR=',1X,E12.6,/)
IF (CHISQ1-CHISQR) 12,13,12
12 CHISQ1=CHISQR
ISUM=ISUM+1
IF (ISUM-10) 14,13,13
13 DO 11 I=1,NPTS
11 YFITI(I)=1./YFIT(I)
PRINT 10
10 FORMAT(' ',13X,'IND.VAR.',12X,'DEP.VAR.',11X,'INV.DEP.VAR.',/)
PRINT 15,(X(I),YFIT(I),YFITI(I),I=1,NPTS)
15 FORMAT(' ',10X,E12.6,8X,E12.6,8X,E12.6)
STOP
END
```

CURFIT

```
SUBROUTINE CURFIT(X,Y,SIGMAY,NPTS,NTERMS,MODE,A
1,DELTAA,SIGMAA,FLAMCA,YFIT,CHISQR)
DOUBLE PRECISION ARRAY
DIMENSION X(100),Y(100),SIGMAY(100),A(20),DELTAA(20),SIGMAA(20),
1YFIT(100),WEIGHT(100),ALPHA(20,20),BETA(20),DERIV(20),ARRAY(20,
120),B(20)
11 NFREE=NPTS-NTERMS
   IF (NFREE) 13,13,20
13 CHISQR=0.
   GO TO 110
C EVALUATE WEIGHTS
20 DO 30 I=1,NPTS
21 IF (MCDE) 22,27,29
22 IF (Y(I)) 25,27,23
23 WEIGHT(I)=1./Y(I)
   GO TO 30
25 WEIGHT(I)=1./(Y(I))
   GC TO 30
27 WEIGHT(I)=1.
   GO TO 30
29 WEIGHT(I)=1./SIGMAY(I)**2
30 CONTINUE
C EVALUATE ALPHA AND BETA MATRICES
31 DO 34 J=1,NTERMS
   BETA(J)=0.
   DO 34 K=1,J
34 ALPHA(J,K)=0.
41 DO 50 I=1,NPTS
   CALL FDERIV(X,I,A,DELTAA,NTERMS,DERIV)
   DO 46 J=1,NTERMS
      BETA(J)=BETA(J)+WEIGHT(I)*(Y(I)-FUNCTN(X,I,A))*DERIV(J)
   DO 46 K=1,J
46 ALPHA(J,K)=ALPHA(J,K)+WEIGHT(I)*DERIV(J)*DERIV(K)
50 CONTINUE
51 DO 53 J=1,NTERMS
   DO 53 K=1,J
53 ALPHA(K,J)=ALPHA(J,K)
C EVALUATE CHISQR AT STARTING POINT
61 DO 62 I=1,NPTS
62 YFIT(I)=FUNCTN(X,I,A)
63 CHISQ1=FCHISQ(Y,SIGMAY,NPTS,NFREE,MODE,YFIT)
C INVERT CURVATURE MATRIX TO FIND NEW PARAMETERS
71 DO 74 J=1,NTERMS
72 DO 73 K=1,NTERMS
73 ARRAY(J,K)=ALPHA(J,K)/SQRT(ALPHA(J,J)*ALPHA(K,K))
74 ARRAY(J,J)=1.+FLAMDA
80 CALL MATINV(ARRAY,NTERMS,1)
81 DO 84 J=1,NTERMS
```

CURFIT

```
B(J)=A(J)
DO 84 K=1,NTERMS
84 B(J)=B(J)+BETA(K)*ARRAY(J,K)/SQRT(ALPHA(J,J)*ALPHA(K,K)).
C IF CHI SQUARE INCREASED, INCREASE FLAMDA
91 DO 92 I=1,NPTS
92 YFIT(I)=FUNCTN(X,I,B)
93 CHISQR=FCHISQ(Y,SIGMAY,NPTS,NFREE,MODE,YFIT),
IF (CHISQ1-CHISQR) 95,101,101
95 FLAMDA=10.*FLAMDA
GO TO 71
101 DO 103 J=1,NTERMS
103 A(J)=B(J)
FLAMDA=FLAMDA/10.
110 RETURN
END
```

ORIGINAL PAGE IS
OF POOR QUALITY

FDERIV

```
SUBROUTINE FDERIV(X,I,A,DELTAA,NTERMS,DERIV)
DIMENSION X(100),A(20),DELTAA(20),DERIV(20)
11 DO 18 J=1,NTERMS
AJ=A(J)
DELTAA=DELTAA(J)
A(J)=AJ+DELTAA
YFIT=FUNCTN(X,I,A)
A(J)=AJ-DELTAA
DERIV(J)=(YFIT-FUNCTN(X,I,A))/(2.*DELTAA)
18 A(J)=AJ
RETURN
END
```

MATINV

```
SUBROUTINE MATINV(ARRAY,NTERMS,MCODE)
DOUBLE PRECISION ARRAY,B
DIMENSION ARRAY(20,20),B(210)
DO 1 I=1,NTERMS
DO 1 J=1,NTERMS
CALL LOC(I,J,IJ,NTERMS,NTERMS,MCODE)
1 B(IJ)=ARRAY(I,J)
EPS=1.0E-16
CALL DSINV(B,NTERMS,EPS,IER)
IF (IER) 2,4,3
2 PRINT 10
10 FORMAT(' ','NO RESULT',/)
GO TO 4
3 PRINT 11
11 FORMAT(' ','WARNING',/)
4 DO 5 I=1,NTERMS
DO 5 J=1,NTERMS
CALL LOC(I,J,IJ,NTERMS,NTERMS,MCODE)
5 ARRAY(I,J)=B(IJ)
RETURN
END
```

ORIGINAL PAGE IS
OF POOR QUALITY

FCHISQ

```
FUNCTION FCHISQ(Y,SIGMAY,NPTS,NFREE,MODE,YFIT)
DIMENSION Y(100),SIGMAY(100),YFIT(100)
SUM=0.
DO 5 I=1,NPTS
IF(MODE) 1,2,3
1 W=1./Y(I)
GO TO 4
2 W=1.
GO TO 4
3 W=1./(SIGMAY(I)**2)
4 SUM=(Y(I)-YFIT(I))*(Y(I)-YFIT(I))*W
5 CONTINUE
FCHISQ=SUM/NFREE
RETURN
END
```

ORIGINAL PAGE IS
OF POOR QUALITY

C
C
C SUBROUTINE DSINV
C
C PURPOSE
C INVERT A GIVEN SYMMETRIC POSITIVE DEFINITE MATRIX
C
C USAGE
C CALL DSINV(A,N,EPS,IER)
C
C DESCRIPTION OF PARAMETERS
C A - DOUBLE PRECISION UPPER TRIANGULAR PART OF GIVEN
C SYMMETRIC POSITIVE DEFINITE N BY N COEFFICIENT
C MATRIX.
C ON RETURN A CONTAINS THE RESULTANT UPPER
C TRIANGULAR MATRIX IN DOUBLE PRECISION.
C N - THE NUMBER OF ROWS (COLUMNS) IN GIVEN MATRIX.
C EPS - SINGLE PRECISION INPUT CONSTANT WHICH IS USED
C AS RELATIVE TOLERANCE FOR TEST ON LOSS OF
C SIGNIFICANCE.
C IER - RESULTING ERROR PARAMETER CODED AS FOLLOWS
C IER=0 - NO ERROR
C IER=-1 - NO RESULT BECAUSE OF WRONG INPUT PARAM-
C ETER N OR BECAUSE SOME RADICAND IS NON-
C POSITIVE (MATRIX A IS NOT POSITIVE
C DEFINITE, POSSIBLY DUE TO LOSS OF SIGNI-
C FICANCE)
C IER=K - WARNING WHICH INDICATES LOSS OF SIGNIFI-
C CANCE. THE RADICAND FORMED AT FACTORIZA-
C TION STEP K+1 WAS STILL POSITIVE BUT NO
C LONGER GREATER THAN ABS(EPS^K*A(K+1,K+1)).
C
C REMARKS —
C THE UPPER TRIANGULAR PART OF GIVEN MATRIX IS ASSUMED TO BE
C STORED COLUMNWISE IN N*(N+1)/2 SUCCESSIVE STORAGE LOCATIONS.
C IN THE SAME STORAGE LOCATIONS THE RESULTING UPPER TRIANGU-
C LAR MATRIX IS STORED COLUMNWISE TOO.
C THE PROCEDURE GIVES RESULTS IF N IS GREATER THAN 0 AND ALL
C CALCULATED RADICANDS ARE POSITIVE.
C
C SUBROUTINES AND FUNCTION SUBPROGRAMS REQUIRED
C DMFSD
C
C METHOD
C SOLUTION IS DONE USING FACTORIZATION BY SUBROUTINE DMFSD.
C
C

```

C      SUBROUTINE DSINV(A,N,EPS,IER)
C
C      DIMENSION A(210)
C      DOUBLE PRECISION A,DIN,WORK
C
C      FACTORIZE GIVEN MATRIX BY MEANS OF SUBROUTINE DMFSD
C      A = TRANSPOSE(T) * T
C      CALL DMFSD(A,N,EPS,IER)
C      IF(IER) 9,1,1
C
C      INVERT UPPER TRIANGULAR MATRIX T
C      PREPARE INVERSION-LOOP
1 IPIV=N*(N+1)/2
IND=IPIV
C
C      INITIALIZE INVERSION-LOOP
DO 6 I=1,N
DIN=1.0/A(IPIV)
A(IPIV)=DIN
MIN=N
KEND=I-1
LANF=N-KEND
IF(KEND) 5,5,2
2 J=IND
C
C      INITIALIZE ROW-LOOP
DO 4 K=1,KEND
WORK=0.0D0
MIN=MIN-1
LHOR=IPIV
LVER=J
C
C      START INNER LOOP
DO 3 L=LANF,MIN
LVER=LVER+1
LHOR=LHOR+L
3 WORK=WORK+A(LVER)*A(LHOR)
C      END OF INNER LOOP
C
C      A(J)=-WORK*DIN
4 J=J-MIN
C      END OF ROW-LOOP
C
5 IPIV=IPIV-MIN
6 IND=IND-1
C      END OF INVERSION-LOOP

```

ORIGINAL PAGE IS
OF POOR QUALITY
DSINV

```
C      CALCULATE INVERSE(A) BY MEANS OF INVERSE(T)
C      INVERSE(A) = INVERSE(T) * TRANSPOSE(INVERSE(T))
C      INITIALIZE MULTIPLICATION-LOOP
DO 8 I=1,N
IPIV=IPIV+I
J=IPIV
C      INITIALIZE ROW-LOOP
DO 8 K=I,N
WORK=0.D0
LHOR=J
C      START INNER LOOP
DO 7 L=K,N
LVER=LHOR+K-I
WORK=WORK+A(LHOR)*A(LVER)
7 LHOR=LHOR+L
C      END OF INNER LOOP
C      A(J)=WORK
8 J=J+K
C      END OF ROW- AND MULTIPLICATION-LOOP
C
9 RETURN
END
```

C
C
C
C SUBROUTINE DMFSD
C
C PURPOSE
C FACTOR A GIVEN SYMMETRIC POSITIVE DEFINITE MATRIX
C
C USAGE
C CALL DMFSD(A,N,EPS,IER)
C
C DESCRIPTION OF PARAMETERS
C A - DOUBLE PRECISION UPPER TRIANGULAR PART OF GIVEN
C SYMMETRIC POSITIVE DEFINITE N BY N COEFFICIENT
C MATRIX.
C ON RETURN A CONTAINS THE RESULTANT UPPER
C TRIANGULAR MATRIX IN DOUBLE PRECISION.
C N - THE NUMBER OF ROWS (COLUMNS) IN GIVEN MATRIX.
C EPS - SINGLE PRECISION INPUT CONSTANT WHICH IS USED
C AS RELATIVE TOLERANCE FOR TEST ON LOSS OF
C SIGNIFICANCE.
C IER - RESULTING ERROR PARAMETER CODED AS FOLLOWS
C IER=0 - NO ERROR
C IER=-1 - NO RESULT BECAUSE OF WRONG INPUT PARAMETER N OR BECAUSE SOME RADICAND IS NON-
C POSITIVE (MATRIX A IS NOT POSITIVE DEFINITE, POSSIBLY DUE TO LOSS OF SIGNIFICANCE)
C IER=K - WARNING WHICH INDICATES LOSS OF SIGNIFICANCE. THE RADICAND FORMED AT FACTORIZATION STEP K+1 WAS STILL POSITIVE BUT NO LONGER GREATER THAN ABS(EPS*A(K+1,K+1)).
C
C REMARKS
C THE UPPER TRIANGULAR PART OF GIVEN MATRIX IS ASSUMED TO BE STORED COLUMNWISE IN $N*(N+1)/2$ SUCCESSIVE STORAGE LOCATIONS. IN THE SAME STORAGE LOCATIONS THE RESULTING UPPER TRIANGULAR MATRIX IS STORED COLUMNWISE TOO.
C THE PROCEDURE GIVES RESULTS IF N IS GREATER THAN 0 AND ALL CALCULATED RADICANDS ARE POSITIVE.
C THE PRODUCT OF RETURNED DIAGONAL TERMS IS EQUAL TO THE SQUARE-ROOT OF THE DETERMINANT OF THE GIVEN MATRIX.
C
C SUBROUTINES AND FUNCTION SUBPROGRAMS REQUIRED
C NONE
C
C METHOD
C SOLUTION IS DONE USING THE SQUARE-ROOT METHOD OF CHOLESKY.

ORIGINAL PAGE IS
OF POOR QUALITY

```
C      THE GIVEN MATRIX IS REPRESENTED AS PRODUCT OF TWO TRIANGULAR
C      MATRICES, WHERE THE LEFT HAND FACTOR IS THE TRANSPOSE OF
C      THE RETURNED RIGHT HAND FACTOR.
C
C      ****
C
C      SUBROUTINE DMFS(a,n,eps,ier)
C
C      DIMENSION a(210)
C      DOUBLE PRECISION dsum, a
C
C      TEST ON WRONG INPUT PARAMETER N
C      IF(n-1) 12,1,1
1   ier=0
C
C      INITIALIZE DIAGONAL-LOOP
C      kpi=0
C      DO 11 k=1,n
C          kpi=kpi+k
C          ind=kpi
C          lend=k-1
C
C      CALCULATE TOLERANCE
C      tol=abs(ep*sngl(a(kpi)))
C
C      START FACTORIZATION-LOOP OVER K-TH ROW
C      DO 11 i=k,n
C          dsum=0.0
C          IF(lend) 2,4,2
C
C          START INNER LOOP
2   DO 3 l=1,lend_
C          lanf=kpi-l
C          lind=ind-l
3   dsum=dsum+a(lanf)*a(lind)
C          END OF INNER LOOP
C
C          TRANSFORM ELEMENT A(ind)
4   dsum=a(ind)-dsum
C          IF(i-k) 10,5,10
C
C          TEST FOR NEGATIVE PIVOT ELEMENT AND FOR LOSS OF SIGNIFICANCE
5   IF(sngl(dsum)-tol) 6,6,9
6   IF(dsum) 12,12,7
7   IF(ier) 8,8,9
8   ier=k-1
C
```

DMFSD

```
C      COMPUTE PIVOT ELEMENT
9  DPIV=DSQRT(DSUM)
A(KPIV)=DPIV
DPIV=1.D0/DPIV
GO TO 11
C
C      CALCULATE TERMS IN ROW
10 A(IND)=DSUM*DPIV
11 IND=IND+I
C      END OF DIAGONAL-LOOP
C
C      RETURN
12 IER=-1
RETURN
END
```

ORIGINAL PAGE IS
OF POOR QUALITY

REFERENCES

1. R.S. Chapman, "Particle Size and X-Ray Analysis of Feldspar Calvert, Ball, and Jordon Soils," NASA TM X-73941, February 1977.
2. M. Born, E. Wolf, "Principles of Optics," Fifth edition, Pergamon Press, (1975), p. 633.
3. M. Kerker, "The Scattering of Light," Academic Press, (1969), Chapters 3 and 4.
4. J.A. Stratton, "Electromagnetic Theory," McGraw-Hill Book Co., Inc. (1941), p. 563.
5. D. Deirmendjian, "Electromagnetic Scattering on Spherical Polydispersions," American Elsevier Publishing Co., Inc., (1969).
6. J.V. Dave, "Subroutines for Computing The Parameters of The Electromagnetic Radiation Scattered by a Sphere," IBM Report No. 320-3237, May 1968.
7. G. Mie, Annid, Physik (4), Vol. 25 (1908), p. 377.
8. P. Debye, Annid, Physik (4), Vol. 30 (1909), p. 57.
9. "Handbook of Chemistry and Physics," Chemical Rubber Publishing Co., (1960), p.-1510.
10. G.W. Grams, et.al., "Complex Index of Refraction of Airborne Soil Particles," Journal of Applied Meteorology, Vol. 13, June 1974, p. 459.
11. N.G. Jerlov, E.S. Nielsen, eds., "Optical Aspects of Oceanography," Academic Press, (1974), p. 152.
12. D.K. Todd, "The Water Encyclopedia," Water Information Center, (1970), p. 86.
13. M. Born, E. Wolf, "Principles of Optics," Fifth edition, Pergamon Press, (1975), p. 24.

REFERENCES (Concluded)

14. D. Deirmendjian, "Electromagnetic Scattering on Spherical Polydispersions," American Elsevier Publishing Co., Inc. (1969), p. 66.
15. D. Deirmendjian, "Electromagnetic Scattering on Spherical Polydispersions," American Elsevier Publishing Co., Inc., (1969), p. 24.
16. W. Houghton, Private Communication.

INTERNAL DISTRIBUTION LIST

A-10

G. MacDonald

D-10

S. Blum

W. Gouse

C. Zraket

D-11

W. Sievers

D-12

H. Benington

C. Grandy

A. Tachmindji

W-50

R. Greeley

R. Ouellette

J. Golden

R. Pikul

R. Forman

D. Sluyter

W-51

E. Sharp

L. Gsellman

W-52

M. Scholl

G. Bennington

S. Goldstein

W-53

E. Friedman

A. Ghovanlou (10)

J. Gupta

R. Henderson (20)

E. Keitz

N. Lord

E. Mangold

E. Ward

T. Wright

W-54

J. Golden

E. Krajeski

W-55

A. Challis**

N. Coates

J. Stone

W-56

L. Thomas

S. Lubore

G. Erskine

W-57

S. Lewis

W-50 Library (5 copies)

METREK Library

Technical Report Center (2)

Document Control (8)

Westpart Storage* (15)

EXTERNAL DISTRIBUTION LIST

| | <u>No. of Copies</u> |
|--|--------------------------|
| NASA Langley Research Center Hampton, VA 23665 Attn: Report & Manuscript Control Office, Mail Stop 180A William M. Houghton, Mail Stop 235A | 1 20 |
| NASA Ames Research Center Moffett Field, CA 94035 Attn: Library, Mail Stop 202-3 | 1 |
| NASA Dryden Flight Research Center P. O. Box 273 Edwards, CA 93523 Attn: Library | 1 |
| NASA Goddard Space Flight Center Greenbelt, MD 20771 Attn: Library | 1 |
| NASA Lyndon B. Johnson Space Center 2101 Webster Seabrook Road Houston, TX 77058 Attn: JM6/Library | 1 |
| NASA Marshall Space Flight Center Marshall Space Flight Center, AL 35812 Attn: Library, AS61L | 1 |
| Jet Propulsion Laboratory 4800 Oak Grove Drive Pasadena, CA 91103 Attn: Library, Mail 111-113 | 1 |
| NASA Lewis Research Center 21000 Brookpark Road Cleveland, OH 44135 Attn: Library, Mail Stop 60-3 | 1 |
| NASA John F. Kennedy Space Center Kennedy Space Center, FL 32899 Attn: Library, NWSI-D | 1 |

EXTERNAL DISTRIBUTION LIST (Continued)

| | <u>No. of Copies</u> |
|--|--------------------------|
| National Aeronautics & Space Administration Attn: RE-4 Washington, DC 20546 | 1 |
| NASA Scientific & Technical Information Facility P. O. Box 8757 Baltimore/Washington International Airport Maryland 21240 | 30 |
| Mr. H. Mark NASA/Lewis Research Center 21000 Brookpark Road Cleveland, Ohio 44135 | |
| Mr. Al Watkins Chief EROS EROS Data Center Sioux Falls, SD 57198 | 1 |
| Mr. William R. Bandeen NASA/Goddard Space Flight Center Code 910 Greenbelt, Maryland 20771 | 1 |
| Mr. Lawrence T. Hogarth NASA/Goddard Space Flight Center Code 903.0 Greenbelt, Maryland 20771 | 1 |
| Mr. Charles Laughlin NASA/Goddard Space Flight Center Code 901 Greenbelt, Maryland 20771 | 1 |
| Dr. Vincent V. Salmonson NASA/Goddard Space Flight Center Code 913 Greenbelt, Maryland 20771 | 1 |

EXTERNAL DISTRIBUTION LIST (Continued)

| | <u>No. of Copies</u> |
|--|--------------------------|
| Dr. Albert Rango NASA/Goddard Space Flight Center Code 913 Greenbelt, Maryland 20771 | 1 |
| Mr. Pitt G. Thome NASA Headquarters Mail Code ERB2 Washington, D.C. 20546 | 1 |
| Dr. Robert A. Schiffer NASA Headquarters Mail Code ERC2 Washington, D.C. 20546 | 1 |
| Mr. John P. Mugler NASA/Langley Research Center Mail Code 422 Hampton, VA 23665 | 1 |
| Dr. James D. Lawrence NASA/Langley Research Center Mail Code 401 Hampton, VA 23665 | 1 |
| Mr. James L. Raper NASA/Langley Research Center Mail Code ERC2 Washington, D.C. 20546 | 1 |
| Mr. Edwin F. Harrison NASA/Langley Research Center Mail Code 271 Hampton, VA 23665 | 1 |
| Mr. E. Brian Pritchard NASA/Langley Research Center Mail Code 270 Hampton, VA 23665 | 1 |

EXTERNAL DISTRIBUTION LIST (Concluded)

| | <u>No. of</u> <u>Copies</u> |
|---|--------------------------------|
| Ms. Ruth Whitman NASA Headquarters Mail Code ERD2 Washington, D.C. 20546 | 1 |
| Dr. S.H. Melfi NASA Headquarters Mail Code ERC2 Washington, D.C. 20546 | 1 |
| Dr. Charles Whitlock National Aeronautics and Space Administration Langley Research Center Mail Stop 322 Hampton, VA 23665 | 1 |
| Mr. Lamont Poole National Aeronautics and Space Administration Langley Research Center Mail Stop 272 Hampton, VA 23665 | 1 |